Fall 2009

Micro-, nano-integrated composites based on cellulose microfibers

Qi Xing
Louisiana Tech University

MICRO-, NANO-INTEGRATED COMPOSITES BASED ON CELLULOSE MICROFIBERS

by

Qi Xing, M.S.

A Dissertation Presented in the Partial Fulfillment
of the Requirements for the Degree
Doctor of Philosophy

COLLEGE OF ENGINEERING AND SCIENCE
LOUISIANA TECH UNIVERSITY

November, 2009

ProQuest LLC
789 East Eisenhower Parkway
P.O. Box 1346
Ann Arbor, MI 48106-1346

LOUISIANA TECH UNIVERSITY

THE GRADUATE SCHOOL

June 30, 2009

Date

We hereby recommend that the dissertation prepared under our supervision by Qi Xing

entitled

MICRO-, NANO-INTEGRATED COMPOSITES BASED ON CELLULOSE MICROFIBERS

be accepted in partial fulfillment of the requirements for the Degree of Doctor of Philosophy in Engineering

Yuri Lvov

Supervisor of Dissertation Research

Head of Department

Department

Recommendation concurred in:

Advisory Committee

Approved:

Director of Graduate Studies

Approved:

Dean of the Graduate School

Dean of the College

GS Form 13a
(6/07)

ABSTRACT

Three different cellulose microfiber based composites have been fabricated through micro-, nano-integrated methods. The morphology, properties and application of these composites were demonstrated.

Biocomposites of cellulose microfibers and enzymes (laccase and urease) were obtained through layer-by-layer assembly by alternate adsorption with oppositely charged polycations and enzymes. The formation of organized polyelectrolyte and enzyme multilayer films of 15–20 nm thickness was demonstrated by quartz crystal microbalance, ζ-potential analysis and confocal laser scanning microscope. These biocomposites retained enzymatic catalytic activity, which was proportional to the number of coated enzyme layers. For laccase-fiber composites, around 70% of its initial activity was retained after 45 days storage at 4°C. The synthesis of calcium carbonate microparticles on urease-fiber composites confirmed urease functionality and demonstrated its possible applications. This strategy could be employed to fabricate fiber-based composites with novel biological functions.

Nanocoating of poly(3,4-ethylenedioxythiophene) - poly(styrenesulfonate) (PEDOT-PSS) and aqueous dispersion of carbon nanotubes (CNT-PSS) on cellulose microfibers has been developed to make a conductive cellulose microfibers based composite. To construct the multilayers on cellulose microfibers, cationic poly(ethyleneimine) (PEI) has been used in alternate deposition with anionic conductive PEDOT-PSS and solubilized

CNT-PSS. Using a Keithley microprobe measurement system, current–voltage measurements have been carried out on single composite microfibers after deposition of each layer to optimize the electrical properties of the coated microfibers. The conductivity of the resultant wood microfibers was in the range of 10^{-2} to 2 $S.cm^{-1}$, depending on the architecture of the coated layer. Further, the conductivity of the coated wood microfibers increased up to 20 $S.cm^{-1}$ by sandwiching a multilayer of conductive co-polymer PEDOT-PSS with CNT-PSS through a polycation (PEI) interlayer. Moreover, paper hand sheets were manufactured from these coated wood microfibers with conductivity ranging from 1 to 10 $S.cm^{-1}$. A paper composite structure consisting of conductive/dielectric/conductive layers that acts as a capacitor, has also been fabricated and is reported.

Cellulose microfibers were combined with cross-linked gelatin to make biocompatible porous microscaffolds for the sustained growth of brain cell and human Mesenchymal Stem Cells (hMSCs) in a three dimensional (3-D) structure. Live imaging, using confocal microscopy, indicated that 3-D microscaffolds, composed of gelatin or cellulose fiber/gelatin, both supported brain cell adhesion and growth for 16 days *in vitro*. Cellulose microfiber/gelatin composites containing up to 75% cellulose fibers can withstand higher mechanical load than gelatin alone, and composites also provided linear pathways along which brain cells could grow compared to more clumped cell growth in gelatin alone. Therefore, the bulk cellulose microfiber provides a novel skeleton in this new scaffold material. The cellulose fiber/gelatin scaffold supported hMSCs growth and extra cellular matrix formation. hMSCs osteogenic and adipogenic assays indicated that hMSCs cultured in cellulose fiber/gelatin composite preserved the multi-lineage

differentiation potential. As natural, biocompatible components, the combination of gelatin and cellulose microfibers, fabricated into 3-D matrices, may therefore provide optimal porosity and tensile strength for long-term maintenance and observation of cells.

APPROVAL FOR SCHOLARLY DISSEMINATION

The author grants to the Prescott Memorial Library of Louisiana Tech University the right to reproduce, by appropriate methods, upon request, any or all portions of this Dissertation. It is understood that "proper request" consists of the agreement, on the part of the requesting party, that said reproduction is for his personal use and that subsequent reproduction will not occur without written approval of the author of this Dissertation. Further, any portions of the Dissertation used in books, papers, and other works must be appropriately referenced to this Dissertation.

Finally, the author of this Dissertation reserves the right to publish freely, in the literature, at any time, any or all portions of this Dissertation.

Author Qi Xing

Date 11/10/2009

TABLE OF CONTENTS

LIST OF TABLES

LIST OF FIGURES

ACKNOWLEDGEMENTS

I wish to express my sincere gratitude and appreciation to my advisor Dr. Yuri Lvov. His guidance, encouragement and trust have supported me throughout all aspects of my doctoral education and research. I would like to thank my committee members: Dr. Mark DeCoster, Dr. Tabbetha Dobbins, Dr. David Mills and Dr. James Palmer for their time and contributions. Special thanks to Dr. Mark DeCoster for his guidance and generous support in the cellulose fiber scaffold work. I would also like to thank Dr. Kody Varahramyan for his support on conductive paper work.

I am grateful to Dr. Feng Zhao who introduced me to graduate research in the U.S.A. and helped me with stem cell culture experiments. I want to thank Dr. Mangilal Agarwal for his efforts, incite and supervisions on conductive composite work. I also want to thank Dr. Zonghuan Lu and Dr. Tatsiana Shutava for their invaluable help and experience in my research.

A number of fellow graduate students I have been closely working with gave me much useful advice and assistance, and I want to take this opportunity to thank all of them. Ms. Si Chen deserves special credit for her brain cell culture experiment. Additionally, I would like to thank Dr. George Grozdits for his helpful discussion about wood cellulose microfibers and Dr. Sidney Sit for use of his mercury intrusion porosity instrument.

Finally, I would like to thank my family. My parents and my brother have encouraged and supported me with their love and patience throughout my life and study.

CHAPTER ONE

INTRODUCTION

1.1 Motivation and Background

Wood cellulose microfibers are traditionally used to make paper, cardboard and other paper-based materials. They are also widely employed as reinforcement filler for the manufacture of polymer composites which have been used in a variety of low-end applications, such as construction, transportation and consumer products. The increasing concern for environmental preservation and resource sustainability has created dramatic interest in renewable materials, such as wood cellulose microfibers. The pulp and paper industry are also seeking for new technology or innovation hoping to improve the decreasing market profits. Cellulose microfiber based composites for high-end applications are highly desired. In recent years, the advancement of micro-, nanotechnology provides a revolutionary platform for development of higher-value and higher-performance composite products based on wood cellulose microfibers. Magnetic particles[1] and noble metal nanoparticles[2] have been successfully synthesized in the presence of cellulose fibers. These nanoparticle-containing cellulose fibers were used to make special paper with magnetic properties, and high-performance catalysis for chemical reactions under mild conditions. Cellulose micro and nanofibrils were extracted from fiber cell walls and used to prepare light cellulose composites of high strength.[3,4]

Layer-by-layer (LbL) self-assembly is a versatile method to form tailored multilayer thin films on substrates with different shapes. The basic idea of the LbL method is the alternate deposition of polycations and polyanions through electrostatic interactions. Polyelectrolyte and nanoparticle multilayers created by LbL nanoassembly have been utilized to modify the surface of cellulose fibers.[5-8] These modified fibers obtained special functions without losing their basic structure and properties.

1.2 Previous Work and Contribution

The application of the LbL nanoassembly technique on wood cellulose microfiber to make better paper has been investigated in our group. Polyelectrolytes were coated on the wood fiber surface producing negatively and positively charged fibers. The confocal images of wood cellulose microfibers with negative and positive surface potential are shown in Figure 1.1.

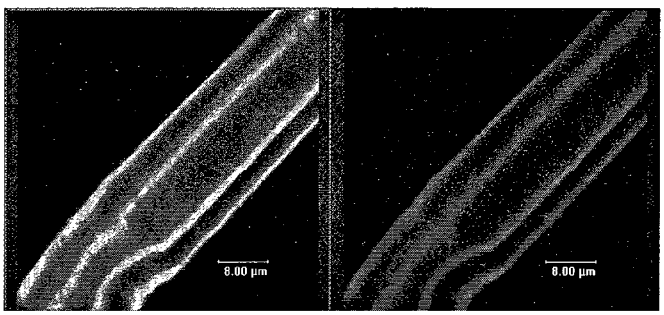

Figure 1.1 Confocal images of longitude cross section of softwood microfibers coated with $(PAH/PSS)_3$ multilayers. PAH was labeled with FITC (green) and PSS was labeled with RBITC (red).

These oppositely charged fibers were mixed to make paper which introduced electrostatic interaction in addition to the traditional hydrogen bonding between fibers. The resulting paper strength was increased up to 100% more than virgin paper.[7] This

strategy is very helpful for recycling broken fiber material from paper mills. Old corrugated cardboard broken fibers were coated with polyelectrolyte multilayer films of (PAH/PSS/PAH). Handsheets made from 50% treated fibers and 50% untreated fibers showed increased tensile index, tear index, stiffness index and modulus compared to the control (100% untreated fibers).[9] Different nanoparticles and nanotubes were deposited on the wood fiber surface using the LbL approach. The brightness and porosity of the resulting paper handsheets were enhanced.[8] We have developed a series of methods to characterize the LbL multilayer thin film growth, and also a setup specifically for the LbL nanocoating of cellulose microfibers, as schematically shown in Figure 1.2.

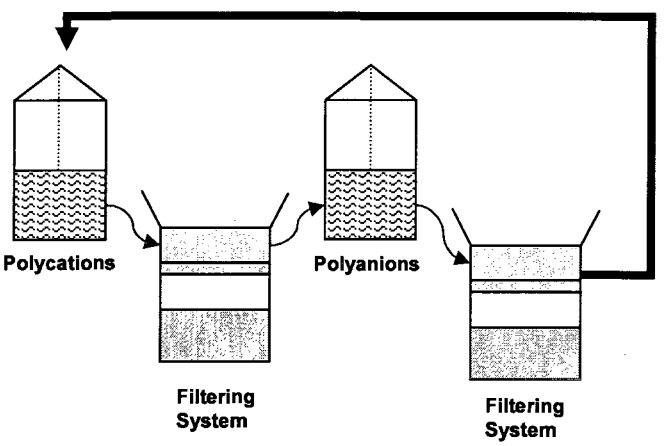

Figure 1.2 Set-up for LbL nanocoating on wood cellulose microfibers.

1.3 Objectives

The overall objective of this research work is to explore and demonstrate one possibility of developing wood cellulose microfiber based composites with novel functionalities by utilizing the LbL nanoassembly method and phase- separation method. Specifically:

(1) Modify wood cellulose microfibers systematically with different enzymes using the LbL nanoassembly method; characterize the morphology and LbL film growth.

(2) Monitor the enzyme activity and stability variation over multilayer thin film architecture.

(3) Demonstrate the application of cellulose microfiber/enzyme biocomposites.

(4) Modify wood cellulose microfibers with PSS modified carbon nanotubes using LbL approach. Investigate the conductivity of the resulting composite by changing the assembling conditions.

(5) Examine the influence of PEDOT-PSS incorporated in the LbL films.

(6) Make conductive paper handsheets using the obtained conductive microfibers; measure the conductivity and demonstrate the application for making electronic devices.

(7) Fabricate cellulose microfiber/gelatin composite using phase separation and freez-drying method.

(8) Characterize material properties, such as porosity, pore size, mechanical strength, water uptake capacity and protein adsorption ability.

(9) Demonstrate the biocompatibility of cellulose microfiber/gelatin composite by culturing different cells in the scaffold. Observe cell adhesion, proliferation and differentiation.

1.4 Outline of Dissertation

Chapter One introduces the motivation and some background information about this research work. Previous related work done by this author and other group members is presented. The research goals and the organization of this dissertation are shown.

Chapter Two gives a brief literature review covering the knowledge needed for this dissertation: cellulose microfibers, LbL nanoassembly, laccase and urease, carbon nanotubes, conductive polymer PEDOT-PSS, three-dimensional scaffold for tissue engineering and regenerative medicine, etc.

Chapter Three discusses the fabrication of cellulose microfiber/enzyme biocomposites using the LbL technique. The physical and biochemical characteristics are investigated for laccase-fiber and urease-fiber composites, respectively. The application of urease-fiber composite in biomineralization is presented.

Chapter Four describes making conductive cellulose microfibers and the resulting conductive paper handsheets through LbL assembly. Conductivity is investigated upon the assembling conditions of carbon nanotubes and PEDOT-PSS polymer. A conductive paper based capacitor and conductive paper based glucose sensor were fabricated and characterized.

Chapter Five demonstrates the possibility of making a cellulose microfiber/gelatin composite as a cell culture scaffold for tissue engineering and regenerative medicine applications. Various methods are employed to investigate the material properties of this cellulose microfiber based composite. Brain tumor cells and human mesenchymal stem cells are seeded into the scaffold for long term culture and observation.

Chapter Six concludes the results of the dissertation. Some issues and topics for future work are recommended.

CHAPTER TWO

LITERATURE REVIEW

2.1 Cellulose Microfibers

Cellulose microfiber is one of the most abundant and renewable polymer sources in nature including plants, such as wood, cotton and bacterial. With the increasing awareness of the importance of renewable materials in protecting the environment and natural resources, cellulose microfibers were studied extensively in different areas as candidate to replace materials derived from non-renewable sources.

2.1.1 Chemical Structure

Wood cellulose microfibers are composed of different chemical components, such as cellulose, hemicellulose, and lignin. Cellulose, the main component, holds the framework of wood microfibers in the form of cellulose microfibrils.[10] Cellulose is the most abundant organic polymer in the world. It is a linear polysaccharide of D–glucose units linked by β (1→4) glucosidic bonds where every other glucose residue is rotated approximately 180°.[11] Figure 2.1 shows the chemical structure of cellulose. Cellulose is quite evenly distributed throughout the wood cell walls, therefore, the surface of lignocellulose fibers is rich in hydroxyl groups. Hemicellulose is a branched polysaccharide composed of not only glucose but also other sugar unit including xylose, manose, galactose, etc. Hemicellulose fills the space between the cellulose microfibrils as a matrix substance. Lignin functions as an encrusting substance solidifying the cell wall.

After Kraft (sulfate) pulping of wood chips, less than 1% of lignin is present in the resulting fibers. These delignified fibers were simply called cellulose fibers in our work.

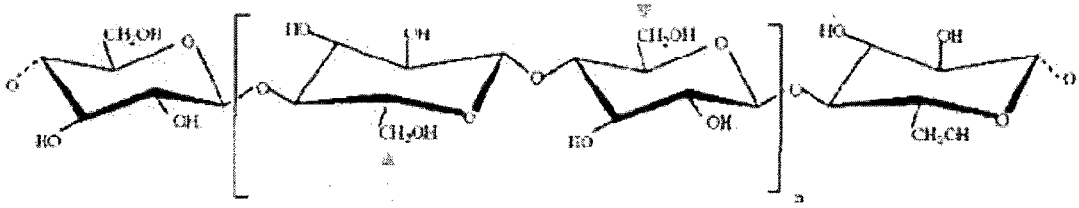

Figure 2.1 Cellulose structure. The arrows point to the basic repeating unit.[11]

2.1.2 Physical Structure

Figure 2.2 shows scanning electron microscopy images of soft wood cellulose fibers after the Kraft pulping process, as supplied by International Paper Co. The diameter of these cellulose fibers is approximately 20 μm. The length can reach 3 mm. There are some pits on fiber surface with a diameter around 1-2 μm.

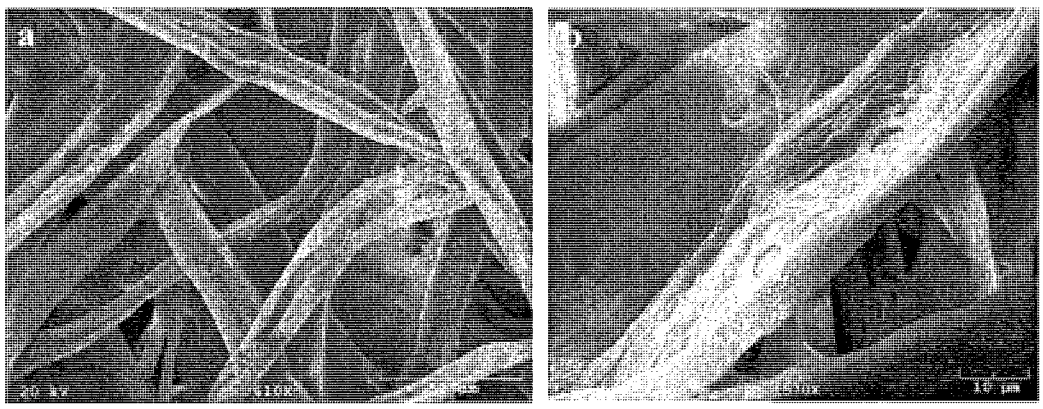

Figure 2.2 SEM images of unrefined soft wood cellulose fibers. (a) low magnification; (b) high magnification.

The microstructure of the wood cell wall was shown in Figure 2.3. The outmost layer is the primary wall. Inside of the primary wall is the secondary wall S1, S2, S3.[10] The

middle layer S2 is thickest and contains most of the cell wall materials. The cellulose microfibrils network is present in each layer with different orientation. Cellulose crystals are present in cellulose fibers in the form of cellulose microfibrils. Wood cellulose microfibril is approximately a few of nanometers in width. Cellulose microfibril is highly crystalline with a core crystalline region of cellulose surrounded by paracrystalline cellulose and short-chain hemicelluloses.[1] These microfibrils can significantly influence the physical, chemical and mechanical properties of the wood.

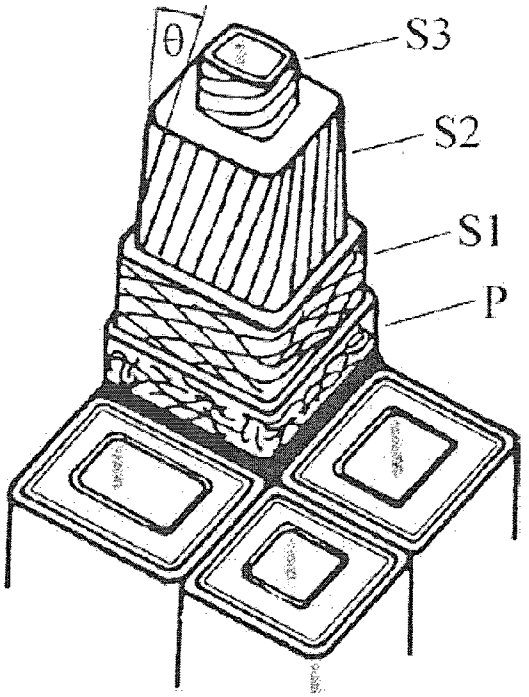

Figure 2.3 Microstructure of wood fiber cell wall. P: primary cell wall, S1: outerlayer, S2: middle layer, S3: inner layer of secondary wall. θ is the microfibril angle.[3]

2.1.3. Cellulose Fiber Reinforced Composite

Cellulose fiber reinforced composites have been accepted worldwide for various applications due to their excellent properties, such as high strength and stiffness, low

density and low cost as compared to conventional fillers of glass and aramid fibers. Cellulose fiber reinforced starch composite has been extensively studied by using cellulose fibers from various resources and different types of starch. Thermoplastic wheat starch, reinforced with cellulose fibers, was four times stronger than without fibers.[12] Starch-based foams were mixed with cellulose fiber (2.5 to 15 wt%) to increase strength.[13] One of the advantages of using cellulose fiber as reinforcement material is the availability of a wide variety of fiber resources: wood, cotton and straw, even recycled fibers. Huda et al. reported on the study of a bicomposite made from recycled newspaper cellulose fiber and poly(lactic acid).[14] The tensile and flexural moduli of biocomposites with 30 wt% cellulose fibers are significantly higher than virgin resin. Wood cellulose fiber/plastic composite is rising in the market to compete with wood and other materials. However, the main issue of using cellulose fiber as a filler for thermoplastics is the poor interaction of polyolefins with the wood cell wall. This problem results in low thermal stability in processing and decreased strength of composite materials. Modification of the cellulose fiber surface is important for improving adhesion between cellulose fiber and thermoplastics.

2.1.4 Cellulose and Cellulose Fiber Modification

There have been many efforts to modify cellulose and cellulose fiber for the purpose of either improving final product properties or exploring new applications of cellulose fibers. A lot of modification methods have been commercially realized in the paper or paper-related industry. The most common and versatile method is chemical modification including esterification, the process to convert hydroxyl groups into ester groups; silanization, the formation of hydrogen bond with hydroxyl groups on cellulose fiber

surface; modification by isocyanates, the formation of covalent bonds between hydroxyl groups and isocyanate groups (-N=C=O). Plasma and ozone treatment is another method for cellulose fiber modification. Gas phase ozonation was employed to improve the wetting and absorption properties of lignocellulosic fibers.[15] After treatment by dielectric-barrier discharge, the compatibility between cellulose fibers and synthetic polymers was greatly improved.[16] The third modification method is graft copolymerization. Polyacrylic acid can be grafted onto the cellulose fiber surface after surface activation by epoxy silane.[17] Hydrogel microstructures were successfully grafted on the cellulose fiber surface to make new functional materials.[18] The fourth modification method is irreversible adsorption of polymers on the cellulose fiber surface. Different block copolymers can be adsorbed on the cellulose fiber to change surface properties, such as hydrophobicity and adhesive ability. LbL nanoassembly is one of the most simple and versatile methods for cellulose fiber surface modification.

2.2 Layer-by-Layer Nanoassembly

By building multilayers of oppositely charged colloids, the LbL nanoassembly method was first reported by Iler in 1966.[19] The method was then rediscovered and explored further by Decher, et al. in the early 1990s.[20,21] The basis of the methods involves the resaturation of charged molecules adsorbed on a charged surface, leading to the reversal of the surface charge of the films after each layer of deposition. The scheme of the LbL nanoassembly process is described in Figure 2.4. Through sequential deposition of oppositely charged molecules, a dense multilayer structure up to 500 nm thick can be achieved. Depending on the size of the molecules and the deposition conditions, the thickness of each layer is controllable in the order of a few nanometers.

This method provides the opportunity to produce molecularly organized ultrathin films similar to the ones obtained with highly sophisticated and expensive molecular beam epitaxy technology used for metals and semiconductors. Therefore, this technique is call "molecular beaker epitaxy" by Mallouk T.[22]

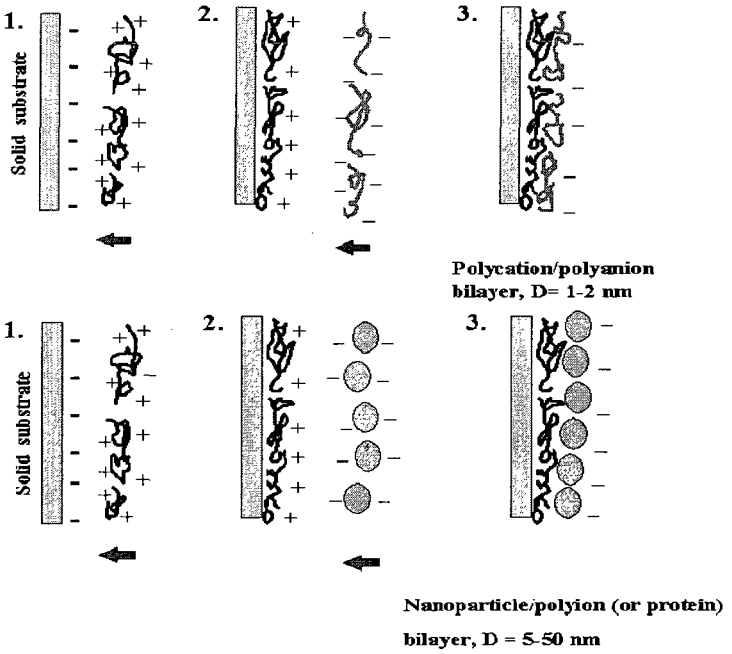

Figure 2.4 Scheme of the LbL nanoassembly process. 1. polycation adsorbed on negatively charged solid substrate; 2. polyanion or negatively charged nanoparticles or proteins adsorbed on polycation covered surface; 3. formation of electrostatic bond immobilized thin films.

2.2.1 LbL Nanoassembly Procedure

Figure 2.5 illustrates the LbL nanoassembly operation procedure. A cleaned substrate of any shape and dimension is immersed into a dilute solution of a polycation for a period of time optimized for the adsorption of a single monolayer (around 1~2 nm thick). If the concentration of polycation is high enough, surface charge is effectively reversed. The reversed surface charge prevents further polycation adsorption. Then it is rinsed in

deionized water and air dried or blow dried with N_2 to remove any non-specific adsorbed molecules. The next step is the immersion of the polycation covered substrate into a dilute solution of polyanion, also for a time period optimized for the adsorption of a monolayer. Then it is rinsed and dried. The above steps complete one cycle of the LbL self-assembly of polycation/polyanion coating on the substrate. By repeating the operations, a multilayer assembly with precisely controllable thickness can be obtained.

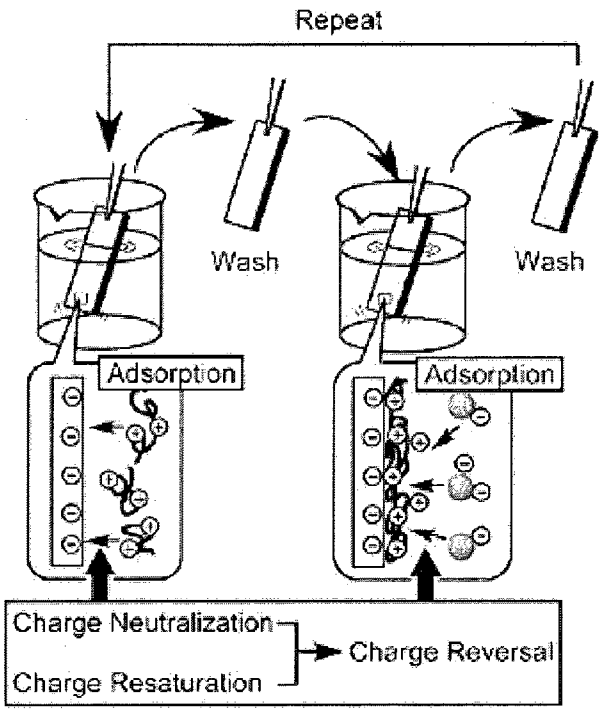

Figure 2.5 Operation procedure of LbL nanoassembly through electrostatic interaction.[23]

The first polyion layer on a weakly charged solid substrate does not cover the whole surface, thus forming an island-type pattern. In the following two to three adsorption cycles these islands spread and cover the entire surface. Therefore, at the beginning of the LbL assembly, non-linear film growth is often observed; the further multilayer growth is linear.[24] Due to this particular phenomenon, three to four precursor polyeletrolyte layers

are first deposited on the substrate when we study the possibility of using new compounds in the assembly. The precursor layers provide a well defined charge of "polyion blanket" for assembly of proteins, nanoparticles and other compounds.

The forces holding LbL multilayers together are primarily due to multiple electrostatic bonds, but other types of interactions like hydrogen bonding and hydrophobic force can also be involved.

2.2.2. Nanoblocks for LbL Nanoassembly

There is no major restriction to the choice of charged molecules. A great variety of substances including polyelectrolytes, nanoparticles (or other nano-sized blocks) and proteins (i.e. DNA, enzymes) have been employed for LbL self-assembly. The structural formula of the predominately used polyelectrolytes is shown in Figure 2.6.

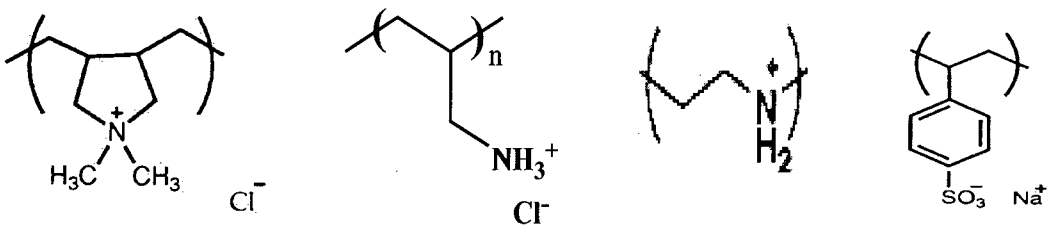

(1) (2) (3) (4)

Figure 2.6 Structure formula of predominately used polyelectrolytes: (1) PDDA; (2) PAH; (3) PEI; (4) PSS.

Polyions predominately used in the LbL self-assembly are as follows: 1) Polycations: poly(dimethyldiallylammonium chloride) (PDDA), poly(allylamine) (PAH), poly(ethylenimine) (PEI), poly-lysine, chitosan; 2) Polyanions: poly(styrenesulfonate) (PSS), poly(vinylsulfate) (PVS), poly(acrylic acid) (PAA), dextran sulfate, sodium alginate, gelatin, and many proteins. The pH of the polyion solution has to be adjusted

away from the isoelectric point so that the polyions have sufficient charge to be adsorbed and reverse the substrate charge. The isoelectric point of major polyions is listed the Table 2.1.

Table 2.1. Isoelectric point of some polyelectrolytes, nanoparticles, and proteins.

Compound	Isoelectric Point	Compound	Isoelectric Point
PDDA	12.0	PSS	1.0
PAH	8.2	PAA	4.2
PEI	11.5	TiO_2 nanoparticle	4.5
Poly(lysine)	8.0-9.0	Silica nanoparticle	4.0
Lysozyme	11.0	Glucose oxidase	4.2
Chitosan	8.0	Urease	5.1
Gelatin	4.7-5.2	BSA	4.9

Many types of nanoparticles and nanotubes were assembled with polymers by the LbL approach to tune optical, magnetic, electrical and mechanical properties. These nanoblocks include, but are not limited, to SiO_2, TiO_2, Fe_2O_3, CdSe, Au nanoparticles, carbon nanotubes and clay nanotubes. Figure 2.7 shows the images of multilayer thin films assembled through the LbL approach by using different polyelectrolytes and nanoblocks.

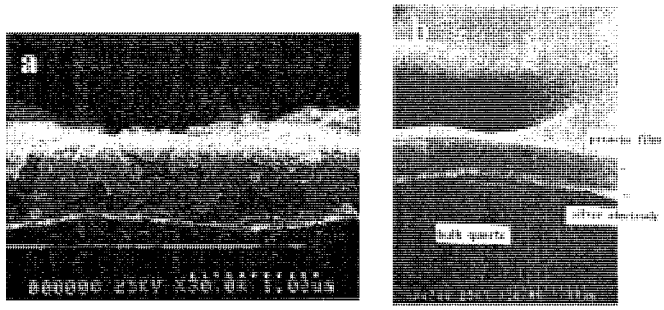

Figure 2.7 SEM images of (a) multilayer films of $(PDDA)(SiO_2/PDDA)_{24}$ on silver electrode.[25] (b) multilayer films of $(PEI/PSS)_2(PEI/Glucose\ Oxidase)_8PEI$ on silver-coated QCM resonator.[26]

2.2.3 LbL Nanoassembly Application in Fiber Modification

LbL nanoassembly has been introduced as a new method to modify fiber surfaces in the last decade. A wide range of polymers and nanoparticles can be employed to prepare nanocomposite fibers with enhanced properties or new functions. It has been demonstrated by Lvov Y. and Wågberg L. that different polyelectrolytes can be deposited on the surface of paper pulp fibers through LbL nanoassembly to vary the surface charge.[27,28] The paper handsheets made with the mixture of positively and negatively charged modified fibers had 100% increased tensile strength for the best case.[7] By using this new technique, electrostatic interaction between fibers was enhanced, which may account for the paper strength increase. Nanoparticles, such as TiO_2, were also used to modify the pulp fiber surface in order to improve the brightness of the paper handsheets by using LbL method.[8] Besides the application on pulp fibers, LbL nanoassembly was employed to modify many other different types of fibers. Dubas, et. al. demonstrated that silk or nylon fibers coated with antimicrobial silver nanoparticles by using the LbL method exhibited antibacterial activity.[29] The antibacterial activity increased with deposition of more nanoparticle layers. Shiratori, et. al. found that a smoke filter showed extremely high performance by forming PAH/PAA multilayer thin films on the surface of glass fibers. The adsorption behavior of smoke can be optimized by changing the deposition conditions used to modify the filter.[30]

2.3 Enzyme Immobilization

An enzyme is a protein category composed of more than 20 amino acids. Enzymes are capable of catalyzing chemical reactions under mild conditions. Due to the broad

application in biotechnology, different proteins, including enzymes, were immobilized for immunoassay, catalysis, biosensing and bioseparation. The advantages of enzyme immobilization on solid substrate are: simplified separation and purification process, improved operational stability and repeatedly used enzymes. There are many methods to immobilize enzymes on a substrate including physical entrapment, covalent bonding, crosslinking and electropolymerization. Each approach has advantages and limitations. For example, physical entrapment is the simplest method with high load efficiency, but the enzyme-substrate composite is not quite stable when the environment changes. Covalent bonding provides the strongest and most stable link to the enzyme, but the enzyme density is low.

2.3.1 LbL Enzyme Multilayer Films

LbL nanoassembly is a promising approach to fabricate highly organized protein multilayer films with a high density of protein. The LbL enzyme multilayer films on a colloid particle surface are permeable to substrates, have high surface areas and controllable biocatalysis activity. In addition, magnetic nanoparticles could be incorporated in the system to enhance the surface area as well as produce magnetic properties of the particles.[31,32] Figure 2.8 illustrates the incorporation of nanoparticles into the LbL enzyme assembly. LbL deposited enzyme multilayer thin films on micro- or nano-scale cores or channels were used to create biocatalysis nanoreactors. Different enzymes, such as glucose oxidase, urease, horseradish peroxidase, organophosphorous hydrolase have been demonstrated for this application.[33-36] Another application is for biosensors. Glucose oxidase and PEI was immobilized using the LbL method on a microcantilever for glucose measurement, which has better performance than the

chemical conjugation method.[37] Dendrimers were LbL deposited with glucose oxidase on an Au surface for bioelectrocatalytic analysis.[38] It was found that the sensitivity is significantly enhanced with enzyme multilayer growth.

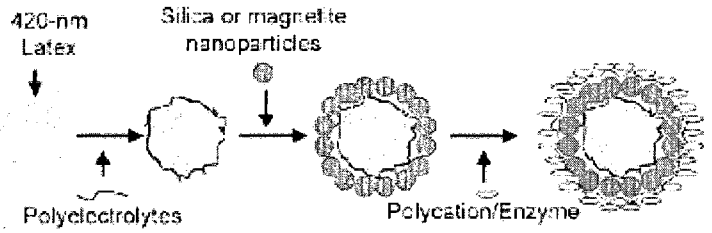

Figure 2.8 Illustration of polyelectrolytes, nanoparticles and enzymes assembled on latex nanoparticles through LbL approach.[31]

2.3.2 Laccase

Laccase is an oxidoreductase able to catalyze the oxidation of various aromatic compounds (particularly phenols) with the concomitant reduction of oxygen to water.[39] The four copper atoms distributed in the laccase molecule are important to the enzyme catalytic mechanisms. One T1 copper forms a mononuclear site, responsible for the blue color, and one T2 copper and two T3 copper forms a trinuclear site.[40] The structure of laccase is shown in Figure 2.9. Laccase is one of the oxidoreductase used widely in industry. It was used with a mediator for pulp delignification and bleaching. The handsheets made of laccase treated wood fibers showed improved strength properties.[41] There are many efforts to immobilize laccase on a solid support for the purpose of degrading phenolic compounds in waste water or monitoring polar pollutants. Laccase from Trametes versicolor was immobilized on APTES-GLUTAL-activated glass for batch reaction. The immobilized laccase showed highly retained activity even after six runs of oxidative cycles.[42] Immobilized laccase was also employed to make a biosensor.

Laccase was covalently bound onto the surface of glassy carbon electrode to detect inhibitor azide.[43]

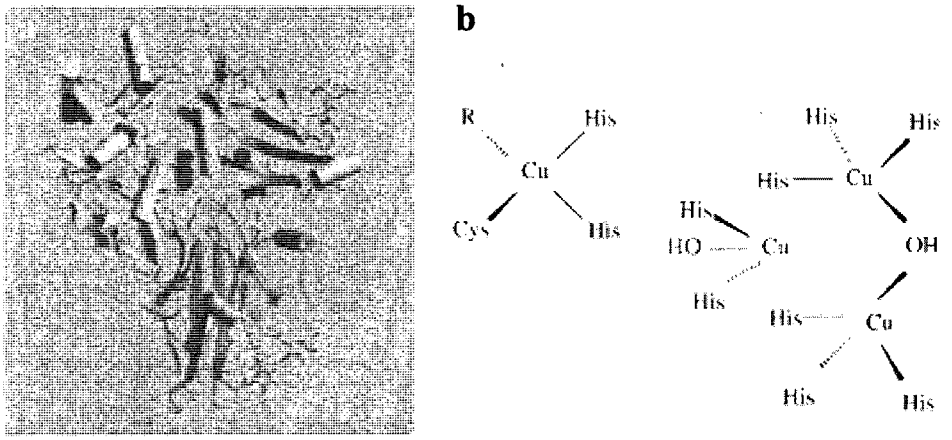

Figure 2.9 (a) Ribbon diagram of Trametes versicolor laccase. (b) Pictorial model of laccase copper center.[40]

2.3.3 Urease

Urease is an enzyme intensively investigated in many research areas due to its possible applications in technical and medical fields. Urease can catalyze the hydrolysis of urea into ammonia and carbon dioxide. The reaction occurs as follows:

$$(NH_2)_2CO + H_2O \rightarrow CO_2 + NH_3.$$

The bi-nickel center contained at each active site regulates the catalytic mechanism of urease. Karplus proposed a mechanism of urease catalysis which is demonstrated in Figure 2.10.

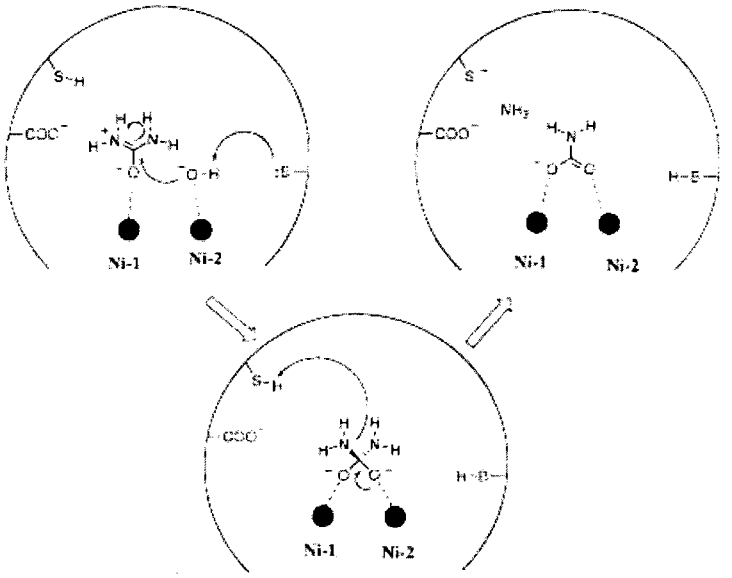

Figure 2.10 Reaction mechanism of urease catalysis of urea.[44]

Urease has been immobilized on different substrates including carboxymethylcellulose,[45] polystyrene nanoparticles,[46] polyaniline,[47] chitosan,[48] and silicon microchannels.[33] The method involved includes covalent bonding, entrapment and LbL nanoassembly. In these works, the activity and stability of immobilized urease were studied in detail. It can be applied in the measurement or removal of urea in blood and waste water. Immobilized urease was also used for biomineralization.[49] The carbon dioxide from urea hydrolysis reacts with calcium ions in solution, and then calcium carbonate crystals were formed at room temperature and under mild conditions. This reaction provides a new biomimetic approach for synthesis of inorganic/organic hybrid composites.

2.4 Carbon Nanotubes and Conductive Polymers

2.4.1. Carbon Nanotubes

Carbon nanotubes (CNTs) are cylinders of graphite sheets which were first discovered by Iijima in the 1990s.[50] CNTs possess unique electrical conductivity, high chemical and thermal stability, high surface area and high mechanical strength. These remarkable properties make them very attractive in a wide range of application areas: nano-electronic devices, fuel cells, biosensor energy storage.[51-54] A tube made of a single graphite layer is called a single-walled nanotube (SWNT); a tube comprised of several, concentrically arranged cylinders is called a multi-walled nanotube (MWNT). The diameter of CNTs varies from several nanometers to hundreds of nanometers. The length is usually in the range of 100 nm to a few millimeters.[55] SWNTs exhibit three structures: armchair, zigzag or chiral nanotubes, as illustrated in Figure 2.11.

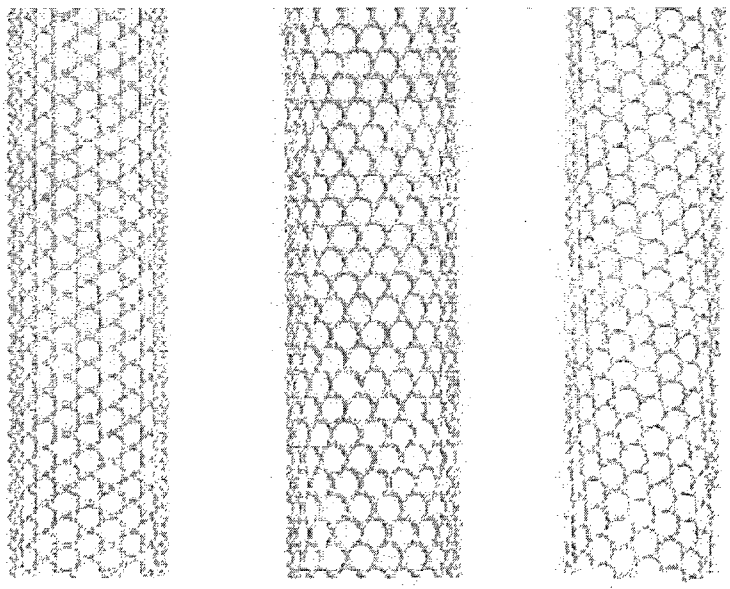

Figure 2.11 Three structures of SWCNT: (a) armchair; (b) zig-zag; (c) chiral.[56]

CNTs with the armchair structure is conducting; CNTs with the other two structures is usually semiconducting. The high electrical conductivity of CNTs comes from the complex both above and below the plane containing the carbon atoms.

The chemical modification and functionalizaiton of CNTs is important because CNTs are hydrophic and tend to aggregate in solvents. Attachment of molecules or functional groups can improve the solubility and dispersion of CNTs. Poly(sodium 4-styrene sulfonate) (PSS),[57] sodium dodecylbenzene sulfate[58] and many proteins[59] have been successfully immobilized on CNTs through non-covalent bonding. Esters,[60] enzymes,[61] and carboxylic acid[62] were functionalized on CNTs by covalent bonding. Preparation of PSS modified CNTs is very simple. CNTs in solution were mixed with PSS solutions, stirred or sonicated for 6 h, then centrifuged and washed with deionized water. After wrapping with PSS, the CNTs showed a negative surface charge and diameter increased to around 30 nm[63] as shown in Figure 2.12 (a). The sulfonyl group ($-SO_3$) on each PSS monomer strongly and uniformly entangled on the side of the CNTs resulting in excellent stability and dispersion.

The modified CNTs can be used to fabricate multilayer thin films through LbL nanoassembly. Positively charged chitosan was alternately assembled with negatively charged β-cyclodextrin modified CNTs on a glass carbon electrode. The resulting films exhibit higher electrocatalytic activity than unmodified CNT multilayer films.[64] β-1,3-glucans was used to functionalize CNTs to prepare cationic and anionic CNTs which were LbL deposited on silica microspheres as shown in Figure 2.12 (b).[65] The silica core can be removed to form hollow capsules composed of CNTs. PDDA modified CNTs and PSS modified CNTs were assembled through electrostatic interaction to make conducting

films. The electrical properties experiment showed that the conduction mechanism of the CNTs-polyelectrolytes films is quantum mechanical tunneling.[66]

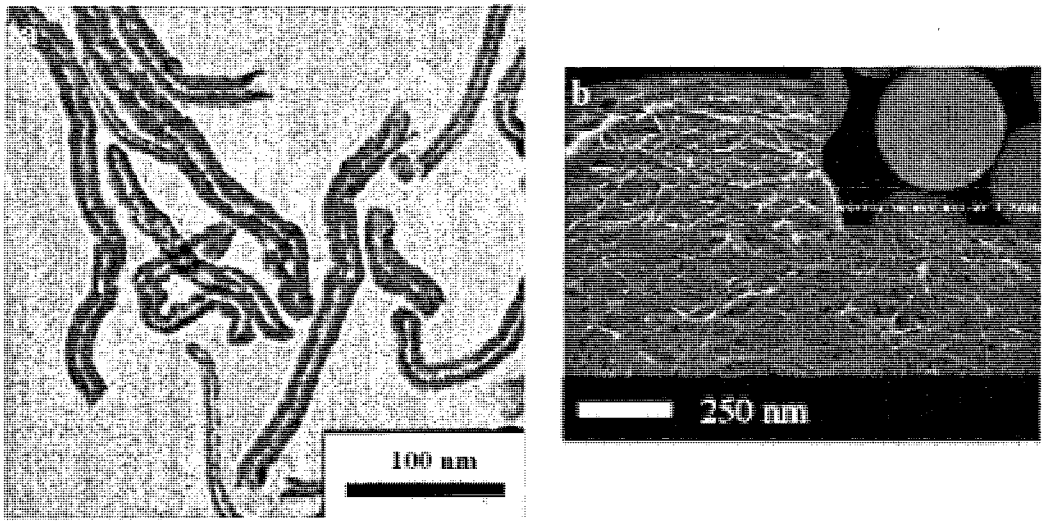

Figure 2.12 (a) TEM image of PSS coated SWCNTs;[63] (b) SEM image of modified SWCNTs coated silica particle.[65]

2.4.2. Conductive Polymer PEDOT-PSS

Recently, there is an increasing interest in the application of conductive polymers in the fabrication of electronic and optical devices. Conductive polymers have considerable advantages over other conductive materials, such as low cost, easy fabrication, more robust than molecular crystals, and soluble in common solvents. The conjugation of Π electrons extending over the length of the polymer backbone is the important conductive mechanism of conductive polymers. The electrical conductivity of conductive polymers varies, the highest conductivity being around 10^7 S/m.[67] Additionally, the conductivity can be tuned by doping with an oxidizing or reducing agent.

"Poly(3,4-ethylenedioxythiophine) (PEDOT) belongs to a novel class of polythiophenes with very high electrochemical stability in oxidized states and a moderate

band-gap with good stability in the doped state".[68] Despite its attractive electrical and optical properties, PEDOT is not soluble in aqueous solution. PEDOT carries positive charges, therefore it can form a complex with negatively charged polyelectrolyte PSS. This complex is called PEDOT-PSS with good chemical stability and high conductivity. The chemical structure of PEDOT-PSS is shown in Figure 2.13.[69] The original PEDOT-PSS conductivity is about 10 S/cm, which can be improved up to 500 S/cm after the doping process.[70] Compared with other conductive polymers, PEDOT-PSS exhibits high conductivity, superior stability, a wide potential window and environment-friendly behavior. PEDOT-PSS has been employed to fabricate antistatic coating for photographic films,[71] conducting layer for field effect transistors,[72] hole injecting layer for polymeric light emitting diodes[73] and sensing films for humidity and gas sensors.[74]

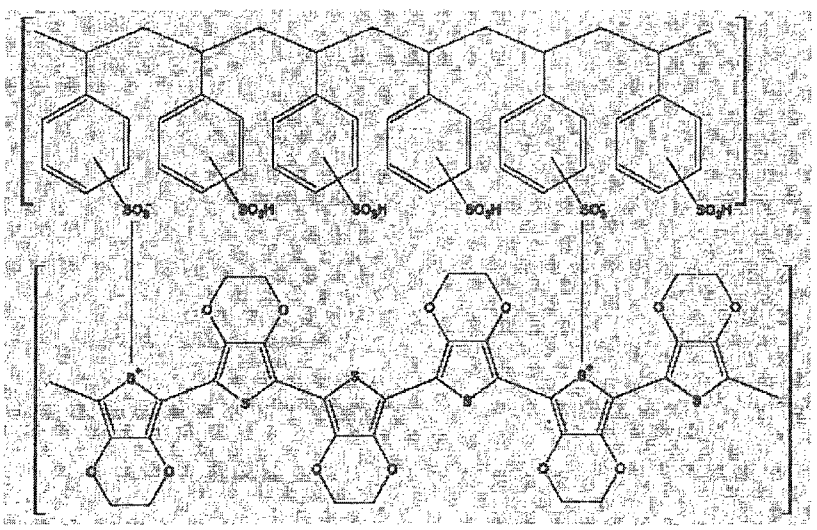

Figure 2.13 PEDOT-PSS chemical structure.[69]

2.5 Three Dimensional Scaffold for Tissue Engineering and Regenerative Medicine

Tissue engineering and regenerative medicine are rapidly developing areas aiming at repairing or replacing lost or damaged tissues by using cells and scaffolds. Three dimensional (3-D) biomaterial scaffold plays a vital role in tissue engineering and regenerative medicine because it better mimics the 3-D environment of living tissues including the different interactions as shown in Figure 2.14. "It refers to the way in which a bulk material is distributed in space from the macro-, micro- to nanoscales (corresponding to tissue, cellular, and molecular scales in a specific tissue, respectively)".[76]

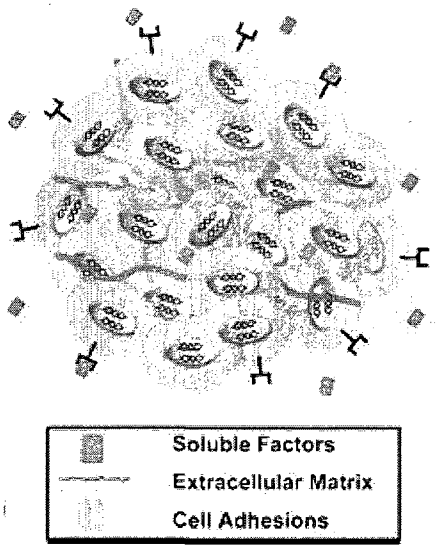

Figure 2.14 Scheme of three-dimensional cell culture, including cell-cell interaction, cell-extracellular matrix interaction and cell-scaffold interaction from a 3-D direction.[75]

Three dimensional scaffolds usually have an open and porous structure which provides space for cell ingress, proliferation and differentiation as well as transport of nutrients. An ideal scaffold also should be biocompatible, biodegradable and exhibiting enough mechanical strength, proper surface topography and chemistry property for cell

adhesion and growth. There is a wide range of synthetic or natural materials which have been investigated as cell culture scaffolds. The current trend is to use natural-origin polymers for tissue engineering scaffolds due to their intrinsic interaction with cells, low cost and availability, biocompatibility and biodegradability. The protein-based natural polymers best mimic many features of the extracellular matrix, which is a 3-D proteinaceous network naturally occurring around cells, and directing and supporting cell growth. Protein-based polymers include collagen, gelatin, elastin and silk firoin. Another type of natural polymer are polysaccharides which are composed of different sugar monomers. These biological polymers include chitosan, alginate, hyaluronan, cellulose and chondroitin sulphate. Compared with protein-based polymers, polysaccharides are less expensive, allow for simpler processing and promise easier control over final product quality and properties.

2.5.1 Gelatin Based 3-D Scaffolds

Gelatin is a protein-based polymer obtained by acid or alkaline processing of collagen. There are two types of gelatin depending on the different process of collagen treatment. An alkaline process yields gelatin with a high density of carboxyl groups by hydrolysis of amid groups of collagen, so the resulting gelatin is negatively charged. An acid process is relatively milder, seldom changing the isoelectrica point of collagen. At elevated temperature, gelatin solution is in the sol state, and gelatin macromolecules exhibit a similar conformation to linear-chain synthetic polymers.[77] At low temperature, the gelatin solution transforms from sol to gel state. It is believed that during the gelation process the concentration of helix fraction is greatly increased, therefore, hydrogen bonds formed both intermolecular and intramolecular connections between neighboring

peptides.[78] This gelation behavior is thermally reversible, while chemical crosslinking is stronger and non-reversible. Various crosslinking agents were used to form gelatin gels: glutaraldehyde, formaldehyde, carbodiimides, and genipin. Carbodiimides, such as 1-Ethyl-3-(3-dimethylaminopropyl)carbodiimide (EDC) can activate carboxylic acid to bind amine groups of lysine. The reaction scheme is demonstrated in Figure 2.15.

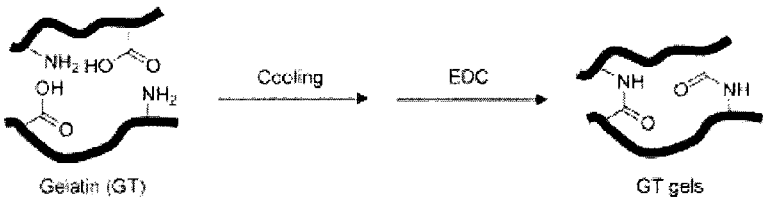

Figure 2.15 Reaction scheme of EDC crosslinking gelatin molecules to form gel.[79]

The phase separation method was employed to form a porous sponge using gelatin gel. First, the gelatin gel was frozen to induce phase separation between solidified gelatin and growing ice crystals. Second, the frozen gel was put into a freeze-dryer for lyopholization. After the sublimation of ice crystals, a porous sponge with interconnected pores was formed, as shown in Figure 2.16.

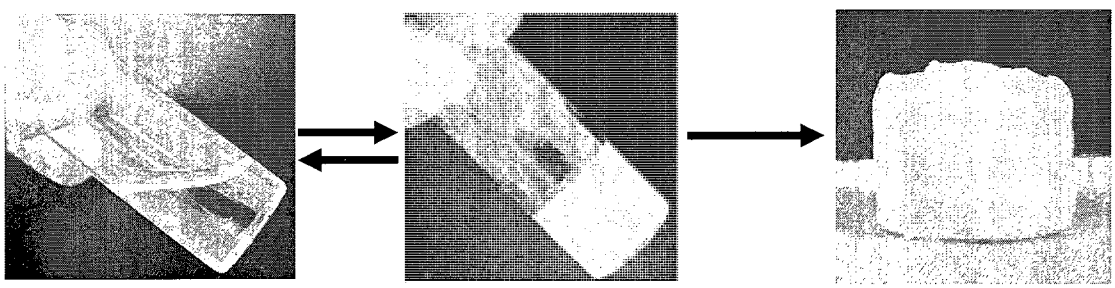

Figure 2.16 The fabrication procedure of gelatin sponge.

Different concentrations of crosslinking reagent results in foams with different pore size. As shown in Figure 2.17, the average pore diameter decreases with higher concentration of EDC.

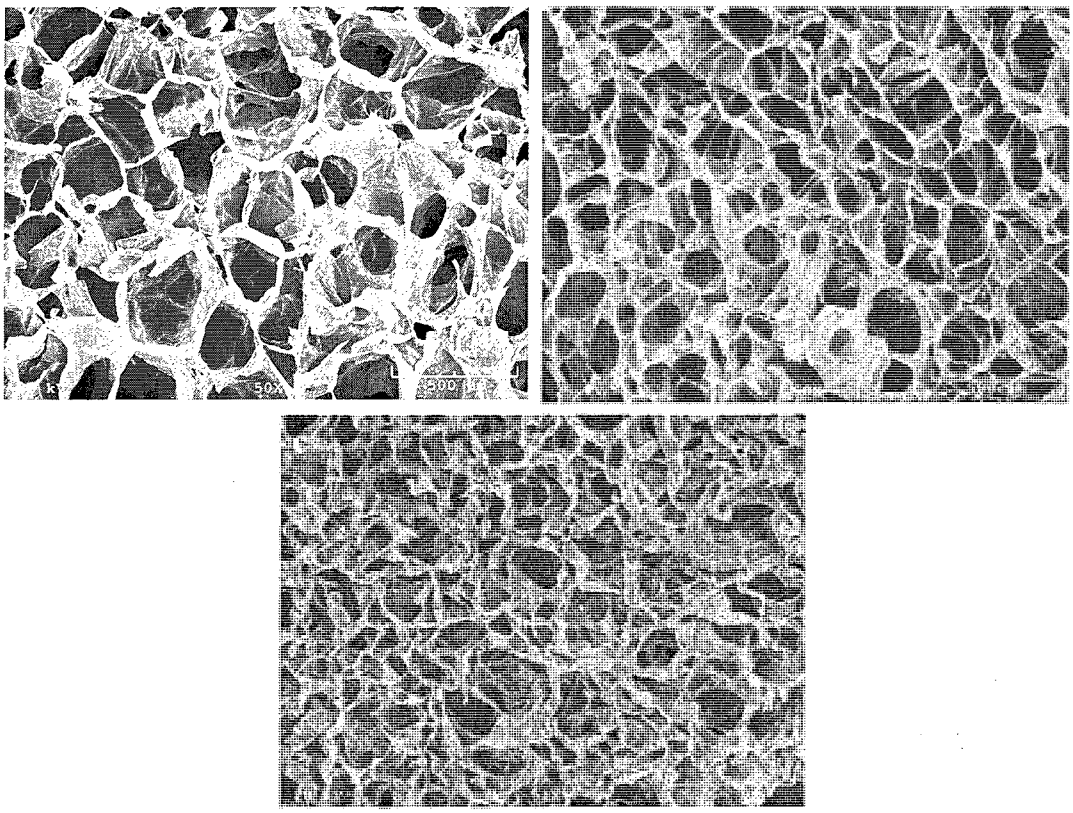

Figure 2.17 SEM images of gelatin foams cross-linked with different concentrations of EDC: (a) 2.5 mM; (b) 5.0 mM; (c) 10 mM.

Gelatin based foams have been widely used in both soft and hard tissue engineering as 3D scaffolds. A series of human cells: endothelial, epithelial, fibroblast, glial and osteoblast cells were seeded into gelatin scaffold. The visualization of calcein-acetoxy methyl ester (CAM)-labeled cells confirmed that cells attached, spread and proliferated on the gelatin scaffolds.[80] Gelatin is usually combined with other materials, such as chitosan, poly(vinyl alcohol), alginate, chondroitin-6-sulphate and hyaluronan to improve

material properties.[81-83] Growth factors, hydroxyapatite and plasmid DNA were incorporated into gelatin gels to enhance cell attachment, migration, proliferation and differentiation.[84,85]

2.5.2 Cellulose Based Scaffolds

Being the most abundant polymer in nature, cellulose is readily available and inexpensive. Due to the presence of hydroxyl groups on the surface, cellulose is easily converted to derivatives through esterification, etherification, and oxidation reactions. These cellulose derivatives, such as cellulose nitrate, cellulose acetate, cellulose xanthate and carboxymethylcellulose are industrially important. The non-toxicity, exceptional strength, low water solubility and hydrophilicity make cellulose suitable for applications in drug delivery and tissue engineering. Table 2.2 presents some examples of cellulose or cellulose fiber based matrices used in tissue engineering. Although there is some research about the application of cellulosic materials in tissue engineering and regenerative medicine, the study related to a 3-D cellulose microfiber based scaffold is rare due to the lack of intrinsic macro-scale 3-D architecture for cell growth.

Table 2.2 Cellulosic materials for tissue engineering application

Cellulosic materials	Tissue engineering (TE) application	Active biomolecule/ modification	Seeded cell type/ implantation	Ref.
Cellulose hollow fibers	Not defined	Fibronectin	Bovine coronary artery smooth muscle cells	86
Cellulose porous scaffold	Cartilage TE	-	Bovine and human chondrocytes	87
Cellulose acetate and regenerated cellulose	Cardiac TE	Fibronectin	Rat cardiac fibroblasts and myocytes	88
Viscose cellulose sponge	Bone TE	-	Implanted in Rat bone marrow cavity	89
Lyocell® cellulose fabric	Cartilage TE	Calcium phosphate	Bovine chondrocytes	90
Methylcellulose	Brain TE	-	Rat astrocytes and neurons	91
Viscose cellulose sponge	Wound healing	Collagen	Subcutaneous implantation	92
Microporous cellulose	Artificial liver TE	Collagen	Rat hepatocytes	93
Co-polymer of cellulose acetate and nitrocellulose	Bone TE	-	Mouse osteoprogenitor cells	94
Regenerated cellulose hollow fiber	Artificial liver TE	-	Rat hepatocytes	95
Cellulose acetate	Not defined	-	Human hematopoietic progenitor cells	96

CHAPTER THREE

CELLULOSE FIBER-ENZYME COMPOSITES

3.1 Introduction

This chapter is based on my contribution to the publication titled "Cellulose fiber-enzyme composites fabricated through layer-by-layer nanoassembly," *Biomacromolecules*, 2007.[97] The LbL technique appeared to be an advantageous method to immobilize bioactive molecules, such as enzymes adsorbed on top or inside LbL polyelectrolyte films, due to the possibility to maintain the structure and functionality of enzymes.[98,99] In addition, compared with other non-covalent binding methods of immobilizing enzyme on cellulose, LbL is more versatile without the assistance of carbohydrate-binding modules or cellulose-binding polysaccharides.[100,101] In this chapter, laccase and urease were immobilized on cellulose fibers through electrostatic LbL nanoassembly to fabricate functional biocomposites. Such enzyme modified composites could be used to decompose urea or lignin, or synthesize inorganic nanoparticles or polyphenols. The enzyme nanocoating on cellulose fibers was systematically analyzed by quartz crystal microbalance (QCM), ζ-potential, and confocal laser scanning microscope. The activity and storage ability of enzymes in these biocomposites were evaluated, and biomineralization application of urease-coated fibers was demonstrated.

3.2 Materials and Methods

All chemicals and enzymes were purchased from Sigma-Aldrich and used without further purification. Poly(dimethyldiallyl ammonium chloride) (PDDA, MW 100k-200k dal), sodium poly(styrene sulfonate) (PSS, MW 70k dal) were used as polycation and polyanion, respectively. Laccase from Trametes versicolor has an activity of 22.6 U/mg, urease type IX from Jack beans has an activity of 65.7 U/mg. Fluorescein isothiocynate (FITC) was used to label the enzyme for confocal imaging. Beaten bleached Kraft softwood fiber sheets, supplied by International Paper Company, were dispersed in water to obtain cellulose fibers.[7]

In order to maximize the enzyme activity, the experiments were performed under optimum pH conditions. Both enzymes are negatively charged under optimum pH conditions, and can be assembled alternately with polycations. For the assembly of laccase, all chemicals were prepared at a concentration of 2 mg/mL in 0.05 M sodium acetate buffer at pH 4.5. Dry fibers (4.5 mg) were dispersed in deionized water. Then a standard LbL assembly procedure[7] was applied with an adsorption time of 10 min for polyelectrolytes and 20 min for the enzyme. After three precursor polyelectrolyte layers, laccase and PDDA were alternately deposited, with the enzyme layer as the outermost layer. For the assembly of urease, all chemicals were prepared at a concentration of 2 mg/mL in 0.02 M Tris-HCl buffer at pH 7.2.

The thickness of the coating was estimated using the Quartz Crystal Microbalance technique (QCM, USI-system, Japan). Multilayer films were deposited on a silver QCM resonator in the same way as was done for coating the fibers. The frequency shift was monitored after each adsorption cycle, and converted to thickness using the Sauerbrey

equation: ΔD (nm) = $-0.017\ \Delta F$ (Hz). The surface potential variation was monitored using a Brookhaven Zeta Plus microelectrophoretic instrument. A scanning electron microscope (AMRAY, model 1830) was used to image the dried cellulose fibers and $CaCO_3$ microparticles. A confocal laser scanning microscope (Leica TCS SP2) was used to analyze the nanocoatings on the cellulose fibers.

The activity of laccase was measured by monitoring the oxidation of ABTS.[102] A 0.01g sample was mixed with 2.9 mL, 0.4 mM ABTS in 0.05 M sodium acetate buffer (pH 4.5). UV absorbance data at 420 nm was continuously recorded for 20 min. For each sample, the same amount of enzyme-coated fibers was added to the test solution. An activity was calculated from the slope of the absorbance curve of each test. Urease activity was measured by a colorimetric assay based on the hydrolysis of urea, as reported in previous work.[103] Briefly, a test solution was made by mixing 25 mM urea, 0.015 mM bromcresol purple, 0.2 mM EDTA and was adjusted to pH 5.8. A 0.01g sample was put into the test solution, and the kinetics was monitored by UV-vis at 588 nm. The slope of the absorbance vs. time curve was used to characterize the urease activity.

After laccase was LbL assembled on the cellulose microfibers, handsheets at 200 $g.m^{-2}$ target basis weight were made according to the Technical Association of Pulp and Paper (TAAPI) T 205T standard using a set-up developed in-house. The scheme of the set-up is shown in Figure 3.1.

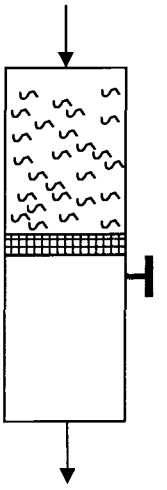

Figure 3.1 The scheme of handsheet-making set-up. The well-mixed solution containing modified cellulose microfibers were poured into the upper column. The valve was immediately opened to filter the water. Fibers were left on the mesh forming handsheet.

3.3 Results and Discussion

3.3.1 Laccase-Fibers Composites

First, the assembly was elaborated on silver QCM resonators in order to determine the optimal conditions for the multilayer growth. After deposition of each layer, the change in frequency was recorded; this corresponded to the amount of mass deposited on the electrode. The assembly results are shown in Figure 3.2. A step-wise growth of laccase/polycation (LAC/PDDA) multilayer on the QCM resonator was observed. The average frequency shift (-ΔF) for the alternate LAC/PDDA adsorption cycle was 253 ± 63 Hz, 276 ± 26 Hz for laccase adsorption and a small negative frequency change for PDDA. This is a typical phenomenon that happens in protein/polyelectrolytes LbL assembly.[26] When PDDA was deposited on top of the protein layer, its flexible linear structure enabled PDDA to penetrate between protein molecules. At the same time, strongly charged PDDA peeled off some of the weakly attached outermost proteins and recharges the surface. The enzyme layer thickness calculated from Sauerbrey equation

was 4.7 ± 0.4 nm. This value is consistent with the molecular dimension of laccase (6.5×5.5×4.5 nm),[104] suggesting a relatively uniform laccase monolayer formation.[97]

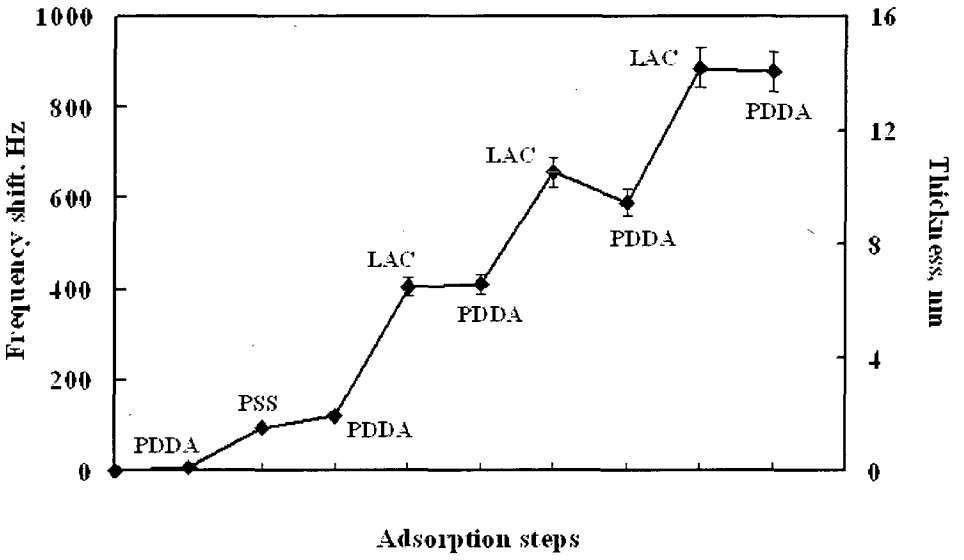

Figure 3.2 QCM monitoring (frequency and thickness change vs. adsorption steps) of laccase (LAC)/PDDA assembly. The first three polyion layers (PDDA/PSS/PDDA) were precursor films.[97]

One of the prerequisites for the sequential deposition of polyelectrolytes and enzymes onto cellulose fibers is charge inversion at every deposition step. Figure 3.3 shows the ζ-potential changes for laccase layers alternated with PDDA during the assembly on cellulose fibers. The cellulose fibers have a negative potential of –43.8 ± 2.5 mV. The first three precursor polyelectrolyte layers provided even coating and showed regular alternation of surface potential with +45 ± 3.7 mV for cationic PDDA and –33 ± 6.2 mV for anionic PSS. The isoelectric point (IP) of laccase from *Trametes versicolor* is around 4.0.[105] The charge of laccase is weakly negatively charged at pH 4.5. Therefore when laccase formed the outermost layer, the surface has a small negative potential, –8.5 ± 1.2 mV. A deposition of the next PDDA layer recharged the surface and restored positive

potential of +52.6 ± 2.1 mV. Then, again –10.2 ± 1.0 mV for laccase and +43.1 ± 1.9 mV for PDDA. For each layer deposited, the underneath layer could have different molecule distribution and conformation, which may have resulted in the slight variations of the measured values.[106] Overall, alternate ζ-potential changes were observed for all laccase/PDDA multilayer films, depending on whether the polyelectrolyte or the enzyme formed the outermost layer. This result proves that the LbL assembly of laccase and PDDA is in organized multilayers.[97]

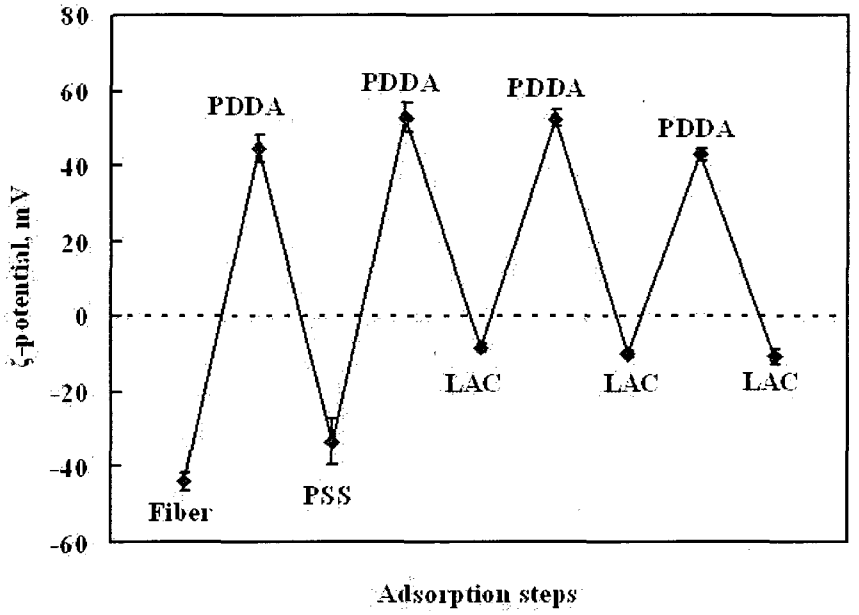

Figure 3.3 ζ-Potential of the coated short cellulose fiber vs. adsorption steps for multilayer film assembly of {PDDA/PSS/(PDDA/laccase)$_3$}. Data are shown as mean ± SD (n=3).[97]

The confocal laser scanning microscope was employed to visualize the location of the laccase multilayer nanocoatings on cellulose fibers. For this purpose, laccase was labeled with FITC (green fluorescence) and assembled with PDDA, as described above. Figure 3.4 demonstrates uniform laccase coatings on the surface of the fibers. Our previous work has shown that only low molecular weight polyelectrolytes may penetrate into the fiber

walls.[7] Due to the resolution limitation of the microscope, it is impossible to accurately estimate how deep the polymer can penetrate. In this work, we deposited precursor PDDA/PSS/PDDA layers before we assembled the enzyme. These polyelectrolytes formed complexes which block the small cell-wall pores-the mean pore width of cell-wall voids around 5 nm.[107] In addition, the test of activity versus enzyme layer showed no difference from the result of enzyme adsorbed on a solid surface.[31] Therefore, it is unlikely that the major part of the enzyme molecules penetrated into the fiber cell-wall, in this case.[97]

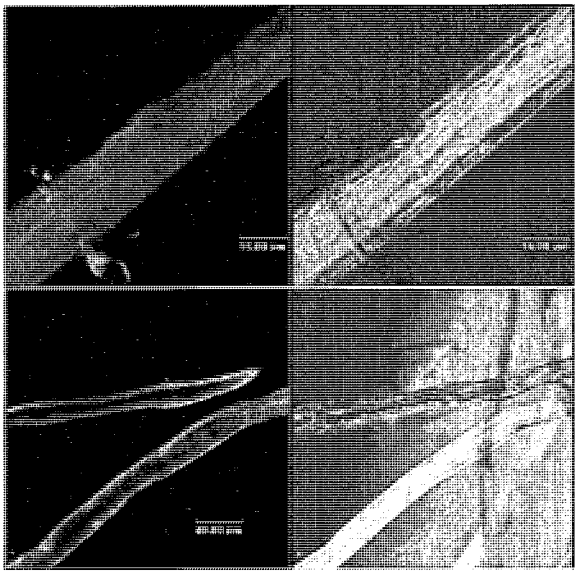

Figure 3.4 Laser scanning confocal microscope images of cellulose fibers coated with three layers of FITC-labeled laccase (green fluorescence) in fluorescent mode and transmission mode.[97]

Figure 3.5 shows the activity for cellulose fibers coated with one to three PDDA/laccase bilayers. As expected, an increase in the enzymatic activity proportional to the enzyme layer number was detected. This demonstrates that the embedded first, second and third enzyme layers remain accessible to the ABTS substrate. A linear

proportionality for the enzyme layers indicates homogeneous laccase adsorption for each layer. It is established that protein / polymer LbL-multilayers are permeable for small molecules and the ABTS substrate rapidly penetrates into the films.[106] There are only three bilayers of PDDA / laccase on cellulose fibers (around 14 nm thickness), so diffusion limitation did not play an important role in the enzyme activity test. Since the reaction is kinetically controlled by the enzyme, the reaction velocity, which represents activity in this case, must have a linear relationship with enzyme concentration (enzyme amount or enzyme layer).[97]

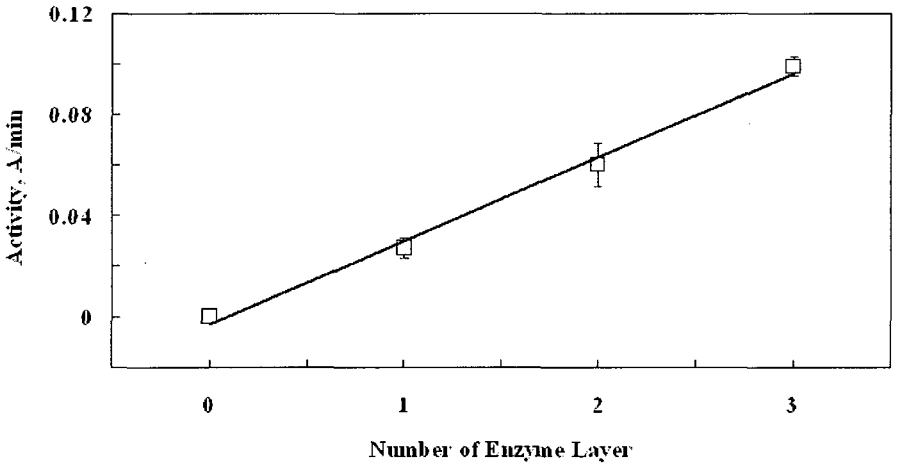

Figure 3.5 Catalytic activity of laccase-fiber biocomposites with one to three (PDDA/laccase) multilayers on cellulose fibers. Data are shown as mean ± SD (n=3).[97]

One of the advantages for assembling enzyme thin films via the LbL method is that the enzymatic activity could be tuned by varying the number of enzyme layers. This has been demonstrated on flat substrates[108,109] and colloid particles.[31,106] Our work shows this tunable feature is also valid on a hollow tubular substrate with a rough surface coated with a three-layer polyelectrolyte precursor.[97]

To determine the stability of laccase immobilized in the biocomposites, samples with architecture of one to three bilayer of PDDA/laccase were stored in deionized water at 4°C for up to 14 days. In all cases, laccase was the outermost layer. Figure 3.6 shows the biocomposite activity changes during the 14 days. All samples have declined enzymatic activities with elapsed time. Especially in the first 7 days, activity decreased about 40% for $(PDDA/laccase)_2$ and $(PDDA/laccase)_3$ biocomposites. The rapid loss of activity could be attributed to the laccase desorption from the outermost enzyme layer or the denaturing of enzymes over time. A similar protein desorption from polyelectrolyte multilayer films assembled on flat substrates or on colloids has also been reported[110] However, from 7 to 14 days, the biocomposites only lost around 10% of its activity, and maintained around 50% of its initial enzymatic activity at day 14. Additionally, there was no significant difference between these two data points. During this period, the activity of the biocomposites had reached a stable stage.[97] A similar enzyme activity decrease has been observed in other LbL enzymatic research. After exponentially losing activity at the initial stage, immobilized enzymes maintained fairly stable activity for more than 30 days.[111] It is possible that the laccase-fiber biocomposites could maintain high activity for months. Laccase is a phenol oxidase that catalyzes the oxidation of various aromatic compounds (particularly phenols, including lignin). It was used to fabricate a biosensor to detect polyphenols in wastewater.[112] In the paper-making process, laccase was studied either as a bio-bleaching catalysis or fiber modification agent.[113,114] The laccase-fiber biocomposites could find possible application in these areas.

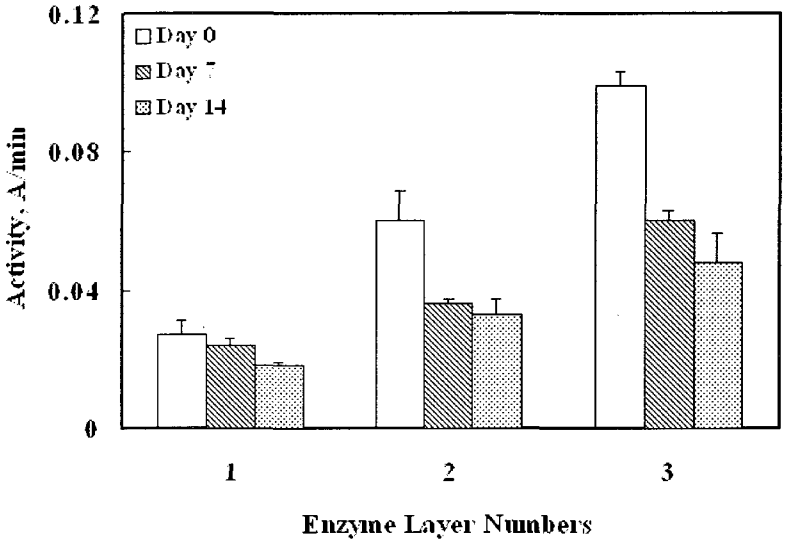

Figure 3.6 The storage ability of enzyme-fiber biocomposites with one to three (PDDA/laccase) layers at 4°C. Data are shown as means ± SD (n=3). For two and three bilayer samples, day 7 and day 14 data points have no significant difference.[97]

The laccase coated cellulose fibers were used to make handsheets for investigation of long-term enzyme activity under dry conditions. The handsheets were stored at 4°C and room temperature separately. As Figure 3.7 shows, the activity of both handsheets gradually decreased. During the first 32 days, there is no significant decrease of activity for handsheets stored at 4°C. On day 45, handsheets stored at 4°C maintained about 72% of its original activity; while handsheets stored at room temperature only maintained about 38% of its original activity. For dry handsheets, the activity decrease was mainly caused by the denaturing of the enzyme.

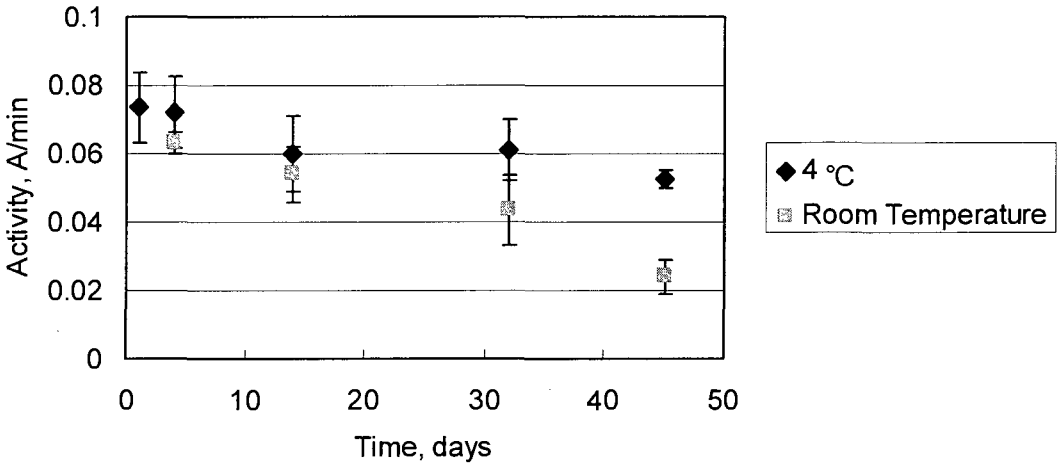

Figure 3.7 Bioactivity of handsheets made with laccase-coated cellulose microfibers stored under different temperature.

3.3.2 Urease-Fiber Composites

Urease was also successfully assembled with PDDA on cellulose fibers. The resulting biocomposites were characterized using the same methods. QCM results indicated a step-by-step urease thin film formation with 6.9 ± 1.4 nm thickness, as shown in Figure 3.8 (a). Figure 3.8 (b) shows the ζ-potential alternating change with the layer number for oppositely charged urease and PDDA. The surface potential of the urease layer decreased from –10 mV to –5 mV, indicating a decrease in surface charge density. Therefore, the subsequent PDDA adsorption became less and the resulting surface potential also decreased from +40 mV to +24 mV.[97]

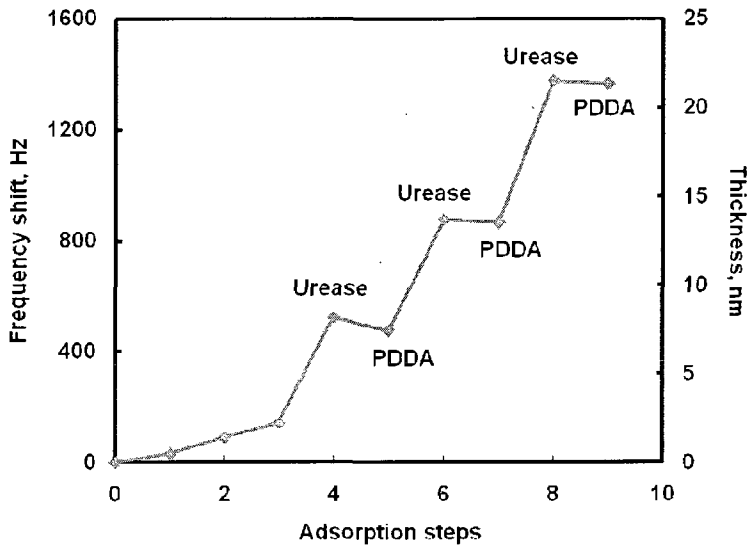

(a)

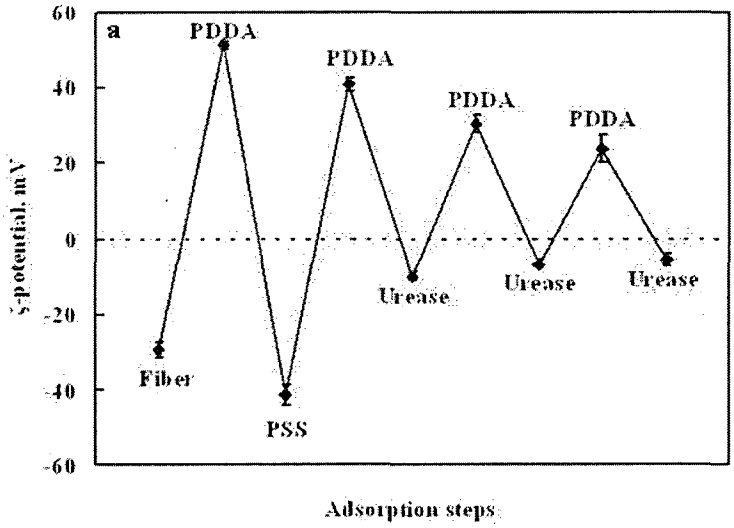

(b)

Figure 3.8 (a) Characterization of PDDA/urease multilayer thin film growth on QCM resonator; (b) ζ-potential during LbL assembly of PDDA and urease on fibers.[97]

Obviously, the urease/PDDA layers assembled on fibers showed an increase in activity with layer number, as revealed by Figure 3.9 (a). The original activity is normalized as 100%. After 7 days storage at 4°C, the biocomposites activity also decreased around 50% and continued decreasing. It was reported that enzymes embedded

in multilayer polyelectrolyte films prevent desorption.[115] We also found that with two bilayers of PDDA/PSS on top of the outermost urease layer, the biocomposites could retained 70% activity after 7 day, as shown in Figure 3.9 (b). However, the coverage of polyelectrolyte on adsorbed enzyme layer reduced its bioactivity; the initial activity decreased by about 40%. The polyeletrolyte layer cover possibly stabilizes the electrostatic and steric interaction between molecules in LbL films.

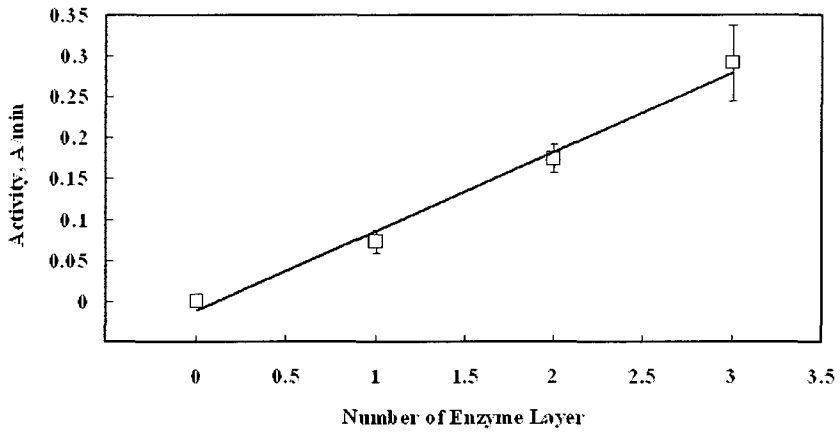

(a)

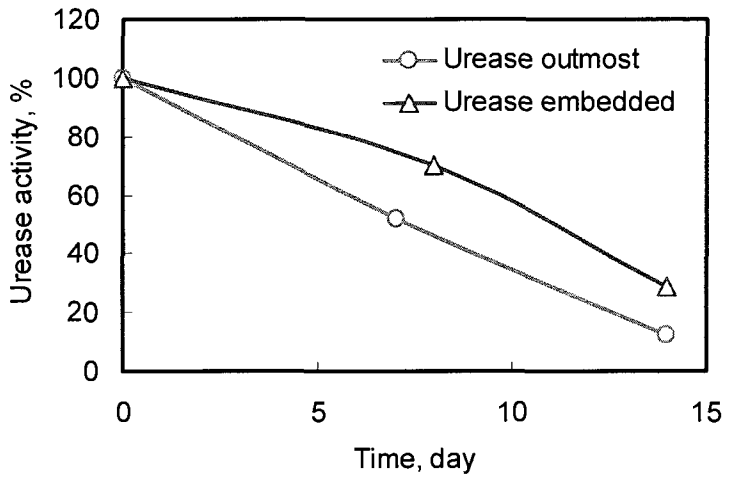

(b)

Figure 3.9 (a) Enzymatic activity for one to three (PDDA/urease) multilayers on cellulose fibers; (b) fraction of enzyme activity in the case of urease as outmost layer or urease topped with $(PDDA/PSS)_2$.

Urease has been widely used as catalysis for a biomineralization reaction. Biomimetic synthesis of inorganic composites is a developing research area lying at the nexus of chemistry, biology, medicine, and materials science. Moreover, biomineralization is one of the most promising methods to form hybrid inorganic/organic nanomaterials, which often display unique and desirable morphological, structural, and mechanic properties and represent informative models for the design of complex functional structures.[116] This process usually occurs at room temperature and mild conditions and requires the presence of organic nano-templates like Langmuir monolayers, self-assembled monolayers, micelles, and emulsions.[117]

We demonstrated the application of urease-fiber biocomposites in biomineralization to produce hybrid inorganic/organic composites. Urease-fiber biocomposites were introduced into a mixture of 0.5 M urea and 1 M $CaCl_2$ for 10 min. Then the biocomposites were washed in deionized water three times. The formation of $CaCO_3$ precipitates starts immediately after urea decomposition into ammonia and CO_3^{2-} catalyzed by urease in the LbL multilayer. Urea decomposition and CO_3^{2-} formation occur on the fiber surface, whereas calcium cations diffuse from the surrounding solution. According to previous work,[118] to prevent the undesirable formation of $CaCO_3$ in bulk solution, a higher concentration of Ca^{2+} is required, so that it consumes all CO_3^{2-} produced in the vicinity of the surface. Using a Ca^{2+} concentration below 0.1 M leads to the formation of $CaCO_3$ particles in the solution.[97]

Before initiation of calcium carbonate microparticle formation, urease-coated fibers looked similar to the uncoated fibers (no particles were detected). The surface was rough and cell wall openings were still visible (Figure 3.10 (a)). After reaction with urea and

$CaCl_2$, calcium carbonate microparticles were formed on the surface of the cellulose fibers, as shown in Figure 3.10 (c). Most of these particles have a spherical shape with diameter of 1-7 μm (Figure 3.10 (d)). Formation of such a composite may be useful for the paper making industry where $CaCO_3$ microparticle loading is an important technique to improve paper brightness.[119] A negative control proved that the addition of Ca^{2+} to polyelectrolyte coated fibers would not cause reconstruction of films without biocatalysis (Figure 3.10 (b)).[97]

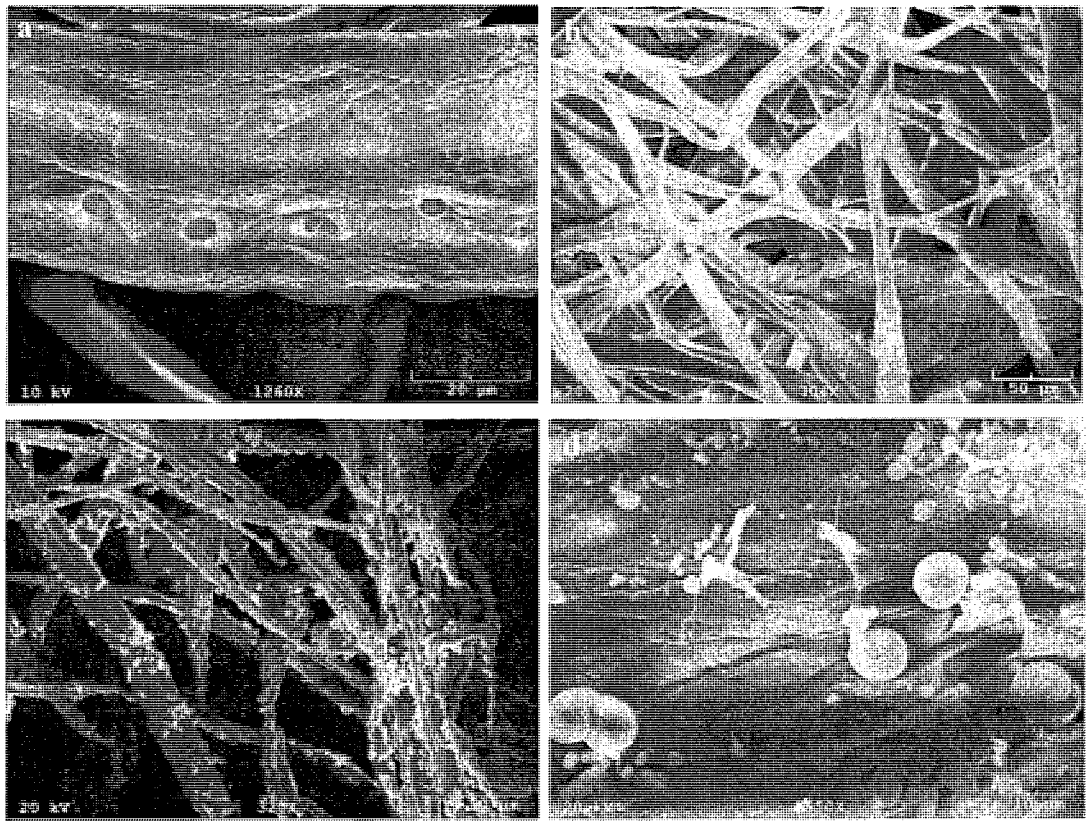

Figure 3.10 SEM images of enzyme-fiber biocomposites. (a) biocomposites with three (PDDA/urease) layers; (b) negative control: fibers with $(PDDA/PSS)_3$ coating reacted with Ca^{2+} - no microparticles formation observed; (c) and (d) composites after biocatalytic $CaCO_3$ microparticle formation.[97]

3.4 Conclusions

The possibility of employing cellulose microfibers as a support to fabricate bioactive composites with organized enzyme multilayers was demonstrated. Through LbL nanoassembly, laccase and urease were sequentially deposited with polycations which acted as electrostatic glue between proteins. The biocomposites were enzymatically active, and this activity could be tuned by varying the number of enzyme layers in the coating. For laccase-fiber composites, around 50% of its initial enzyme activity was preserved after 14 days of storage in water. Handsheets made with laccase-fiber composites could maintain more than 70% of initial enzymatic activity after 45 days under 4°C. Urease-fiber composites were successfully applied for biomineralization to grow the calcium carbonate microparticles needed for paper whitening. The strategy presented could be used for creation of cellulose fiber based biocomposites with various functions which can be precisely controlled by film nano-architecture.[97]

CHAPTER FOUR

CONDUCTIVE CELLULOSE MICROFIBERS AND BULK PAPER COATED WITH CONDUCTIVE NANOCOMPOSITE

4.1 Introduction

This chapter is based on my contribution to the publication titled "Conductive paper from lignocellulose wood microfibers coated with nanocomposite of carbon nanotubes and conductive polymers," *Nanotechnology*, 2009.[120] The development of smart paper technology is a means of enhancing the properties of traditional paper.[121-123] The paper made with LbL modified wood microfibers (depending on the layers), can have unique abilities such as magnetic, electrical, optical, mechanical, biological, chemical, or a combination of these. These diverse assortments of properties allow for numerous applications within different industries. For example, smart paper technology could be incorporated commercially for Radio Frequency Identification Tags (RFID) that are integrated into the paper, ultrathin circuitry, displays, chemical monitoring, deterring confidential and self-destructing documents. Recently the first examples of RFID devices made by LbL of carbon nanotubes (CNTs) have been demonstrated.[124] In this chapter, substantial increase in the electrical conductivity of paper using a LbL assembly of carbon nanotubes and polyelectrolytes in organized multilayers on cellulose

wood microfibers has been demonstrated. We have used an aqueous dispersion of poly(3,4-ethylenedioxythiophene) - poly(styrenesulfonate) (PEDOT-PSS) conducting polymer and carbon nanotubes as our anionic polyelectrolytes, and poly(ethyleneimine) (PEI) as our primary cationic polyelectrolyte. By creating alternating layers of oppositely charged components on the surface of wood microfibers, we have produced a nanocoating of 20-150 nm thickness that enables the microfibers to exhibit electrical conductivity. To further enhance the conductivity, at the second stage, carbon nanotubes were sandwiched with conductive polyelectrolytes in a nano-organized multilayer coating on the wood microfibers. Subsequently, we have used these modified wood microfibers for the production of paper handsheets that have a measurable and controlled electrical conductivity. The content of carbon nanotubes in the final conductive paper or fabric was within 0.2 wt%; therefore, the price of the resulted nanocomposite paper was not essentially increased, as compared to that of traditional paper, while paving the road to the new generation of paper materials and smart electronic paper.[120] Moreover, the same LbL modification is also applicable for coating cotton microfibers to fabricate electrically active fabrics for bio-monitoring and as a fairly universal protein sensor.[125]

4.2 Materials and Methods

4.2.1 Cellulose Fibers and Polyelectrolytes

The commercial pulp used in the experiments was beaten bleached Kraft softwood microfibers (less than 1% lignin and 99% cellulose), press-dried, and shipped in bundles of 17" x 14" sheets, supplied by International Paper Company, Bastrop, Louisiana. These hollow microfibers are of 2-3 mm in length and 20-50 μm in diameter. PEDOT-PSS

(Baytron P HC V4) was purchased from H.C. Starck Inc. PEI (MW 70,000) was purchased from Sigma Aldrich. In order to get the respective concentrations, both PEDOT-PSS and PEI were diluted in DI water with pH 6.5.

4.2.2 PSS-Modified SWCNT Solution

Preparation of PSS modified SWCNT dispersions was done by following the methods of O'Connel, et al.[126] In this method, purified HiPco SWCNTs (Carbon Nanotechologies Inc.) were dispersed in 0.2 wt% poly(sodium-4-styrene sulfonate) (PSS; Mw 1,000,000, Sigma-Aldrich) solution with a mild sonication in a VWR Model 150HT ultrasonic cleaner. The SWCNTs dispersion was poised at room temperature for more than a week and was centrifuged at 5000 rpm for several minutes. The supernatant was then collected to be used for further LbL coating on wood microfibers using different concentrations in DI water. Hereafter, we will call such modified CNT as CNT-PSS. Generally, uniform dispersion of SWCNTs provides a larger number of charge transport routes in a polymeric composite, such that a much lower percolation threshold for electrical conductance is observed. Thus, in LbL systems, direct adsorption of SWCNTs from a solution allows not only uniform dispersion in a solid state, but also macro-scale measurable electrical charge conductance. The characterization of uniform dispersion can be performed by UV-vis absorption measurements. Only in well dispersed composites, can van-Hove-singularity peaks of SWCNTs be observed. Detailed studies of the mathematical correlation of SWCNT dispersion and electrical conductivities are given in previous publication.[127]

4.2.3 Nanocoating Procedure

Experiments were done using aqueous solutions of different concentrations of CNT-PSS (5 μg/ml, 10 μg/ml, and 25 μg/ml), poly (3, 4- ethylenedioxythiophene) - poly(styrenesulfonate) (PEDOT-PSS) (3 mg/ml), and poly(ethyleneimine) PEI (3 mg/ml) for LbL assembly on wood microfibers. The conducting PEDOT-PSS polymer, CNT-PSS and wood microfibers were measured to be negatively charged at pH 6.5 and were used as anionic components. The detailed LbL nanoassembly procedure was described in Chapter Two. Briefly, after four precursor layers of PEI/PSS, CNT-PSS was deposited alternately with PEI with CNT-PSS as the outmost layer. The combination of PEDOT-PSS and CNT-PSS multilayer architecture was assembled in the following sequence: $(PEI/PEDOT\text{-}PSS\ /PEI/CNT\text{-}PSS)_2$ or $(PEI/CNT\text{-}PSS/PEI/PEDOT\text{-}PSS)_2$.

4.2.4 Nanocoating Characterization

The surface charge of all the polyelectrolytes was measured using a Brookhaven Zeta Plus microelectrophoretic instrument (zeta-potential). Thicknesses of the LbL assembled films using 5, 10 and 25 μg/ml of CNT-PSS solutions, 3 mg/ml of PEDOT-PSS, and the composite of CNT-PSS (25 μg/ml)/PEDOT-PSS (3 mg/ml) were estimated from the parallel experiment on assembly of similar architecture multilayers on silver electrode resonators used with the quartz crystal microbalance (QCM, 9 MHz, USI-System, Japan). Field emission scanning electron microscopy was used to image dried cellulose fibers coated with conductive composite or handsheets made with conductive fibers.

4.2.5 Paper Handsheets Preparation

After LbL assembly of the CNT-PSS, PEDOT– PSS and polyelectrolytes on wood microfibers, hand sheets at 200 $g \cdot m^{-2}$ target basis weight were made according to the

Technical Association of Pulp and Paper (TAAPI) T 205Tstandard using a set-up developed in-house at Louisiana Tech University. The schematic set-up was shown in Figure 3.1.

4.2.6 Electrical Properties Characterization

Current (I) – Voltage (V) characterization of single coated microfibers and bulk conductive paper (both were dried) was done using a Keithley electrical microprobe station system. The conductivity is the reciprocal of resistivity. Equation (4.1) was used to calculate resistivity:

$$\sigma = \frac{1}{\rho} = \frac{I}{V} \times \frac{L}{A} , \tag{4.1}$$

where, σ is the conductivity; ρ is the resistivity; I is the current; V is the voltage; L is the length of measured fiber; A is the cross-section area of fiber.

4.3 Results and Discussion

4.3.1 CNT-PSS and PEDOT-PSS Nanocoating on Fibers

First, Figure 4.1 shows scanning electron microscope (SEM) images of uncoated and coated softwood cellulose microfibers. Uncoated microfibers have a smoother surface as compared with CNT-PSS coated microfibers. Carbon nanotubes are very visible in the coating and are randomly dispersed on the entire microfiber surface. These nanotubes interconnect with each other to form a dense network allowing current transfer along the surface. The only unclear aspect of this architecture is the fact that nanotubes are connected through thin PEI films. For this reason, in our approach we used conductive polymer PEDOT-PSS to facilitate the conductive connections between CNT-PSS.[120] In

the case of CNT-PSS/PEDOT-PSS composite, there are more polymer clusters (PEDOT-PSS) mixed with nanotubes (CNT-PSS) (Figure 4.1 (c)). Overall the distribution of CNT-PSS is similar to that obtained previously for cotton threads.[125]

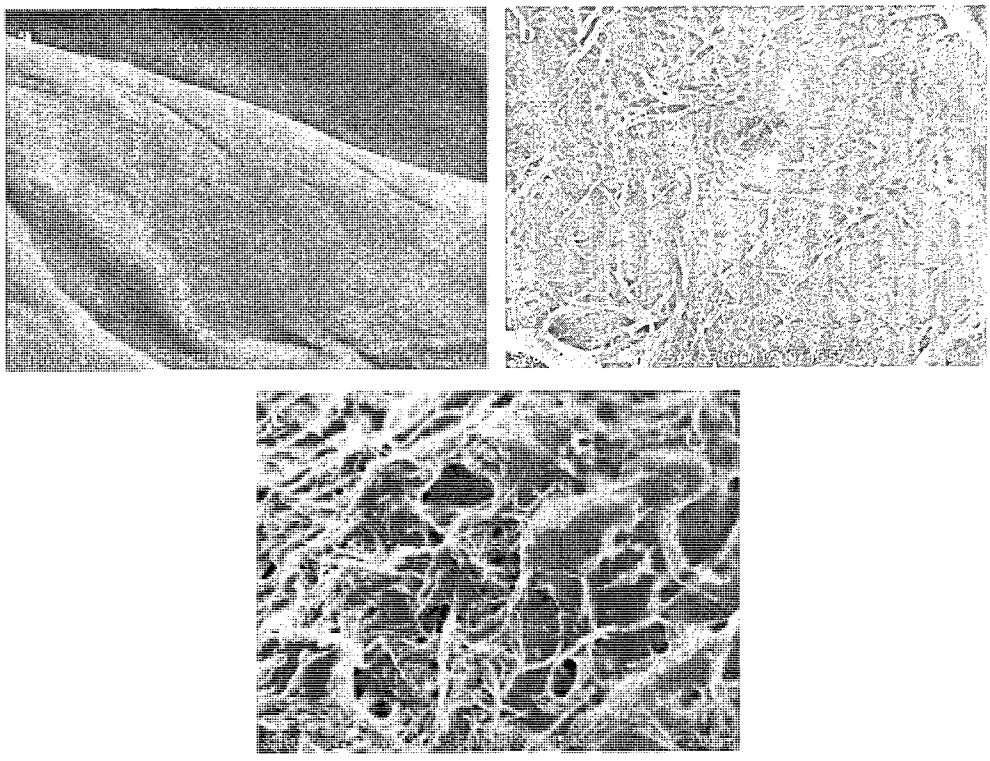

Figure 4.1 SEM images of the wood microfiber surface: (a) uncoated; (b) coated with $(CNT\text{-}PSS/PEI)_4$; (c) coated with composite film of $(CNT\text{-}PSS/PEI/PEDOT\text{-}PSS/PEI)_2$. Bar = 2.00 μm.[120]

Second, the LbL assembly of CNT-PSS and polyelectrolytes on the cellulose fiber surface was demonstrated by surface charge alternation. Initially, the microfibers were coated with two precursor bilayers of PEI/PSS to initiate the LbL process and ensure uniform coverage of the substrate. Then alternating positive/negative layers of PEDOT-PSS/PEI or CNT-PSS/PEI were deposited on the surface of wood microfibers using a centrifugation method. The zeta-potential of the wood microfibers coated with CNT-PSS

and composites of CNT-PSS/PEI-PEDOT-PSS/PEI using LbL nanoassembly is shown in Figure 4.2 (a) and (b), respectively. The charge alternation after each layer confirms that the LbL technique works on the wood microfiber substrate, and alternate layers of polyelectrolytes with anionic CNT-PSS/ PEDOT-PSS and cationic PEI can be coated on its surface. Positively charged PEI in this multilayer serves as electrostatic glue by keeping negatively charged CNT-PSS and PEDOT-PSS together.[120]

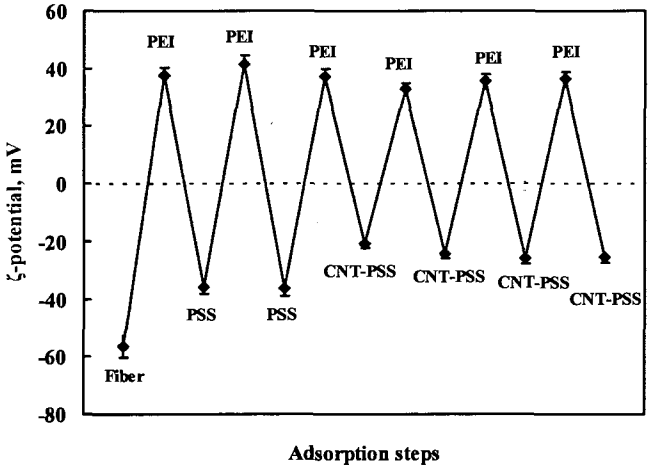

(a)

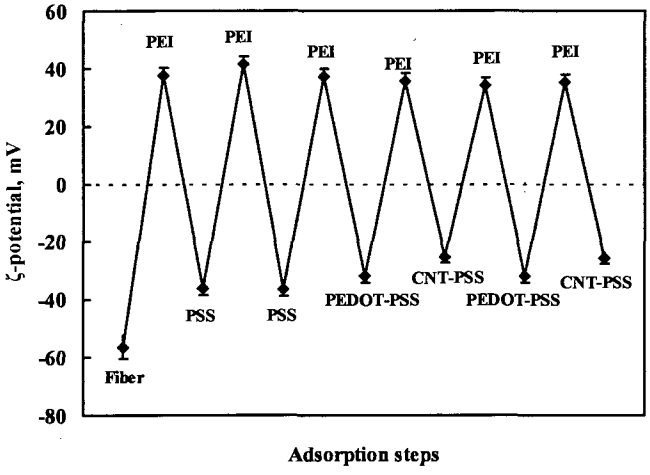

(b)

Figure 4.2 Surface potential of the layers coated using LbL technique on wood microfibers. (a) Carbon nanotubes CNT-PSS alternated with PEI, beginning from the third cycle after precursor layer; (b) Composite of carbon nanotubes, PEI, and PEDOT-PSS.[120]

Third, the amount of deposited nanotubes and polymers was estimated on a QCM resonator. The given results in Figure 4.3 demonstrate a stable growth of CNT-PSS and PEDOT-PSS polymer films during LbL assembly. From Figure 4.3(a), it could be noted that the resulting thickness of CNT-PSS and PEI films increased as the concentration of CNT-PSS solution used for LbL increased.[120]

It was also noted that it is not possible to grow a thin film of CNT-PSS (from LbL process) on a QCM resonator using 5 μg/ml CNT-PSS solution, as discussed below. However, using the same concentration, the film could be deposited on wood microfibers and shows moderate conductivity, probably owing to the rough surface of microfibers. In LbL electrostatic assembly, in order to reverse surface charge during linear polyion adsorption, one needs a concentration greater than 10^{-5} M.[128] Similarly, the LbL assembly of CNT-PSS also needs a concentration higher than the critical concentration, which also depends on the substrate, polycation and so on. On the QCM, 5 μg/ml CNT-PSS is too low to make surface charge reversion, therefore the buildup of the electrostatic by glued thin film is not possible; however, on the rough surface of a cellulose fiber, the conformation of the deposited PEI chain is different, which results in a different adsorption behavior of CNT-PSS. On the other hand, using UV–vis analysis, it was observed that approximately 550 mg of PEDOT–PSS per gram of wood microfibers is consumed after three bilayers have been coated, which is approximately twice as much as the amount measured by the QCM. Better PEDOT–PSS/PEI or CNT-PSS/PEI or a composite of both depositions on the microfibers may be explained by the rough surface of the microfibers as compared with the QCM electrode.[120]

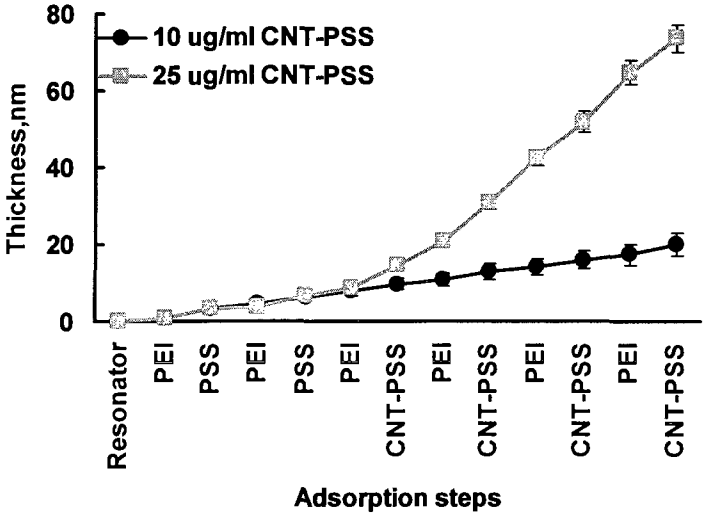

(a)

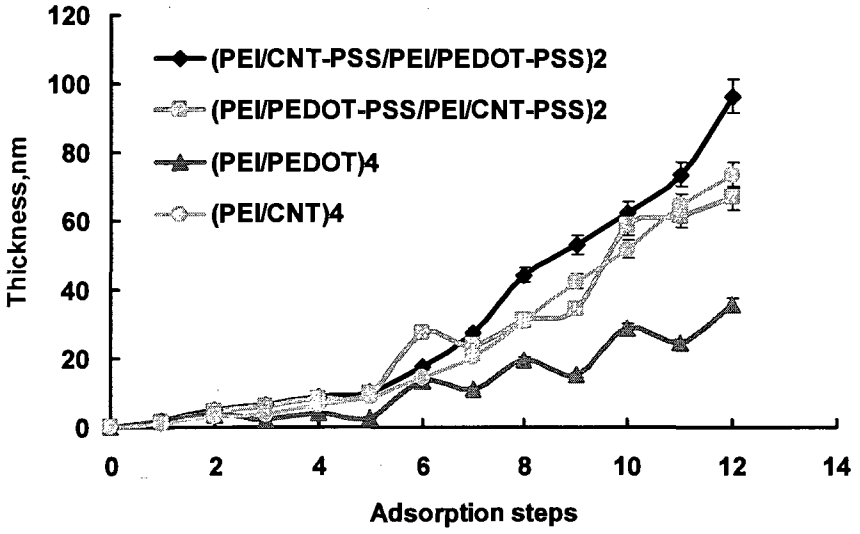

(b)

Figure 4.3 Thickness of the different multilayers prepared with the LbL technique on a QCM resonator by alternating cationic PEI with (a) different concentration of CNT-PSS; (b) different combination of CNT-PSS and PEDOT-PSS.[120]

An interesting phenomenon was observed in the QCM measurement related to PEDOT-PSS/CNT-PSS interaction, which was shown in Figure 4.3 (b). During the PEDOT-PSS/PEI assembly process, PEI always peeled off some molecules from the previous PEDOT-PSS layer due to the strong interaction with PEI in the solution. This

phenomenon is similar to what we observed for the enzyme LbL assembly. Despite the removal of PEDOT-PSS by PEI, there is still 50-80% PEDOT-PSS deposited on the surface. During the combination of PEDOT-PSS with CNT-PSS LbL assembly, PEDOT-PSS was not removed when it is deposited after CNT-PSS. The film growth is continuous. The observation indicated there is strong interaction between PEDOT-PSS and CNT-PSS, which has been reported earlier.[120] Zhang, et. al synthesized PEDOT/PSS modified CNT nanocomposites via *in situ* polymerization. PSS was used to solubilize and disperse CNT as well as tether the PEDOT monomer onto the surface of CNT.[63]

4.3.2 Electrical Characterization of Fiber

Figure 4.4 shows the I-V characteristics of the coated wood microfiber after each bilayer of PEI and CNT-PSS using a 25 μg/ml solution. It can be observed that after each bilayer, the slope of the I-V curve increases, indicating a decrease in the resistance of the coated wood microfiber. This shows that the conductivity of the coated microfiber increases with increasing layers of CNT-PSS even in the absence of PEDOT-PSS in the composite. It is interesting that the curve's increment (representing conductivity) increases proportionally to the number of layers in the coating proving the proposed multilayer architecture. However, there was some inconsistency in the results obtained from fiber to fiber, where the measurement differed approximately in the range of 10%. This discrepancy could be attributed to a physical change in the shape and size of the fibers.[120]

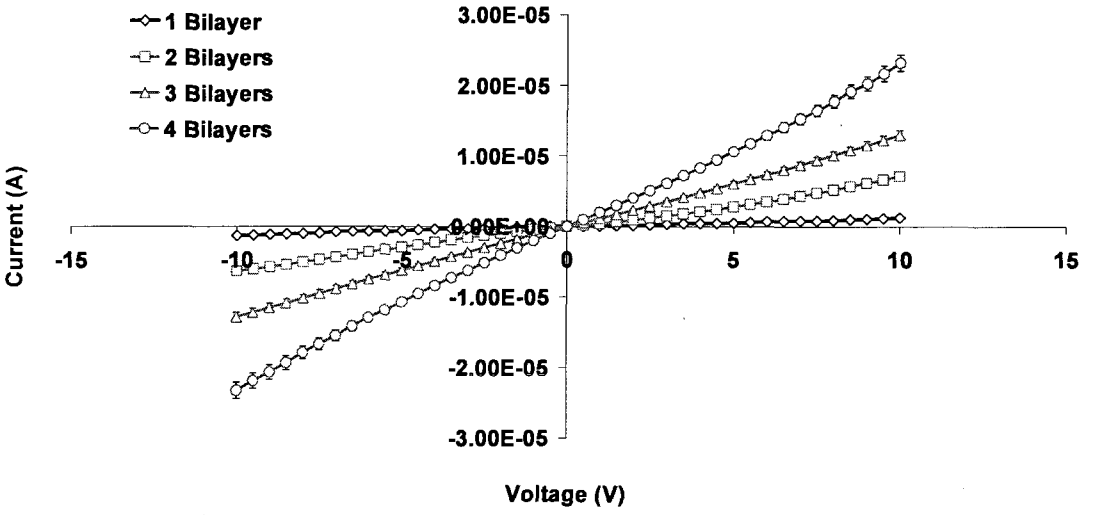

Figure 4.4 I-V characteristics of the wood microfiber coated with different bilayers of carbon nanotubes at 25 μg/ml solution.[120]

Figure 4.5 shows the I-V characteristics for microfibers coated with 4-bilayers of CNT-PSS / PEI using different solution concentrations, and the composite layer of PEDOT-PSS /PEI / CNT-PSS / PEI. Importantly, all the curves almost perfectly agree with Ohm's Law. As the concentration of the CNT-PSS solution increases, the slope of the I-V curve increases, indicating a decrease in resistance. The resistance of the coated wood microfiber decreases with an increase in the concentration of the carbon nanotube solution. A sandwich of a PEDOT-PSS layer in between a CNT-PSS layer enhances the electrical characteristics (reduced resistance) of the coated microfiber, as shown by the steepest plot. The combination assembly of PEDOT-PSS/CNT-PSS has a similar thickness (around 70 nm) to the multilayer architecture of CNT-PSS; however, the conductivity of PEDOT-PSS/CNT-PSS modified cellulose fiber is much higher than the CNT-PSS modified fiber. This is probably due to the electrical path provided by PEDOT-PSS to carbon nanotubes forming a continuous conductive network on the microfiber

surface. PEDOT has been employed to fabricate nanocomposite with CNT, which showed enhanced optical properties and electrical conductivity.[129]

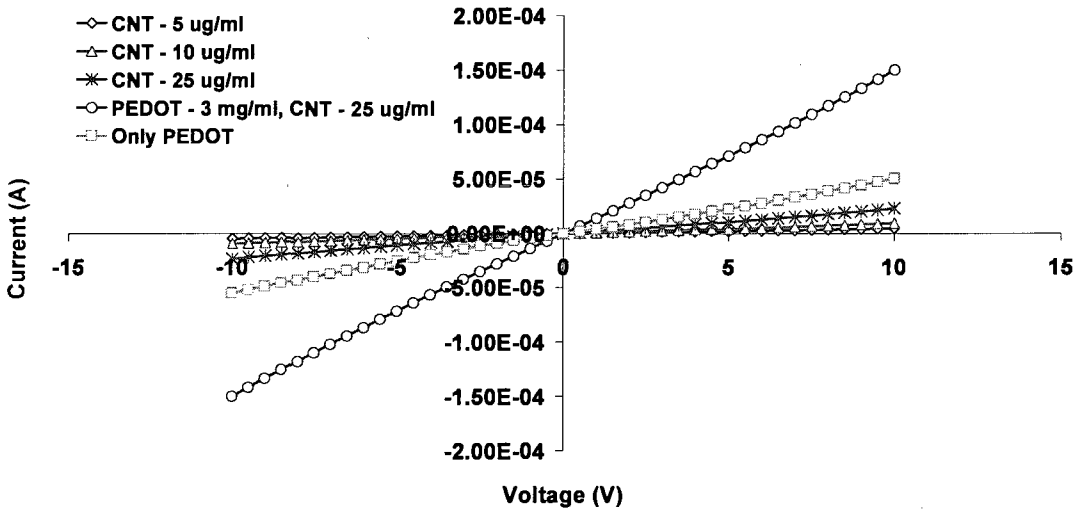

Figure 4.5 I-V data from microfibers coated with 4-bilayers of CNT-PSS/PEI of different concentration, composite of PEDOT-PSS/PEI/CNT-PSS/PEI, and only PEDOT-PSS/PEI. In all cases total number of bilayers was the same.[120]

Figure 4.6 shows the conductivity versus the number of bilayers of wood microfibers coated with CNT using 5, 10, and 25 μg/ml concentration solutions, and a multilayer composite of PEDOT-PSS and CNT-PSS. Conductivity was calculated based on an assumption of the LbL layer thickness are taken from UV-vis analysis. In the case of microfibers coated with PEDOT-PSS using 3 mg/ml concentration solution, the measured conductivity was found to be in the 10^{-2} to 10 $S.cm^{-1}$ range.[12] Comparable conductivity can be achieved when microfibers are coated with CNT-PSS using only a few μg/ml concentration solution, about one thousand times less than PEDOT-PSS. The reason might be that high electron mobility and electrical conductivity along the carbon nanotubes provides more efficient electron transfer. The composite (PEDOT-PSS/PEI & CNT-PSS /PEI)$_2$ multilayer gave the highest conductivity of 20 $S.cm^{-1}$.[120]

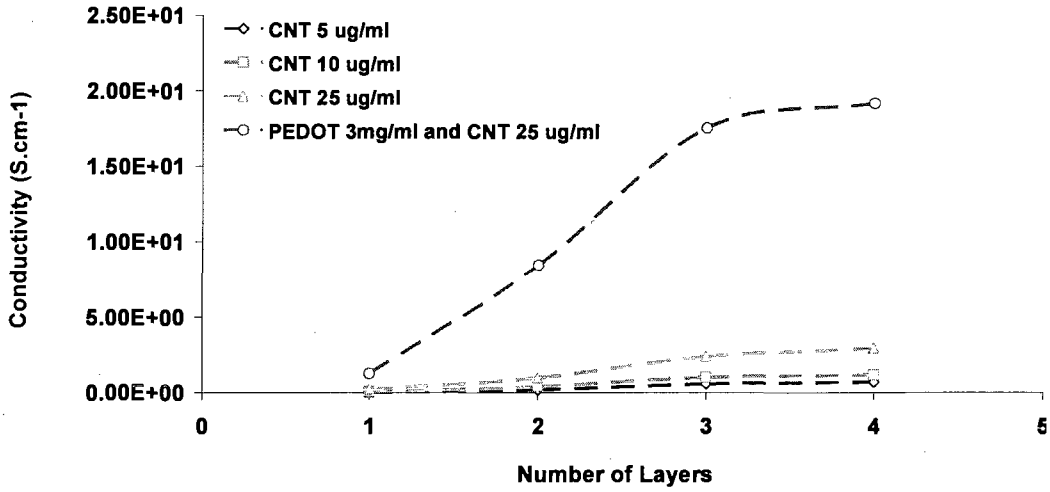

Figure 4.6 Conductivity of wood microfibers coated with 4-bilayers of carbon nanotubes of different concentration in alternation with PEI, and composite of (PEDOT-PSS /PEI & CNT-PSS / PEI)$_2$.[120]

4.3.3 Bulk Conductive Paper

The photographic image of a handsheet made using different proportions of virgin uncoated wood microfibers mixed with fibers coated with a composite of (PEDOT-PSS /PEI / CNT-PSS / PEI)$_2$ is shown in Figure 4.7.

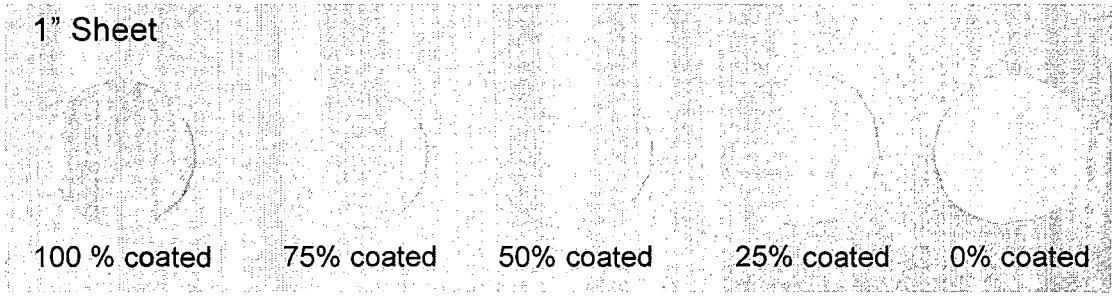

Figure 4.7 Photographic images of the full handsheets made with mixture of wood microfibers coated with composite of (PEDOT-PSS /PEI & CNT-PSS / PEI)$_2$ (100, 75, 50 and 25%), and uncoated wood microfibers (0, 25, 50, 75 and 100 %).[120]

The SEM images of a handsheet are shown in Figure 4.8. The magnified picture showed that the surface of the fibers in the handsheet has random oriented networks of

CNTs. Compared with CNT-PSS coated fibers before making handsheets, the nanotubes seems to be crushed into polymer thin films. Individual nanotubes are not easily recognizable. The handsheet making process pressed the fibers really hard resulting in the deformed network of CNTs.

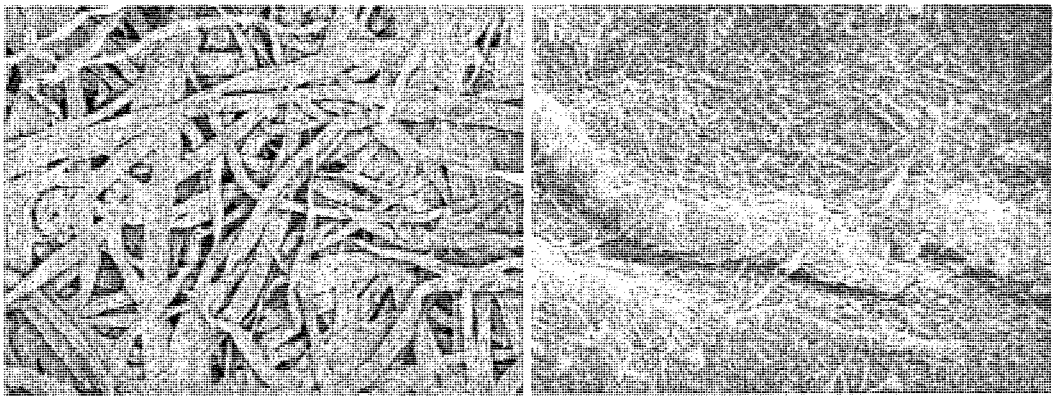

Figure 4.8 SEM images of handsheets made with 100% coated conductive composite of $(PEDOT\text{-}PSS/PEI\&CNT\text{-}PSS/PEI)_2$ (a). low magnification; (b) high magnification.

The electrical characteristics (I-V) of the bulk paper samples are shown in Figure 4.9. The I-V measurements on paper strips were done using an electrode distance of 1 cm. Handsheets made of 100% LbL coated microfiber have the lowest resistance as compared to handsheets made of 25%, 50%, and 75% coated microfibers in a mixture with virgin wood cellulose microfibers. Paper from virgin uncoated fibers was used as the control, which has zero conductivity. This is due to the connections between each fiber and the direct path for the current to flow in the 100% coated fiber is much higher.[120] The measured conductivity of the produced handsheets ranged between 1 to 10 $S.cm^{-1}$. The conductivity is lower than for a coated single fiber because the conductive composite network was destroyed to some extent.

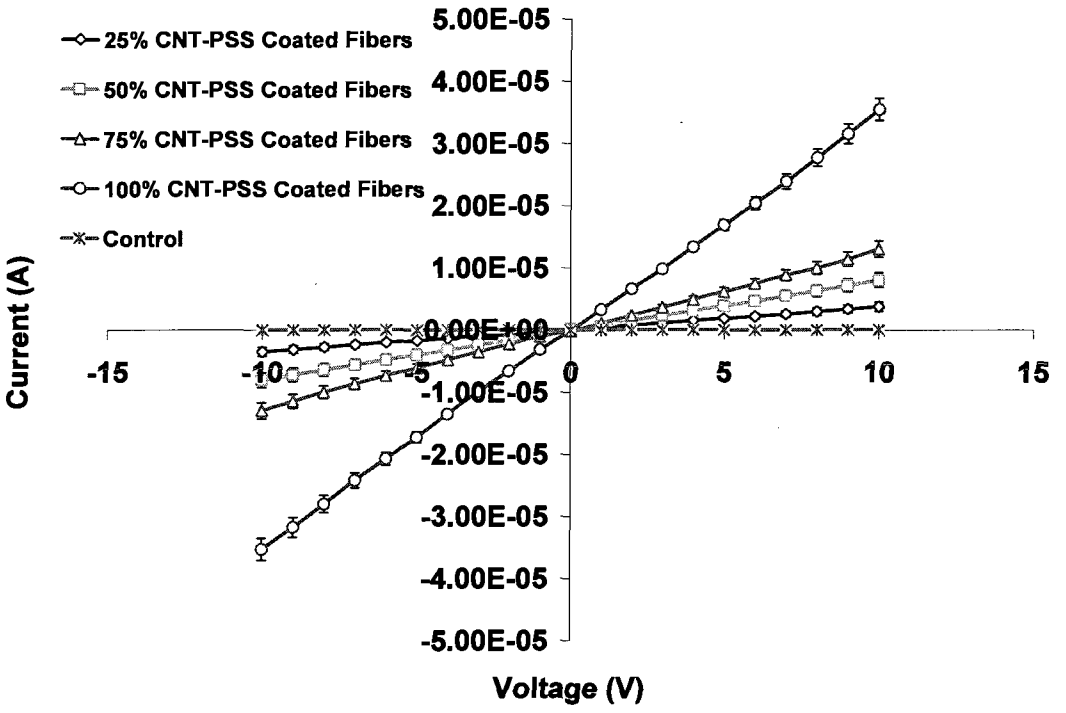

Figure 4.9 I-V characteristics of the hand sheets made with mixture of wood microfibers coated with $(PEDOT\text{-}PSS/PEI/CNT\text{-}PSS/PEI)_2$, and uncoated wood microfibers. Measurements made at room temperature at relative humidity of around 40%.[120]

As shown in Figure 4.10, the electrical characteristics of the handsheet made of 100% LbL coated microfibers along the length of the handsheet at 0.25, 0.5, 1, 1.5, and 2 cm showed a proportional resistivity increase (the current decreases at a given voltage) according to Ohm's law. Therefore, resistance of the handsheet is inversely proportional to its length and the contact resistance is negligible.[120]

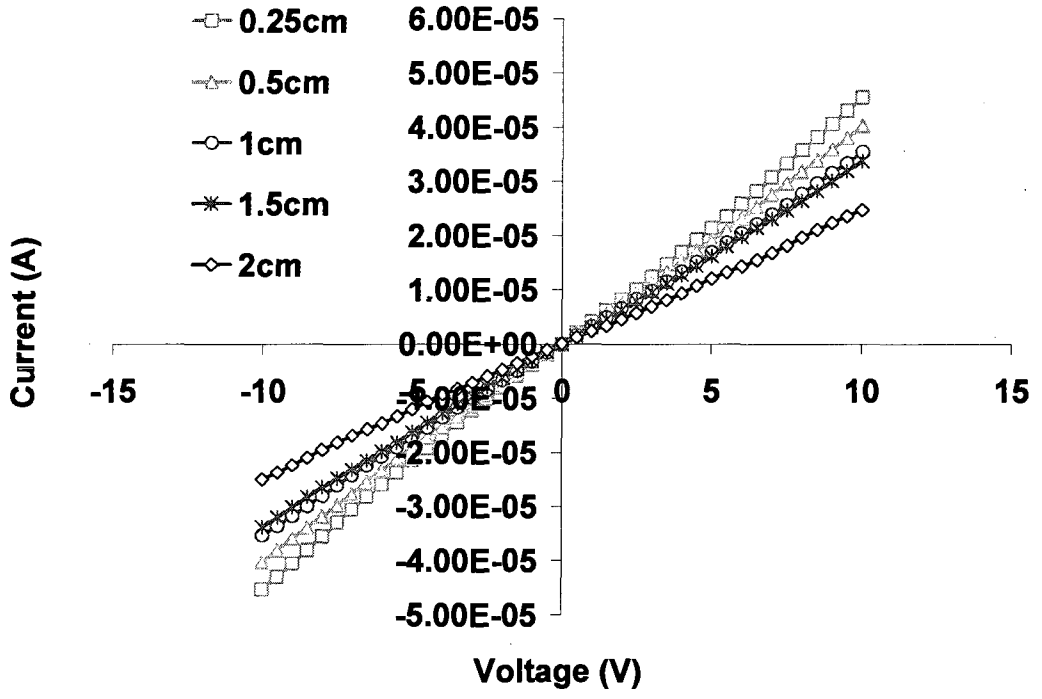

Figure 4.10 I-V characteristics of 100% coated (PEDOT-PSS/CNT-PSS)$_2$ paper as a function of length.[120]

4.3.4 Non-Metallic Paper Capacitor

Using the conductive wood microfibers, a layered paper that can act as a capacitor was fabricated and tested. The schematic diagram of the paper capacitor sample is given in Figure 4.11 (a). Total paper sheet thickness was kept equal to three equal thickness (conductive/dielectric/conductive) layers of 0.6 mm. The measured capacitance of the initial sample made is given in Figure 4.11 (b), which shows that the capacitance of the sandwiched conductive/dielectric/conductive paper is measured to have an approximately constant value of 1.5×10^{-11} F over the given range of applied voltage. It is also observed that this capacitance is much larger than the capacitance of a sample consisting of two flat metal (copper) electrodes of the same area as the conductive paper capacitor, separated by a similarly thick uncoated center paper sheet with a dielectric constant of 3.[120]

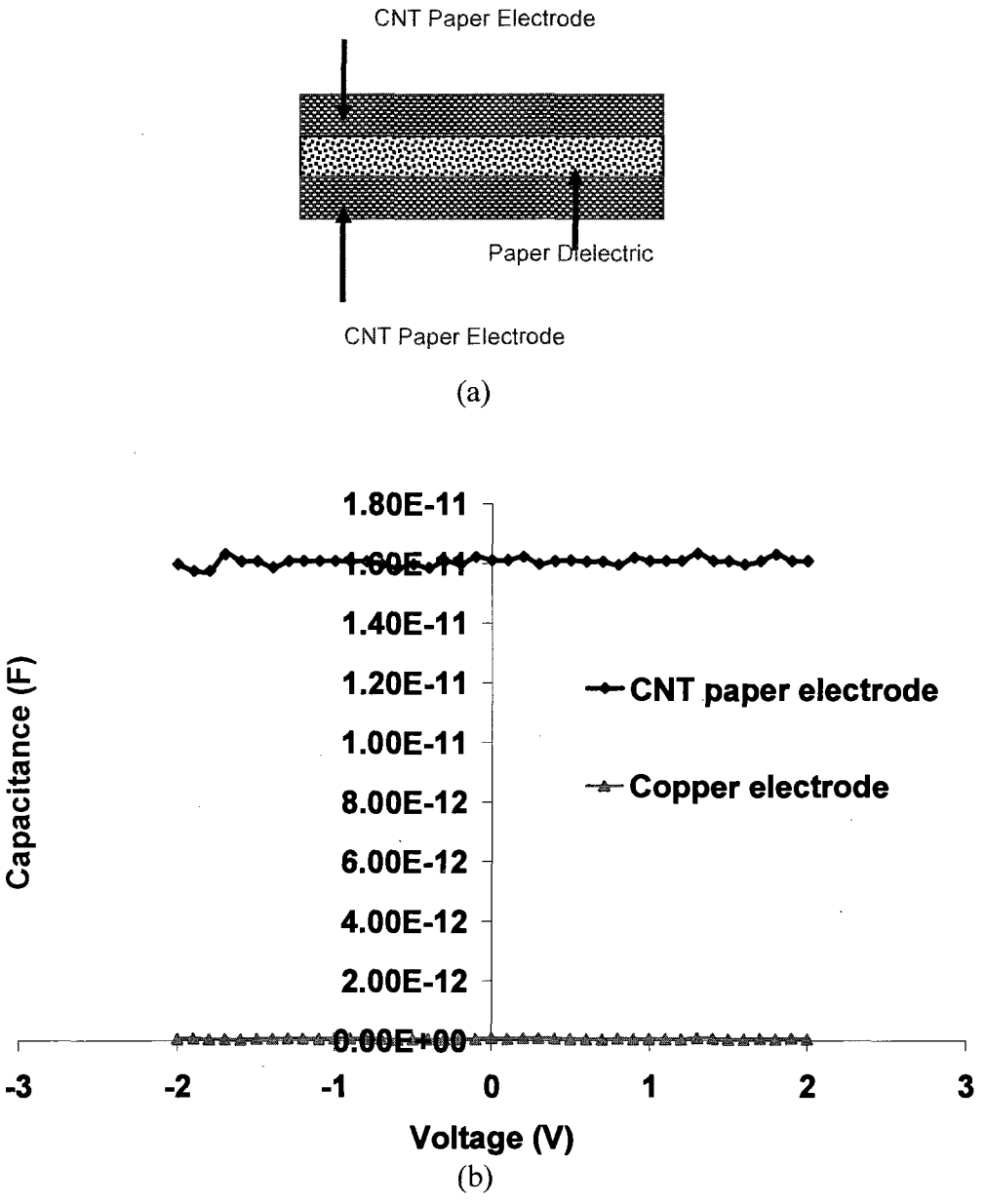

Figure 4.11 (a) Schematic diagram of the capacitor manufactured using conductive paper; (b) Capacitance measured using Keithley measurement system.[120]

The difference is attributed to the nature of the interfacial contact between the electrodes and the dielectric regions of the given two capacitor samples. The interfacial contact between the conductive and non-conductive layer of the paper capacitor is expected to consist of fiber inter-digitations resulting in lower voids or air gaps, which,

however, may exist for the other sample. This simple explanation also assumes that the contact area in the conductive-nonconductive layers of fibers in the paper capacitor is larger compared to the other capacitor sample. The conductive paper itself is also a possible dielectric material since it is porous and having a high surface area which can increase charge storage.[130] The results obtained seem promising for future development of paper-based transistors and batteries.[120]

4.3.5 Conductive Paper Based Glucose Sensor

Attempts to develop a conductive paper based glucose sensor were demonstrated. A conductive handsheet was soaked into glucose oxidase (GOx) solution and air dried. Then a thin film of cellulose acetate was put on the top to fabricate the sensing device. The scheme for the sensor structure is shown in Figure 4.12 (a). Different concentrations of glucose solution were prepared to evaluate the sensor performance. The reaction of GOx enzyme catalyzing glucose was described using the following equations:

$$\text{Glucose} + O2 \xrightarrow{\text{GOx}} \text{Gluconolacton} + H_2O_2$$

The oxidation of H_2O_2 produces electrons which can be detected by a sensing electrode made of conductive materials, thus the glucose concentration can be measured by monitoring the electrical signal of the sensing device. Figure 4.12 (b) shows the electrical behavior of the conductive paper based sensor exposed to a series of glucose solutions with different concentrations. The increased slope of the I-V curve corresponds to the increase in glucose concentration. Higher concentrations of glucose produced more charge carriers during the reaction, thus increasing the current under the same voltage. The result is promising for fabrication of paper-based sensors. However, the issue of the

poor attachment of cellulose acetate membrane on the paper surface remains, which leads to unstable readings.

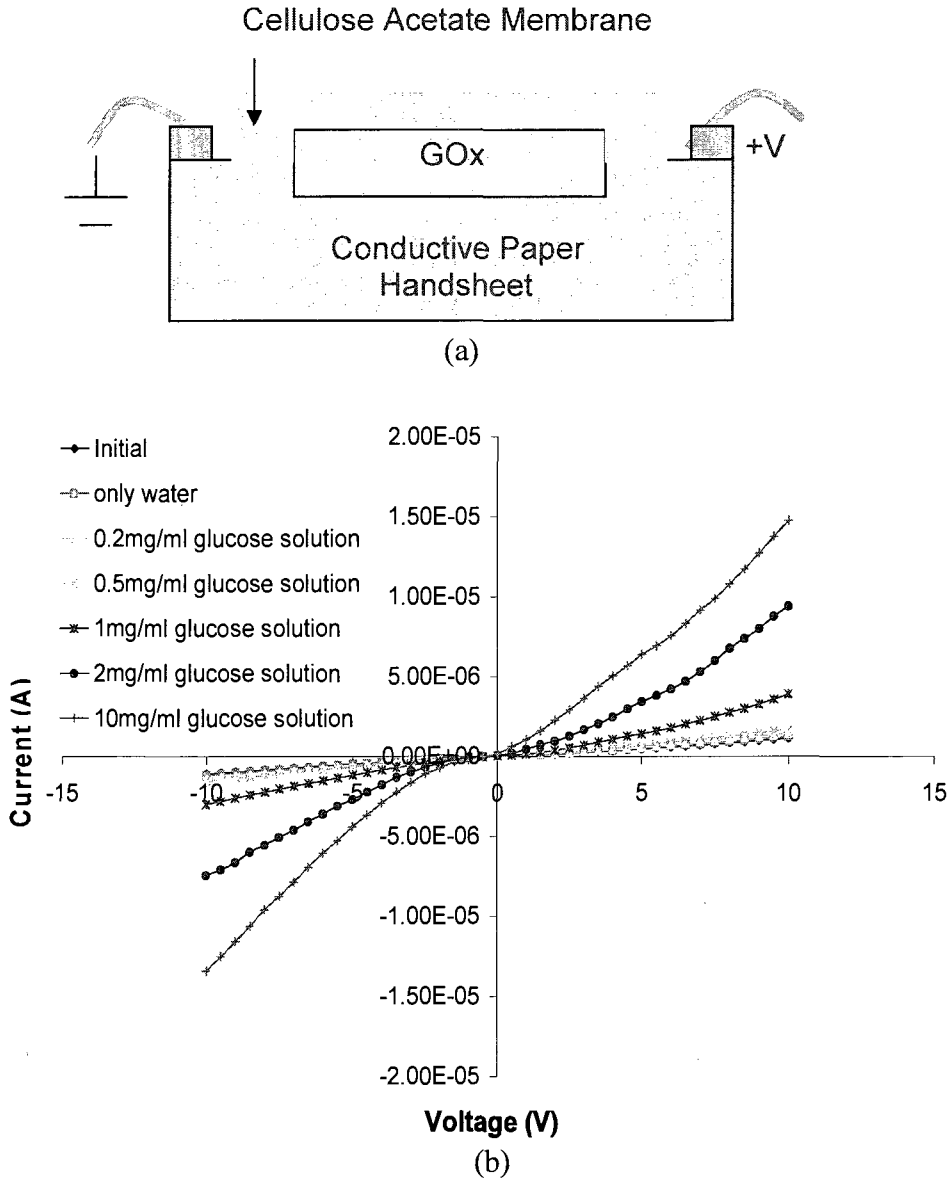

Figure 4.12 (a) Schematic diagram of the conductive paper based glucose sensor structure. (b) I-V characteristics of glucose sensor exposed to glucose solution with concentration of 0.2 mg/ml, 0.5 mg/ml, 1 mg/ml, 2 mg/ml, 10 mg/ml.

4.4 Conclusions

It has been shown that by using the LbL method, very small amounts (around 0.2 wt%) of conductive components (carbon nanotubes bounded through polythiophenes) coated with a thickness of about 148 nm on wood cellulose microfibers can be used to make paper following the traditional manufacturing method, but resulting in functionally enhanced material - bulk conductive paper. Carbon nanotubes were deposited using LbL nanoassembly via alternate adsorption of oppositely charged components on wood microfibers. QCM data, surface potential measurements and SEM images demonstrated that CNT-PSS was successfully coated on the surface of the wood microfibers. The conductivity of the cellulose microfibers was in the range of 10^{-2} to 2 $S.cm^{-1}$ depending upon the architecture of the coated layer. The conductivity of the wood fibers was further increased up to 20 $S.cm^{-1}$ by sandwiching a multilayer of conductive co-polymer PEDOT-PSS with CNT-PSS through a polycation (PEI) interlayer. Paper sheets were made from LbL modified cellulose microfibers and it is demonstrated that the bulk paper conductivity ranged between 1 to 10 $S.cm^{-1}$ depending upon the ratio of LbL coated conductive microfibers to virgin uncoated microfibers. These results show that using the LbL nanoassembly technique, a cellulose microfibers/carbon nanotube composite can be cost effectively realized to make conductive paper sheets. The conductive paper-based capacitor showed enhanced electrical capacitance of 1.6×10^{-11} F per square inch of sample. This technique will help in the realization of cellulose microfiber-based electronic devices (e.g. capacitors, inductors, and transistors) and sensors that can be directly integrated in paper, resulting in "smart" paper products. Moreover, the same LbL

modification is also applicable for coating cotton microfibers to fabricate electrically active fabrics.[120]

CHAPTER FIVE

THREE DIMENSIONAL SCAFFOLD OF CELLULOSE MICROFIBER/GELATIN COMPOSITE FOR CELL CULTURE

5.1 Introduction

Cellulose microfiber is a very promising material for cell culture. First, the major composition of cellulose microfiber is cellulose which has been proved to be biocompatible for both granulation tissue[131] and bone formation.[89] The regenerated cellulose scaffold can promote cardiac cell growth, enhance cell connectivity and electrical functionality.[88] Calcium phosphate coated cellulose fibers were employed to provide a favorable environment for the development of cartilageous tissue.[90] Cellulose fiber has a high density of reactive hydroxyl groups on its surface which facilitates the immobilization of cell adhesive proteins, such as fibronectin.[132] Second, the densely packed glucan chain structure in cellulose fibers gives them sufficient mechanical strength to support cell aggregate structures.[86] Regenerated cellulose was also proved to be very stable under dynamic stress.[133] Third, cellulose does not have good degradability in vivo,[88] but it is biodegradable by hydrolysis with cellulase, and the final product is glucose. Therefore, the cellulose fibers can be removed from a cell culture construct when no longer needed.[86] However, there is very little research studying the application

of cellulose microfibers as a cell culture scaffold due to their absence of self-assemble ability to form an intrinsic macro-scale three dimensional (3-D) architecture for ex vivo study. Use of gelatin may provide additional 3-D architecture for cellulose-based cell scaffolds. Gelatin is a derivative of collagen and it is biodegradable, inexpensive, and non-immunogenic. It was shown that gelatin-based scaffolds have wide applications in different areas of tissue engineering.[134,135]

Here we elaborate on the use of 3-D composites based on cellulose microfibers connected by gelatin as bio-glue for cell culture. Morphology and structure characteristics were observed by scanning electron microscopy. The biocompatibility of the scaffolds was tested by culturing brain tumor cells (BTCs) and human Mesenchymal Stem Cells (hMSCs) *in vitro*. To our knowledge, this is the first report of cellulose fiber/gelatin composites for 3-D cell scaffolds.

5.2 Materials and Methods

5.2.1 Materials

Beaten bleached Kraft hardwood fiber sheets, supplied by International Paper Company, (Bastrop, LA), were dispersed in water to obtain cellulose fibers. All other chemicals were purchased from Sigma-Aldrich or Invitrogen and used without further purification.

5.2.2 Scaffold Fabrication and Characterization

The 3-D microscaffolds were prepared by solid-liquid phase separation and subsequent sublimation of the solvent.[134] Briefly, 1 wt% gelatin solution was prepared by dissolving gelatin B (negatively charged) powder in deionized H_2O heated at 50°C. A

controlled amount of 1-ethyl-3-(3-dimethyl aminopropyl) carbodiimide (EDC) and N-hydroxysuccinimide (NHS) were added to crosslink the gelatin. The final concentration of EDC and NHS was 5 mM at a molar ratio of 1:1. Different amounts of dried cellulose fibers were mixed with the above gelatin solutions and gently rotated for even distribution. The mixture was put in an ice bath to initiate gelation. After being kept in a 4°C refrigerator overnight, the resulting gel was placed at -20°C to freeze. Then the frozen samples were lyophilized in a freeze-dryer for at least 24 h. Samples were cut into thin slices, and a Scanning Electron Microscope (AMRAY, Model 1830) was used to characterize the morphology of the scaffolds. Pore size and porosity was determined using Autopore II mercury intrusion porosity meter.

5.2.3 Mechanical Properties Testing

The mechanical properties of scaffolds was tested with an eXpert 2611 twin screw electromechanical materials testing machine (ADMET, 10KN). The specimens tested were rectangular disks with a length of 7 mm and thickness of 1.5 mm. The gage length was set at 5 mm. Young's modulus, peak stress and break position were recorded at the maximum load.

5.2.4 Swelling Ratio

Swelling ratio, or water sorption capacity, was measured by soaking the sample in 0.01M phosphate buffered saline (PBS) solution at room temperature for 24 hours. The samples were weighed (W_0), then after swelling, the samples were wiped with filter paper to remove excess water and weighed (W_{24}) again. The swelling ratio (S) was calculated from Equation (5.1):

$$S = \frac{W_{24} - W_0}{W_0}. \tag{5.1}$$

5.2.5 Protein Adsorption Characterization

Samples of 3-D cellulose fiber/gelatin scaffolds and pure gelatin scaffolds were weighed and put into complete media [DMEM (American Type Culture Collection) containing 10% FBS (Lonza Group Ltd, Switzerland) and 1% Penicillin/Streptomycin (Sigma)] at 37°C for a specific time period. The samples were taken out and washed in PBS repeatedly, then put into freezer overnight and freeze-dried in the lyophilizer for 24 h. The samples were weighed again and the weight changes were calculated as average percentage increases of three samples. The media was changed every three days.

5.2.6 Brain Cancer Cells Seeding and Culture

Brain cancer cells, CRL-2020, were obtained from American Type Culture Collection. Both gelatin and cellulose fibers/gelatin microscaffolds were cut into thin slices about 1 mm thick, and sterilized using 70% ethanol followed by washing three times with phosphate buffered saline (PBS). A 1 ml cell suspension with 2×10^6 cells was seeded onto the matrix, soaked into 1ml culture media, in a well of a 24-well tissue culture plate. After seeding, the media was changed every other day and the cultures were incubated for 16 days at 37°C and 5% CO_2.

5.2.7 Calcein Staining

After 16 days in culture, the brain cancer cells were stained using a calcein-AM fluorescent dye. Briefly, 5 μL pluronic acid with a concentration of 20% (w/v) in DMSO and 10 μL stock solutions of calcein-AM with a concentration of 1mM were added into 5 ml pre-warmed Locke's solution. The cells were incubated with the pre-warmed solution for 25 minutes and imaged using a LEICA DMIRE2 Confocal Laser Scanning

Microscope (CLSM) or Nikon epifluorescence microscope, as indicated.

5.2.8 hMSCs Seeding and Culture

hMSCs were obtained from bone marrow of health donors in a method described by Noiset et al.[132] Briefly, bone marrow asparites of about 2 ml were drawn from healthy donors ranging in age from 19 to 49 years under an Institutional Review Board approved protocol. The collected cells were expanded using α-MEM media with 20% FBS under 37°C and of 5% CO_2. The sixth passage cells were seeded onto each scaffold in a 24-well plate using 1 mL cell suspension of about 2.5×10^5 cells. The cell culture media was changed every other day and incubated for up to 28 days at 37°C and of 5% CO_2.

5.2.9 DNA Assay

The cell number in the 3-D cellulose fiber/gelatin scaffold was determined by quantifying the DNA number of cells. A series of diluted DNA solutions with different concentration were used to prepare a DNA standard curve. Cell constructs were lysed in TEX (10 mM Tris, 1 mM EDTA, 0.1% Triton X-100) with 0.1 mg/ml Proteinase K at 50°C overnight. A 100 μl sample was extracted and placed in a 96-well plate; then 100 μl Picogreen was added to each well to stain the DNA. After incubation in a dark place at 37°C for 10 min, the plate was read using a fluorescent plate reader. For each time point, three constructs were collected to obtain cell pellets and used for calculating the cell number.

5.2.10 Immunocytochemistry Staining

Cytoskeleton protein F-actin and extracellular matrix (ECM) proteins fibronectin and collagen IV were examined using an immunocytochemistry staining method. The hMSCs grown in the 3-D scaffold were fixed using 0.3% glutaraldehyde solution, permeated with

1.0% Triton X-100, and blocked with 10% fetal bovine serum. Then, cells were incubated with anti-fibronectin or collagen IV primary antibodies for 1 h at 37°C, followed by a mixture of FITC-conjugated secondary antibody and phalloidin conjugated to Alexa Fluor 594 for 1h at 37°C. Before imaging, the samples were mounted using Vectashield with Dapi to counterstain the cell nuclei. The cells were viewed using the Leica SP5 confocal microscope.

5.2.11 Osteoblast Differentiation

After 35 days culture, the cells were tested for osteoblast differentiation potential by using a STEMPRO® osteogenesis differentiation kit (Invitrogen) for 21 days. Control was prepared by continuing to culture the un-induced construct in α-MEM media for an additional 21 days. The mineralized extracellular matrix was detected by Von Kossa staining, as previously described.[137] Briefly, cell constructs were fixed in 10% formalin solution for 1 h and put into silver nitrate solution under UV light. After around 15 minutes, un-reacted silver was removed with 5% sodium thiosulfate. Then the constructs were observed under a Zeiss Axio Imager widefield fluorescence microscope.

5.2.12 Adipocyte Differentiation

After 35 days culture, the cells were tested for adipocyte differentiation ability by using a STEMPRO® adipogenesis differentiation kit (Invitrogen) for 21 days. Control was prepared by continuing to culture the un-induced construct in α-MEM media for an additional 21 days. The cells were fixed and lipid-containing adipocytes were visualized by Nile Red staining, following the method reported before.[137] Dapi was applied as a counterstain. Leica SP5 confocal microscope was employed for observation.

5.3 Results

5.3.1 Cellulose Fibers/Gelatin Composite Morphology

Scanning electron microscope (SEM) images of both gelatin and cellulose fiber/gelatin microscaffolds are shown in Figure 5.1.

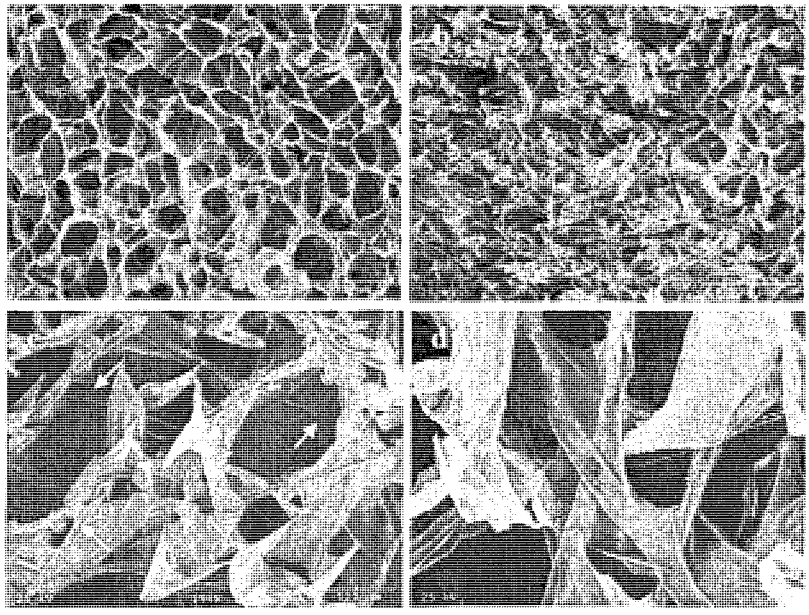

Figure 5.1 SEM images of pure gelatin scaffold (a) and cellulose fiber/gelatin scaffold (b, c, d) containing 75 wt% fibers. Arrows in (c) indicate cellulose fibers within the composite matrix. Scale bars shown in microns.

For an ideal scaffold for cell culture, high porosity is required to allow oxygen and nutrient diffusion into the matrix. Both scaffolds are highly porous with interconnected matrices of components. The average pore diameter of cellulose fiber/gelatin scaffold was determined to be 69 ± 4 μm with a high porosity of about 70%. The pore size is large enough to allow for nutrient transport to support cell growth into the material. Compared to gelatin scaffolds (Figure 5.1 (a)), the cellulose fiber/gelatin composite scaffolds (Figure 5.1 (b)) appeared to be much rougher. Cellulose fibers were randomly distributed

in the matrix at different levels, as shown in Figure 5.1 (c). Some fibers are embedded in the gelatin films, some are wrapped by gelatin films (Figure 5.1 (d)), and others just adsorbed some gelatin molecule.

The scaffolds were also observed under CLSM, as shown in Figure 5.2. After the addition of cellulose microfibers, the pore structure of gelatin foam is more or less retained.

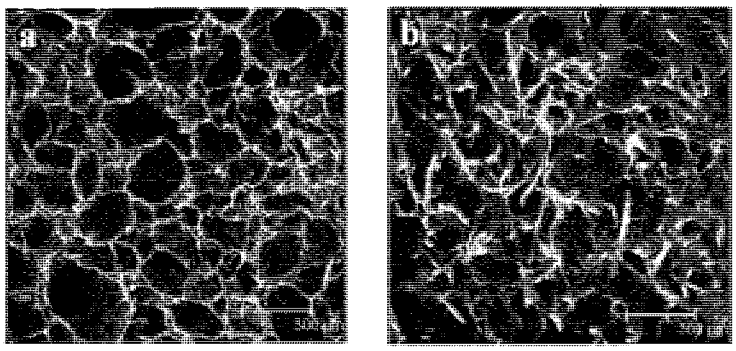

Figure 5.2 CLSM images of (a) gelatin scaffold; (b) cellulose fiber/gelatin scaffold containing 75 wt% fibers.

5.3.2 Mechanical Properties

The results of the mechanical testing are presented in Figure 5.3. The trend suggests an increase in Young's modulus and peak stress with an increase in the amount of cellulose fibers. The sample with 75% cellulose fibers has the highest Young's modulus at 3.1 ± 0.1 MPa, around 8 times higher than the sample without fibers. The highest peak stress is 225 KPa, 4 times the peak stress of pure gelatin samples. The difference between the samples containing 50% and 66.7% fibers is not significant.

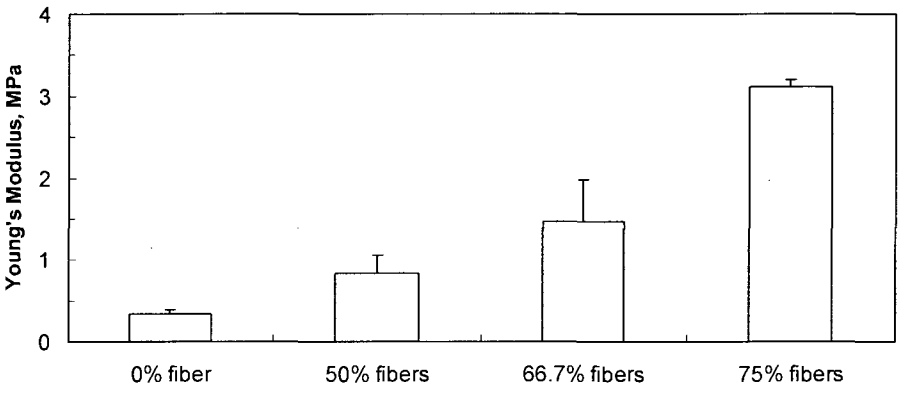

(a)

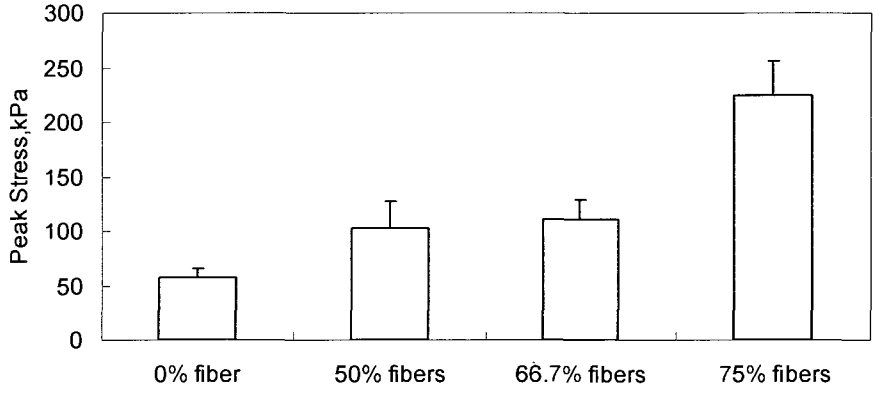

(b)

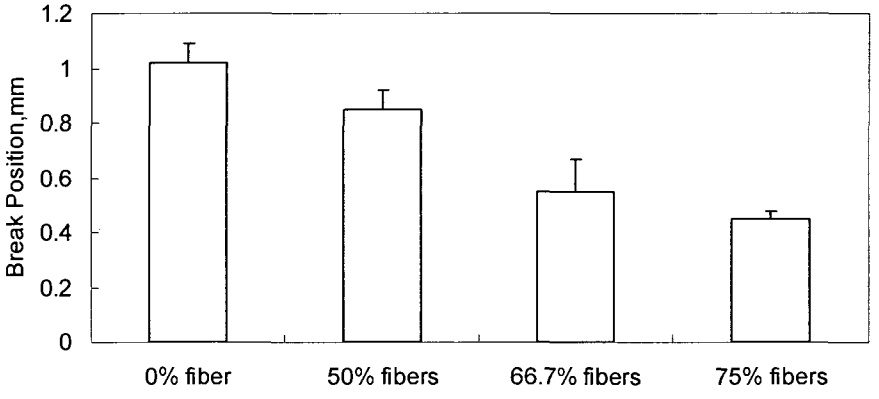

(c)

Figure 5.3 (a) Young's modulus of microscaffolds with various amounts of cellulose fibers; (b) Peak stress of microscaffolds with various amounts of cellulose fibers; (c) Break position of microscaffolds with various amounts of cellulose fibers. In all cases, $n \geq 3$.

The break position data showed a decreasing displacement with an increase of fiber content. This is an indication of good fiber-matrix adhesion.[138] The stiffness makes the composite easily handled under dry conditions. When wetted, however, we observed that samples became much more gel-like, due to a high water sorption capacity.

5.3.3 Adsorption Characteristics

Swelling ratio experiments showed that all the samples have high water sorption capacity. The effect of the cellulose fibers weight percentage on the swelling ratios is illustrated in Figure 5.4. The swelling ratio gradually decreased on increasing the cellulose fiber weight percentage in the microscaffolds.

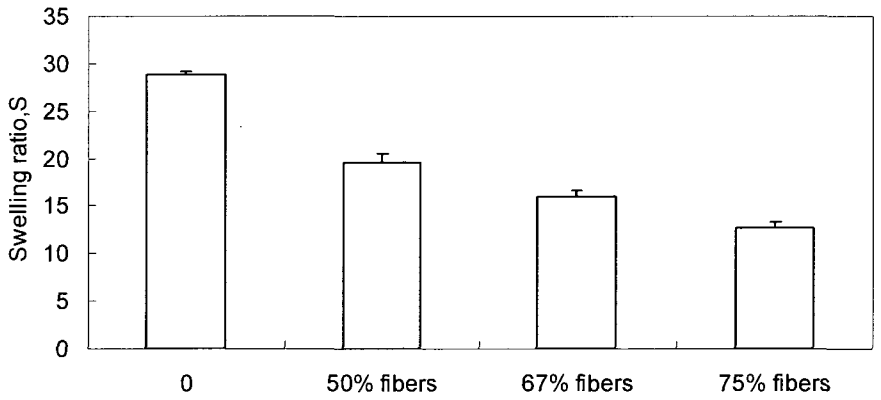

Figure 5.4 The effect of cellulose fiber weight percentage on water uptake capacity of cellulose fiber/gelatin microscaffold.

The weight of both porous samples increased when incubated in media for a certain period of time. This suggests the adsorption of proteins to the scaffolds. As shown in Figure 5.5, during the first 7 days the weight of cellulose fiber/gelatin scaffold increased around 20% , while pure gelatin scaffold only increased 9%. From day 8 to 28, the weight of both scaffolds varied but kept a similar level to what was observed on day 7. In

the last 7 days, there is an increase in weight for the cellulose fiber/gelatin scaffold. In contrast, the tendency for the gelatin scaffold is a decrease in weight.

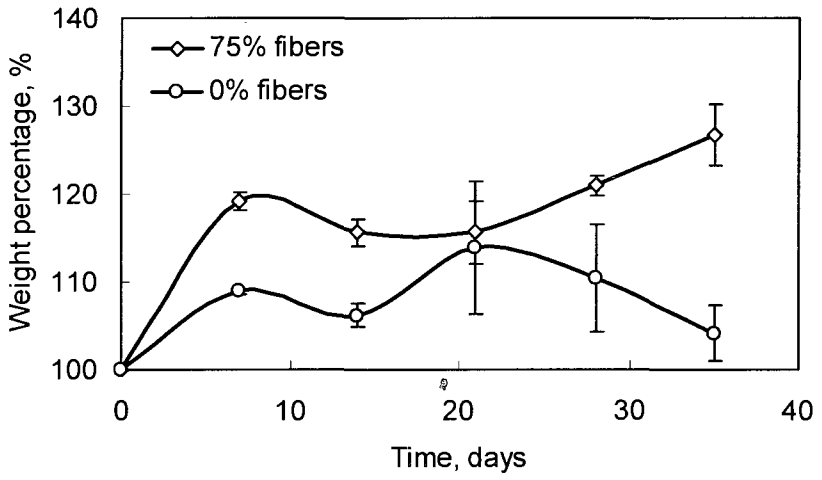

Figure 5.5 Weight changes of cellulose fiber/gelatin and gelatin microscaffold incubated in the complete media with 10% FBS as a function of time.

After 5 weeks adsorption, SEM images of cellulose fiber/gelatin composite showed that protein crystals were deposited on the scaffold surface, as shown in Figure 5.6 (a),(b); while before protein adsorption, no particles was observed on the surface, as shown in Figure 5.6 (c). This result demonstrated that the scaffold may have adsorbed proteins such as, albumin, fibronectin and vitronectin from the serum to support cell adhesion and proliferation.

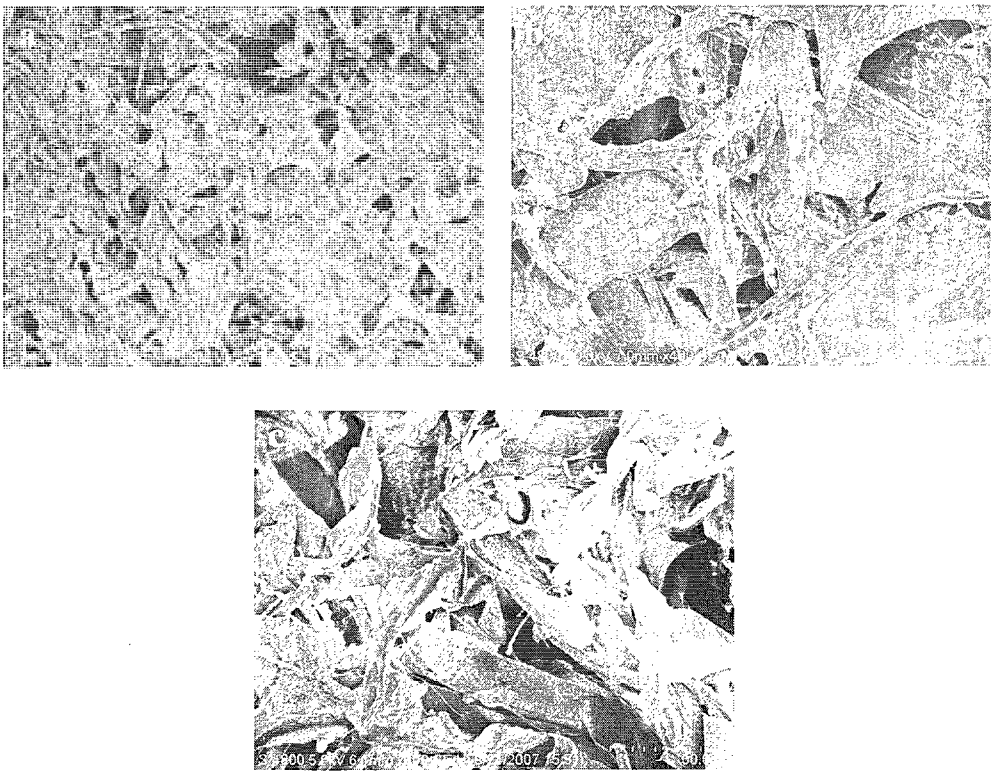

Figure 5.6 SEM images of cellulose fiber/gelatin scaffold: (a), (b) after 5 weeks of proteins adsorption; (c) before protein adsorption.

5.3.4 Brain Cancer Cell Culture

Brain cancer cells were chosen due to their invasive nature and rapid proliferation capability. These cells are an excellent model to study brain cell growth pattern. Brain cancer cell growth patterns in the different scaffolds were assessed after 16 days *in vitro* by staining for viable cells with calcein. Epifluorescence microscopy showed that gelatin matrices caused a more clumped formation of cells (Figure 5.7 (a)-(c), top), compared to gelatin/cellulose fiber composites which clearly allowed for some alignment and separation of cell groups (Figure 5.7 (a)-(c), bottom).

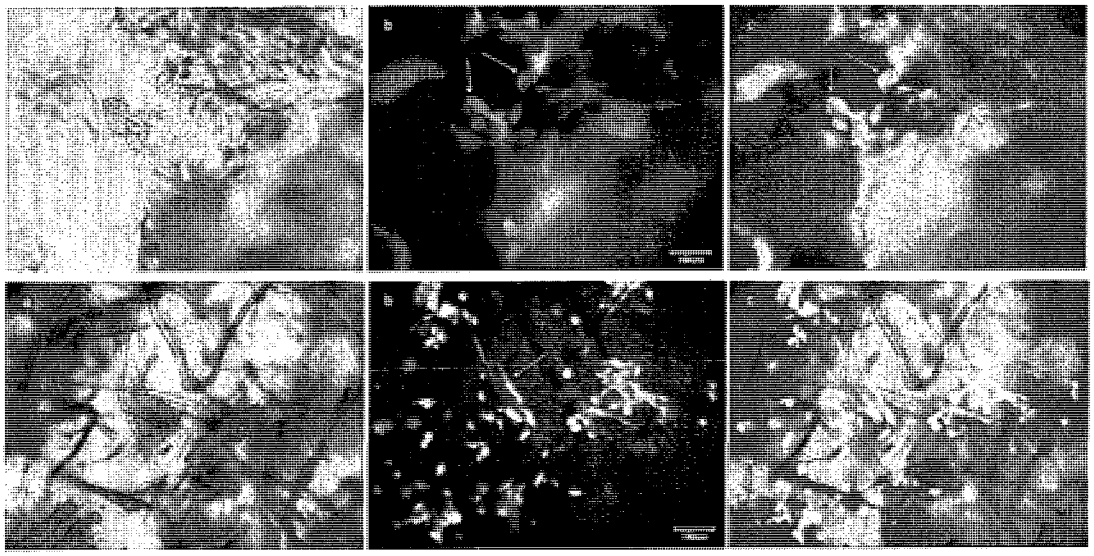

Figure 5.7 Epifluorescence images of CRL-2020 brain tumor cells grown on gelatin (top panel) and cellulose fiber/gelatin (bottom panel) microscaffolds for 16 days *in vitro*. Panel (a) shows phase image of cells and matrix; panel (b) shows monochrome fluorescence indicating calcein staining, and panel (c) shows merged image of panels (a) and (b). Arrows indicate cells bound to the gelatin matrix (top), or fiber matrix (bottom). Scale bar in (b) indicates 100 microns.

Since these scaffolds can serve as three dimensional growth matrices, we next assessed in-focus cell growth at a given depth (Z-plane) using confocal laser scanning microscopy. The confocal laser scanning microscopy images of the matrices confirmed epifluorescence observations: cells can penetrate through, adhere and grow well in both microscaffolds. In the gelatin scaffold, cells tend to grow in clusters (Figure 5.8 (a)-(c), top); while in the cellulose fibers/gelatin scaffold, cells can grow along the fibers, which indicates that the fiber may provide better guidance to control the direction or spacing of cell growth (Figure 5.8 (a)-(c), bottom)

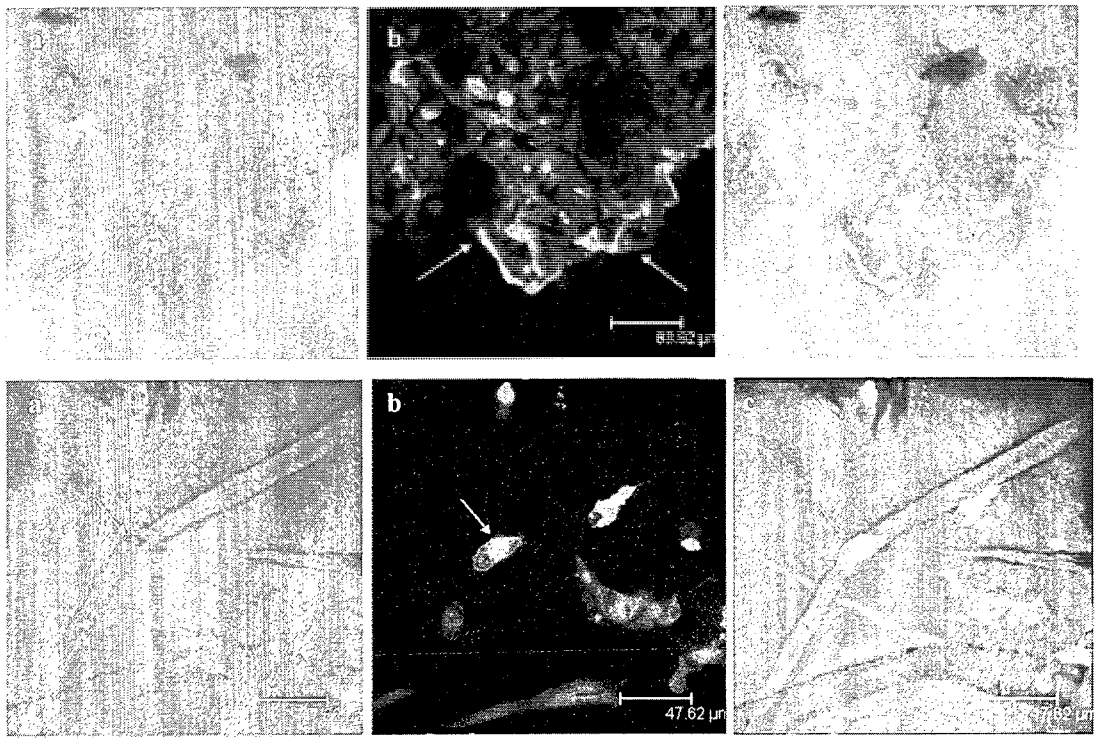

Figure 5.8 Confocal Laser Scanning Microscope (CLSM) images of CRL-2020 brain tumor cells grown on gelatin (top panel) and cellulose fibers/gelatin (bottom panel) microscaffolds for 16 days. Panel (a) shows phase images of cells and matrix; panel (b) shows green fluorescence indicating calcein staining; panel (c) shows merged image of panel (a) and (b). Arrows in top panel indicate the front edge of the gelatin matrix; arrows in bottom panel indicate cells aligned on cellulose microfibers.

5.3.5 hMSCs Adhesion and Growth

hMSCs were also used to evaluate the biocompatibility of the cellulose fiber/gelatin scaffold. After 28 days culture of hMSCs in the cellulose fiber/gelatin scaffold, cells proliferated actively and expressed extensive F-actin and extracellular molecule networks, as shown in Figure 5.9. The F-actin, fibronectin and collagen IV fibrils seemed to be aligned along the fibers, which could be caused by the cells grew along the fibers. But it is also probably caused by the high density of packed hMSCs in that region.

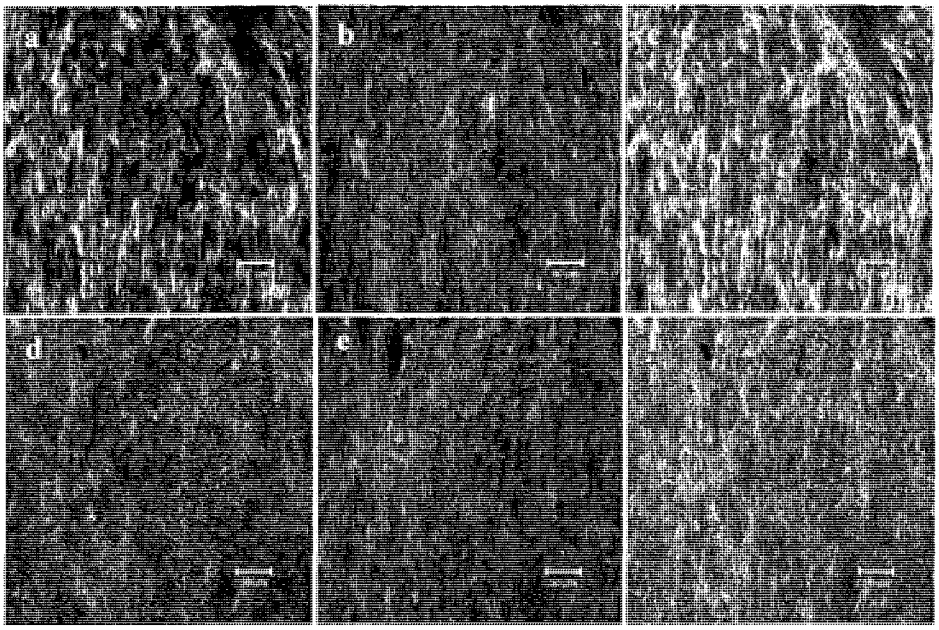

Figure 5.9 hMSCs adhered and proliferated over 28 days in cellulose fiber/gelatin scaffold. Extensive F-actin and extracellular matrix network were formed. Cell nuclei were stained with Dapi(blue), F-actin were stained with Rodamine(red), fibronectin (upper panel) and collagen IV (lower panel) were stained with FITC(green).

About 25% of the cells attached in the scaffold 24 hours after seeding. In the first 7 days, the cell number increased by 34% and remained constant at this level (around 8 $\times 10^6$ cells in scaffold) for the following 21 days (Figure 5.10). Cells did not grow in a typical 3-phase pattern: lag phase, exponential phase and stationary phase. After initial moderate growth for the first week, the stationary phase followed and lasted three weeks. During this period the cell growth rate equals the death rate. The growth kinetics corresponds to the cellulose fiber/gelatin scaffold protein adsorption trend. Both protein adsorption and cell growth increased in the first week, then reached a plateau in the following 3 weeks.

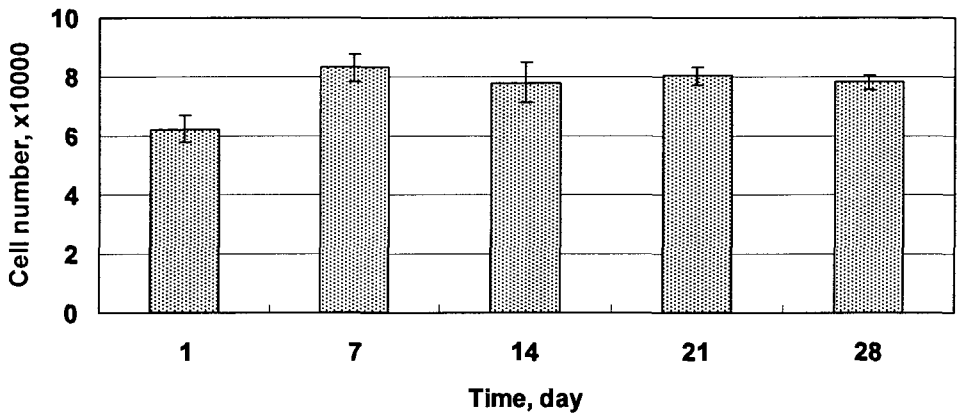

Figure 5.10 hMSCs growth in cellulose fiber/gelatin scaffold over a 28-day period. (n=3)

5.3.6 hMSCs Multi-Lineage Differentiation

After a 35-day culture, hMSCs were induced into osteoblasts and adipocytes respectively to investigate the multi-lineage differentiation potential. Von Kossa staining of induced constructs was used to detect the osteogenic differentiation of hMSCs. Calcium-containing, mineralized ECM was stained black to demonstrate the successful osteoblast differentiation. The induced construct appeared much darker than the control (Figure 5.11 (a)-(c), top). Under microscopy, the presence of many black spots also confirmed that hMSCs retained osteogenic differentiation ability. The majority of black spots were located around fibers, which may indicate cells are preferentially growing along the fibers (Figure 5.11 (a)-(c), bottom).

The most important characteristic of adipogenic differentiation is the presence of mature adipocytes. From the induced constructs shown in Figure 5.12, many clusters of lipid droplets were found. The observation confirmed the hMSCs retained the adipogenic differentiation ability.

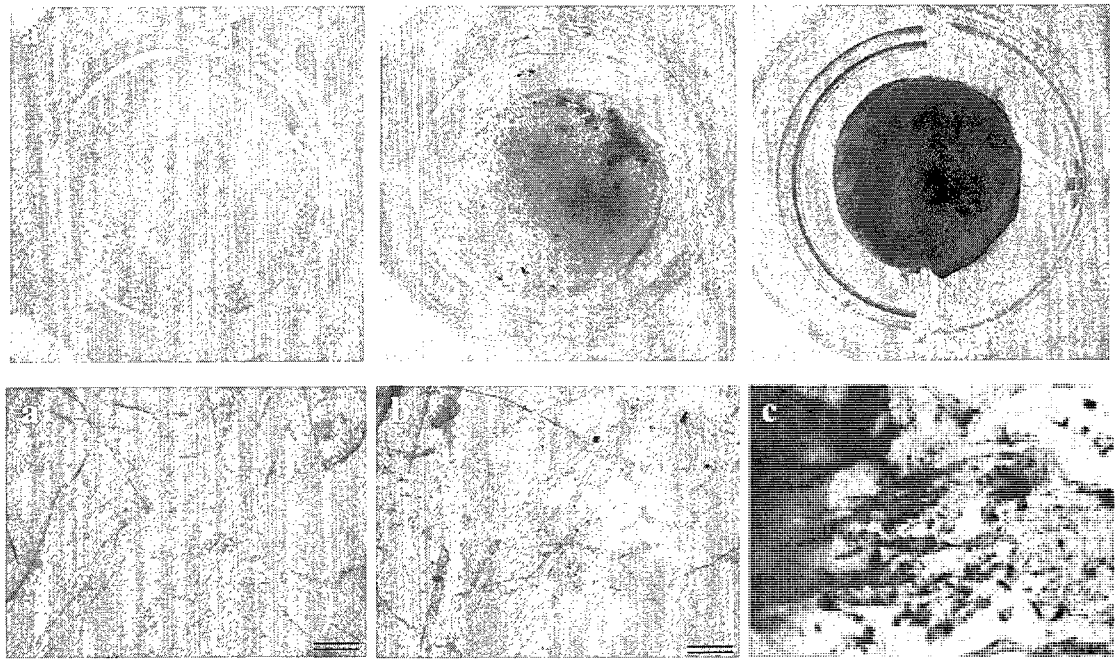

Figure 5.11 Von Kossa staining of osteo-induced hMSCs in cellulose fiber/gelatin scaffold. Top panel: photographic images of scaffolds; Bottom panel: microscopic images of scaffolds. (a) Control, hMSCs construct of 8 weeks culture without induction and staining. (b) hMSCs constructs of 8 weeks without induction but with Von Kossa staining. (c) hMSCs construct of 5 weeks culture and 3 weeks induction with Von Kossa staining. Scale bar in bottom panel indicates 200 μm.

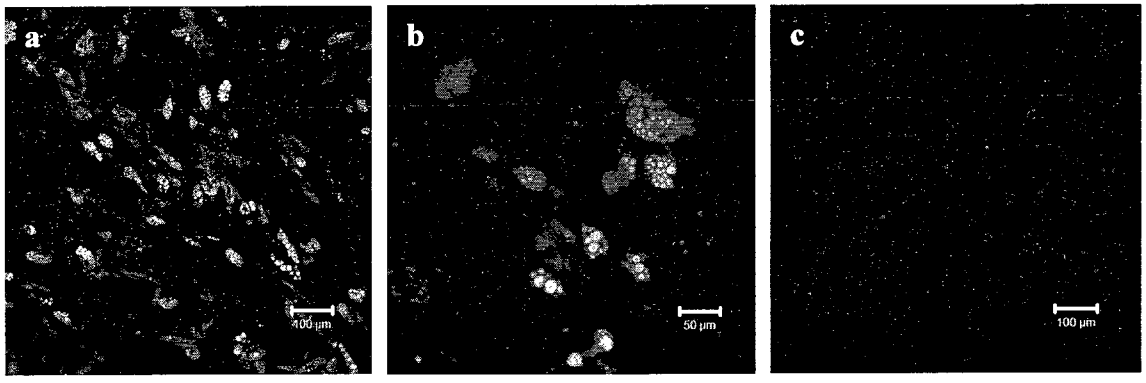

Figure 5.12 Nile red staining of adipo-induced hMSCs in cellulose fibers/gelatin scaffold shown in (a) low magnification and (b) high manification. Samples were obtained after 35 days culture and 21 days induction. There was no detectable signal in control (c).

5.4 Discussion

Cellulosic materials demonstrated good biocompatibility and mechanical strength for use as a biomedical engineering material. It has been shown that different cellulosic materials can be used for bone,[89,139] cardiac[88] and cartilage growth.[87,90] Ko et al. found that there was no cell proliferation observed on native cellulose films; however, cells grew well on fibronectin-immobilized surfaces.[86] In our scaffolds, the gelatin coating rendered the fiber surface suitable for cell culture, as well as providing spacing for the cellulose fibers. The surface and structure of scaffolds can significantly influence the interaction between scaffold and cells as well as cell growth, migration and differentiation.[137,140] The rough structure of the cellulose fiber/gelatin scaffold may also play an important role to promote cell adhesion and interaction with materials. It was reported that the interconnections between microfibers facilitate cells to cover the micro-nano-fiber scaffold.[141] In our cellulose fiber/gelatin scaffold, the interconnection was not limited to between films, but also included between films and fibers. In this way the scaffold may provide better support and guidance to the cells.

Our composite is mostly based on cellulose fibers and contained 50-75 wt% of cellulose fibers providing the scaffold skeleton. The amount of cellulose microfibers in the composite significantly affects the mechanical properties of the samples. Cellulose fibers have been extensively studied as reinforcement material.[14,142] In recycled newspaper cellulose fiber reinforced poly(lactic acid) composite, the tight connection between fiber and matrix were found.[14] Some of the fibers in our composite were also covered in a thin layer of gelatin. This linking facilitated stress transfer between the two materials, which led to better mechanical strength. Compared to the gelatin scaffold,

cellulose fiber/gelatin scaffolds showed 3-8 times higher mechanical strength. At the macroscopic level, gelatin/cellulose fiber composite samples have been scaled up so that they can be more easily cut into pieces and handled. When dry, they also have sufficient stiffness so that they can be easily manipulated (Figure 5.13).

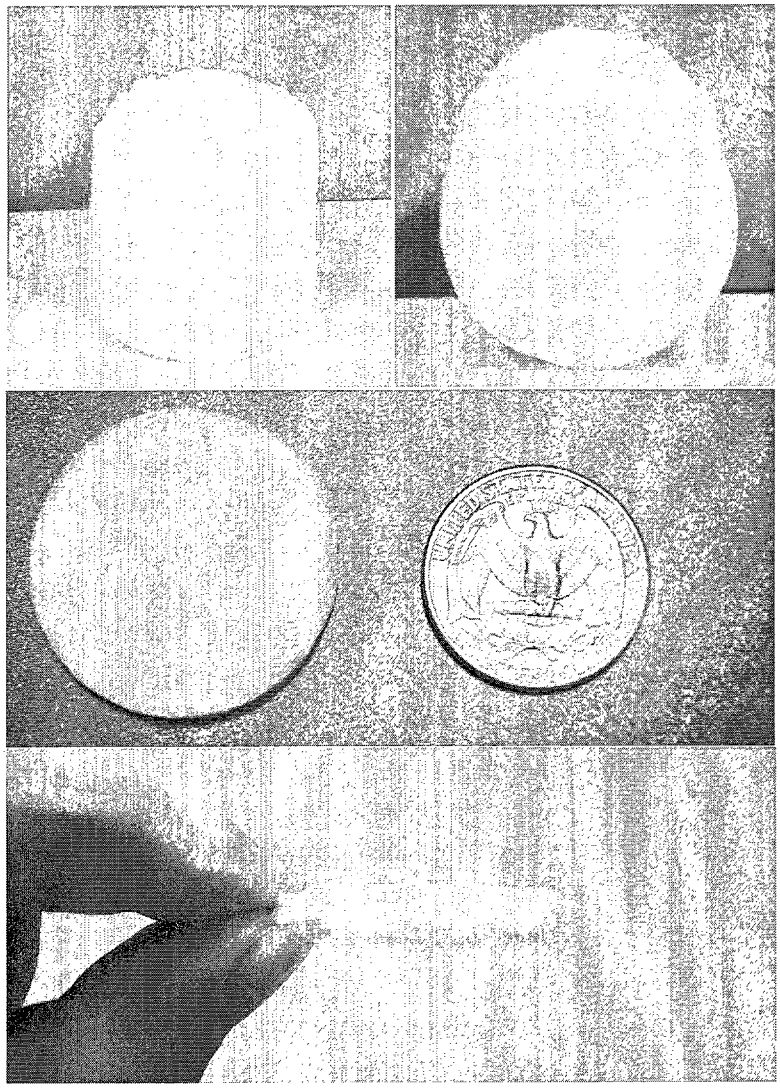

Figure 5.13 Macroscale views of dry cellulose fiber/gelatin scaffold. Top panel: sample in cylinder shape; middle panel: sample sliced and compared with a quarter; bottom panel: dry sample showing sufficient stiffness to be easily handled.

The gelatin/cellulose fiber scaffold provided two important aspects for tissue engineering: a three dimensional structure within which cells could grow, and sufficient porosity and liquid uptake so that cell culture media containing nutrients could penetrate into the matrix. At the microscopic level, cellulose fibers within the gelatin matrix also appear to provide sufficient pattern structure to allow for some alignment of cells. In fact, we chose these fibers in part due to their intrinsic width being sufficient to allow for single cell alignment, such as is shown in Figure 5.8. Here we chose a brain tumor cell line (CRL-2020) as one of the candidates for determining biocompatibility of the constructed 3-D gelatin-cellulose scaffolds due to the intrinsic proliferative and invasive characteristics of brain tumor cells in general and for this cell line in particular.[143] ECM is very important for cell interaction with each other and with the surrounding microenvironment.[144] The intensive expression of F-actin in the hMSCs culture indicated good cell adherence to the scaffold. The secretion of fibronectin and collagen IV demonstrated active signaling and interaction events of hMSCs. Multi-lineage differentiation ability is one of the parameters to indicate the "stemness" of stem cells. hMSCs cultured in cellulose fiber/gelatin scaffold can be differentiated into osteoblastic and adipogenic phenotype which proved that the scaffold provided a favorable microenvironment to stimulate stem cell differentiation.

To our knowledge, this is the first report of cellulose fiber/gelatin composites for 3-D cell culture scaffolds. Cellulose has been used as a solid support for growing bacteria.[145-147] Litwin has reported methods for culturing diploid cells on cellulose fibers in solution.[148] It is interesting to note that in contrast to our results, Litwin found that cells grew in large clumps around cellulose microfibers rather than spread out and aligned

along the fibers, such as we observed. This may be due in part to the spinner bottle suspension culture used in these previous studies.

Since gelatin and cellulose microfibers are both derived from natural products, there is appeal for using such products in biomedical engineering. Biocompatibility concerns may be diminished compared to purely synthetic products, and indeed here we saw excellent growth and attachment of cells in the scaffolds. As has been suggested previously, cellulase may be a method for shaping cellulose tissue scaffolds, since the enzyme is harmless to mammalian cells.[149]

5.5 Conclusions

3-D cellulose fibers/gelatin microscaffolds were fabricated by simply mixing natural wood cellulose microfibers with a small amount of gelatin, and then using a freeze-drying method. Microscopy images demonstrated that this novel scaffold has a porous, interconnected, rough structure with pores of around 70 μm in diameter. Cellulose fibers are randomly present in the scaffold at different space levels, indicating that a 3-D network of cellulose fibers is built with the gelatin glue. Compared with the gelatin scaffold, the cellulose fiber/gelatin scaffold showed 3-8 times higher mechanical strength, which is controllable by varying the fiber amount. CRL-2020 cells attached and grew well on both gelatin and cellulose fiber/gelatin scaffolds. However, cells grew in separated cell pathways rather than cell clumps when cellulose fibers were present. hMSCs cultured in the cellulose fiber/gelatin scaffold showed active ECM secretion and maintained multi-lineage differentiation potentials. The results suggest that 3-D cellulose fiber/gelatin composite will be a promising material for tissue engineering.

CHAPTER SIX

CONCLUSIONS AND FUTURE WORK

6.1 Conclusions

In this dissertation, LbL nanoassembly approach was employed to fabricate cellulose microfiber/enzyme biocomposites and cellulose microfiber/CNT/PEDOT conductive composite. Cellulose microfiber/gelatin composite used for cell culture was first developed by using a phase separation method.

Laccase and urease were used to fabricate bioactive composites with cellulose microfibers. Organized laccase and urease multilayers systematically deposited on a cellulose microfiber surface were demonstrated. The adsorption amount of enzyme at each layer is approximately the same, indicating uniform enzymer monolayer formation. Therefore, the enzyme activity of the biocomposite is linearly proportional to the number of enzyme layers in the coating. Different multilayer architecture can change the initial activity of the biocomposite as well as the stability of the biocomposite. Extra polyelectrolyte layers on top of outmost enzyme layer help slow the activity decay, but the initial activity was also reduced because the outside polyelectrolyte layers limited the enzyme access to the substrate. The laccase-fiber composite maintained around 50% of its initial enzyme activity after 14 days of storage in deionized water at 4°C. Handsheets made with laccase-fiber composites could maintain more than 70% of initial enzymatic activity after 45 days at 4°C. Laccase-fiber composites can be used for degradation of

phenol compounds in waste water. Urease-fiber composites were successfully applied for biomineralization to grow calcium carbonate microparticles. Other water insoluble carbonates such as $ZnCO_3$ and $CuCO_3$ or phosphates could be obtained using a similar approach. These organic/inorganic hybrid composites could find applications in a paper whitening process or biological materials fabrication. The strategy presented could be used for creation of cellulose fiber based biocomposites with various functions which can be precisely controlled by film nano-architecture.

PSS modified CNTs and PEDOT-PSS were used to fabricate conductive composites with cellulose microfibers. Surface charge reversal at each LbL assembly step and a dense network of carbon nanotubes observed on the cellulose fiber surface demonstrated that CNT-PSS was successfully coated on the surface of the cellulose microfibers. The conductivity of the cellulose microfibers was in the range of 10^{-2} to 2 $S.cm^{-1}$ depending upon the architecture of the coated layer. The conductivity of the wood fibers was further increased up to 20 $S.cm^{-1}$ by combining conductive co-polymer PEDOT-PSS with CNT-PSS through a polycation (PEI) interlayer. QCM data indicates that PEDOT-PSS formed a strong complex with CNT-PSS in the combination structure. The complex facilitated the electron transfer through the carbon nanotubes network, and thus greatly enhanced the conductivity. The LbL coated conductive fibers were mixed with uncoated cellulose fibers to make paper handsheets following the traditional manufacturing method. It is demonstrated that the bulk paper conductivity ranged between 1 to 10 $S.cm^{-1}$ depending upon the ratio of LbL coated conductive microfibers to virgin uncoated microfibers. These results show that using the LbL nanoassembly technique, cellulose microfibers/carbon nanotubes composite can be realized cost effectively (only a small

amount, around 0.2 wt%, of CNTs) to make conductive paper sheets. This functionally enhanced material - bulk conductive paper was employed for fabrication of a conductive paper-based capacitor. The results showed enhanced electrical capacitance of 1.6×10^{-11} F per square inch of sample compared with a capacitor using a copper electrode. This technique will help in the realization of cellulose microfiber-based electronic devices (e.g. capacitors, inductors, and transistors) and sensors that can be directly integrated in paper, resulting in "smart" paper products.

3-D cellulose fibers/gelatin microscaffolds were fabricated by simply mixing natural wood cellulose microfibers with a small amount of gelatin, and then using phase separation and freeze-drying methods. The morphology was observed by SEM and CLSM and the microscopy images showed the porous and rough structure of the scaffold. The porosity is around 70% and the diameter of the pores is about 70 μm. The composite demonstrated an ideal open and porous structure favorable for cell seeding and growth. Compared with the pure gelatin scaffold, the cellulose fiber/gelatin scaffold showed 3-8 times higher mechanical strength, which is controllable by varying the fiber amount. The biocompatibility test using brain tumor cells showed that cells attached and grew well on both gelatin and cellulose fiber/gelatin scaffolds. However, cells grew in separated cell pathways rather than cell clumps when cellulose fibers were present. hMSCs cultured in the cellulose fiber/gelatin scaffold showed active proliferation in the first week. Extensive ECM secretion and maintenance in multi-lineage differentiation potentials proved that the scaffold provided a good microenvironment for cellular activity. The microscopy images also indicated that cells are preferentially growing along the fiber orientation. The results

suggest that the 3-D cellulose fiber/gelatin composite will be a promising material for tissue engineering and regenerative medicine application.

6.2 Future Work

6.2.1 Cellulose Microfiber Composites Based on LbL Nanoassembly

LbL nanoassembly introduced a simple and versatile method to fabricate cellulose microfiber composites with novel functions. Enzymes (laccase and urease) and conductive substances (CNTs and PEDOT) incorporated cellulose microfiber composites have been successfully developed in this work. A great variety of other materials can be applied for LbL coating of cellulose microfibers. For example, lysozyme can be deposited on a cellulose fiber surface to enhance antimicrobial properties. Cellulose microfiber composites with magnetic properties can be fabricated by assembling magnetic nanoparticles on the cellulose fiber surface.

In addition, the LbL approach is not limited in modifying cellulose fibers. Other fibers, such as glass fibers and polymer fibers may also be applicable. It may be interesting to use this method to modify electrospun nanofibers, which have been extensively studied in many research areas. The diameter of electrospun nanofibers is typically in the range of 30-2000 nm with length > 100 μm. TiO_2 nanoparticles have been successfully assembled alternately with PAA on electrospun cellulose acetate nanofibers, as shown in Figure 6.1.[150]

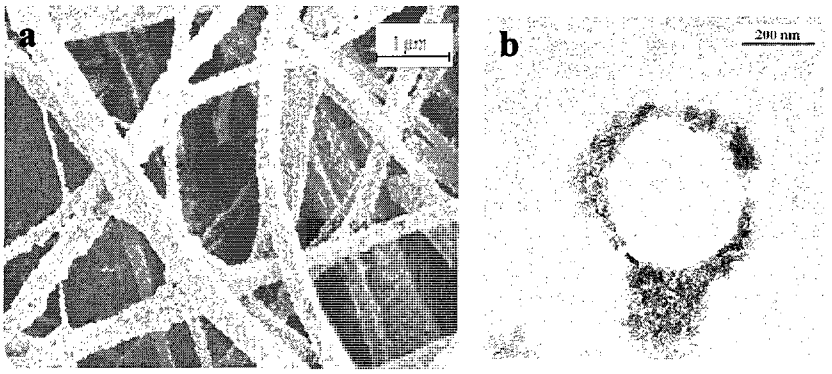

Figure 6.1 (a) SEM image of TiO_2 nanoparticles coated cellulose acetate nanofibers; (b) TEM image of cross-section of coated fiber.[150]

6.2.2 3-D Cellulose Microfiber Based Composite for Cell Culture

Cellulose microfiber (containing up to 75 wt%) / gelatin composite was fabricated and used as a cell culture scaffold for the first time. Cell culture experiments indicated it was a suitable and promising scaffold. However, the main issue is that cellulose microfibers are poorly degradable *in vivo*. This problem could be resolved by introducing cellulase for treatment. Cellulase is a group of enzymes that are able to break down cellulose into glucose units under mild conditions. Cell constructs on cellulose hollow bundles were treated with cellulase solution for two days. Although some cells fell off the construct, the structure retained its original morphology (Figure 6.2). The cardiac myocytes viability and attachment were not significantly influenced by the cellulase treatment.[86]

Microfibrillated cellulose could be introduced for scaffold fabrication instead of cellulose microfibers. Microfibrillated cellulose was obtained by homogenizing kraft paper pulp with diameters in the range of 10 – 100 nm, as shown in Figure 6.3.[3] The tiny fibrils formed an interconnected network which has dramatically increased the surface

areas. It is believed that the cellulose microfibril strength might be as high as 2 GPa.[151] Therefore, the resulting microfibrillated cellulose/gelatin composite is likely to exhibit outstanding mechanical properties.

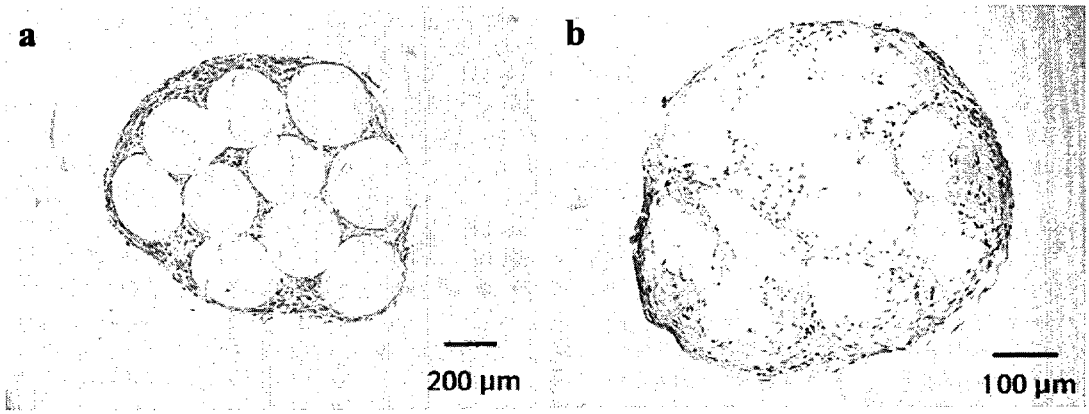

Figure 6.2 Staining of cells before (a) and after (b) cellulase treatment.[86]

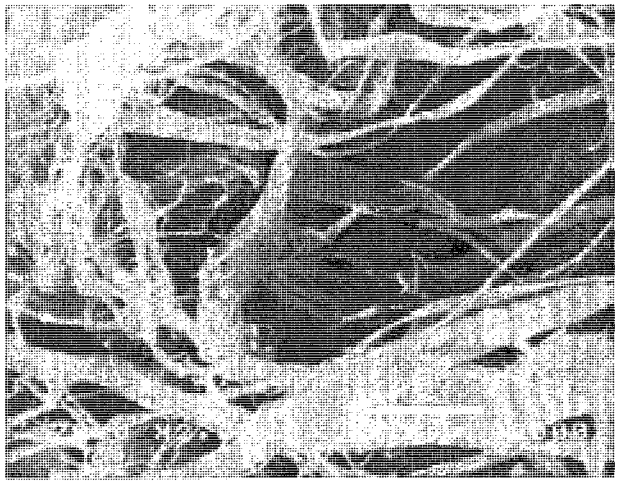

Figure 6.3 SEM image of microfibrillated cellulose.[3]

REFERENCES

(1) He, J.; Kunitake, T.; Nakao, A. *Chem. Mater.* **2003**, *15*, 4401-4406.

(2) Zakaria, S.; Ong, B.; Ahmad, S.; Abdullah, M.; Yamauchi, T. *Mater. Chem. Phys.* **2005**, *89*, 216-222.

(3) Nakagaito, A.; Yano, H. *Appl. Phys. A* **2005**, *80*, 155-159.

(4) Bhatnagar, A.; Sain, M. *J. Reinforced Plas. Compos.* **2005,** *24*, 1259-1268.

(5) Eriksson, M.; Notley, S.; Wågberg, L., *J. Colloids Interface Sci.*, **2005**, *291*, 38-45.

(6) Eriksson, M.; Pettersson, G.; Wågberg, L. *Nord. Pulp Paper Res. J.*, **2005**, *20*, 270-276.

(7) Zheng, Z.; McDonald, J.; Khillan, R.; Shutava, T.; Grozdits, G.; Lvov, Y. *J. Nanosci. Nanotechnol.*, **2006**, *6*, 624-632.

(8) Lu, Z.; Eadula, S.; Grozdits, G.; Zheng, Z.; Xu, K.; Lvov, Y. *Colloids Surf. A*, **2007**, *292*, 56-62.

(9) Lvov, Y.; Zheng, Z.; Lu, Z.; Grozdits, G. *Nordic Pulp Paper Res. J.*, **2006**, *21*, 552-559.

(10) Hon, D.N.-S.; Shiraishi, N. *Wood and Cellulosic Chemistry*, 1st ed.; 1991; pp: 7-9.

(11) Brown, R.W. *J. Polym. Sci. A, Polym. Chem.*, **2004**, *42*, 487-495.

(12) Wollerdorfer, M.; Bader, H. *Ind. Corp. Prod.*, **1998**, *8*, 105-112.

(13) Lawton, J.W.; Shogren, R.L.; Tiefenbacher, K.F. *Ind. Corp. Prod.*, **2004**, *19*, 41-47.

(14) Huda, M.S.; Drzal, L.T.; Misra, M. *Ind. Eng. Chem. Res.*, **2005**, *44*, 5593-5601.

(15) Östenson, M.; Gatenholm, P. *Langmuir*, **2005**, *21* 160-165.

(16) Vander-Wielen, L.C.; Ragauskas, A.J. *Eurp. Polym. J.*, **2004**, *40*, 477-482.

(17) Loria-Bastarrachea, M.; Carrillo-Escalante, H.; Aguilar-Vega, M. *J. Appl. Polym. Sci.*, **2002**, *83*, 386-393.

(18) Karlsson, J.O.; Henriksson, Å.; Michálek, J.; Gatenholm, P. *Polymer*, **2000**, *41*, 1551-1559.

(19) Iler R. *J. Colloid Interface Sci.* **1996**, *21*, 569-594.

(20) Decher, G. *Science*, **1997**, *227*, 1232-1237.

(21) Lvov, Y.; Decher, G.; Möhwald, H. *Langmuir*, **1993**, *9*, 481-486.

(22) Keller, S.; Kim, H-N.; Mallouk, T. *J. Am. Chem. Soc.*, **1994**, *116*, 8817-8818.

(23) Ariga, K.; Hill, J.P.; Ji, Q. *Phys. Chem. Chem. Phys.*, **2007**, *9*, 2319-2340.

(24) Ostrander, J.W.; Mamedov, A.A.; Kotov, N.A. *J. Am. Chem. Soc.*, **2001**, *123*, 1101-1110.

(25) Lvov, Y.; Rusling, J.F.; Thomsen, D.L.; Papadimitrakopoulos, F.; Kawakami, T.; Kunitake T. *Chem. Commun.*, **1998**, *7*, 1229-1230.

(26) Lvov, Y.; Ariga, K.; Ichinose, I.; Kunitake, T. *J. Am. Chem. Soc.*, **1995**, *117*, 6117-6123.

(27) Lvov, Y.; Eadula, S.; Zheng, Z.; Lu, Z.; Grozdits, G. *Nord. Pulp Paper Res. J.*, **2006**, *21*, 552-559.

(28) Eriksson, M.; Torgnysdotter, A.; Wågberg, L. *Ind. Eng. Chem. Res.*, **2006**, *45*, 5279-5286.

(29) Dubas, S.T.; Kumlangdudsana, P.; Potiyaraj, P. *Colloids Surf. A*, **2006,** *289*, 105-109.

(30) Shiratori, S.; Inami, Y.; Kikuchi, M.; Yamada, T.; Yamada, M. *Polym. Adv. Technol.*, **2000**, *11*, 766-771.

(31) Fang, M.; Grant, P.; McShane, M.; Sukhorukov, G.; Golub, V.; Lvov, Y. *Langumir*, **2002**, *18*, 6338-6344.

(32) Lu, Z.; Prouty, M.D.; Guo, Z.; Kumar, C.S.S.R.; Lvov, Y. *Langmuir*, **2005**, *21*, 2042-2050.

(33) Forrest, S.R.; Elmore, B.B.; Palmer, J.D. *Appl. Biochem. Biotech.*, **2005**, *121*, 85-91.

(34) Forrest, S.R.; Elmore, B.B.; Palmer, J.D. *Catalysis Today*, **2007**, *120*, 30-34.

(35) Caruso, F.; Fiedler, H.; Haage, K. *Colloids Surf. A*, **2000,** *169*, 287-293.

(36) Shutava, T.; Zheng, Z.; John, V.; Lvov, Y. *Biomacromolecules*, **2004**, *5*, 914-921.

(37) Yan, X.; Ji, H-F.; Lvov, Y. *Chem. Phys. Lett.*, **2004**, *396*, 34-37.

(38) Yoon, H.C.; Kim, H-S. *Anal. Chem.*, **2002**, *72*, 922-926.

(39) Thurston, C.F. *Microbiology*, **1994**, *140*, 19-26.

(40) Durán, N.; Rosa, M.A.; D'Annibale, A.; Gianfreda, L. *Enzym. Microbiol Technol.*, **2002**, *31*, 907-931.

(41) Mocciutti, P.; Zanuttini, M.; Kruus, K.; Suunakki, A. *TAPPI J.*, **2008**, *7*, 17-22.

(42) Leonowicz, A.; Sarkar, J.M.; Bollag, J.M. *Appl. Microbiol Biotechnol.*, **1988**, *29* 129-135.

(43) Leech, D.; Daigle, F. *Analyst*, **1998**, *123*, 1971-1974.

(44) Karplus, P.A.; Pearson, M.A.; Hausinger, R.P. *Acc. Chem. Res.*, **1997**, *30*, 330-337.

(45) Dumitriu, S.; Popa, M.; Artenie, V.; Dan, F. *Biotechnol Bioeng.*, **1989**, *34*, 283-290.

(46) Liang, Z.; Wang, C.; Tong, Z.; Ye, W.; Ye, S. *Reac. Func. Polym.*, **2005**, *63*, 85-94.

(47) Laska, J.; Wlodarczyk, J.; Zaborska, W. *J. Molec. Catal. B*, **1999**, *6*, 549-553.

(48) Krajewska, B.; Piwowarska, Z. *Biocatal. Biotrans.* **2005**, *23*, 225-232.

(49) Antipov, A.; Shchukin, D.; Fedutik, Y.; Zanaveskina, I.; Klechkovskaya, V.; Sukhorukov, G.; Möhwald, H. *Macromol. Rapid Commun.*, **2003**, *24*, 274-277.

(50) Iijima, S. *Nature*, **1991**, *354*, 56-58.

(51) Martel, R.; Schmidt, T.; Hertel, H.R.; Avouris, P. *Appl. Phys. Lett.*, **1998**, *73*, 2447-2449.

(52) Hertel, T.; Marta, R.; Avouris, P. *J. Phys. Chem. B.*, **1998**, *102*, 910-915.

(53) Planeix, J.M.; Coustel, N.; Coq, B.; Brotons, V.; Kumbhar, P.S.; Dutartre, R.; Geneste, P.; Bernier, P.; Ajayan, P.M. *J. Am. Chem. Soc.*, **1994**, *116*, 7935-7936.

(54) Dai, H.J.; Hafner, J.H.; Rinzler, A.G.; Collbert, D.T.; Smally, R.E. *Nature*, **1996**, *384*, 147-150.

(55) Odom, T.W.; Huang, J.L.; Kim, P.; Lieber, C.M. *J. Phys. Chem. B*, **2000**, *104*, 2794-2809.

(56) Dresselhaus, M.S.; Dresselhaus, G.; Eklaund, P.C. *Science of Fullerences and Carbon Nanotubes*, 1996; pp: 25-28.

(57) Huang, S.C.J.; Artyukhin, A.B.; Wang, Y.M.; Ju, J.W.; Stroeve, P.; Noy, A. *J. Am. Chem. Soc.*, **2005**, *127*, 14176-14177.

(58) Arnold, M.S.; Stupp, S.I.; Hersam, M.C. *Nano Lett.*, **2005**, *5*, 713-718.

(59) Pantarotto, D.; Partidos, C.D.; Graff, R.; Hoebeke, J.; Briand, J.P.; Prato, M.; Bianco, A. *J. Am. Chem. Soc.*, **2003**, *125*, 6160-6164.

(60) Riggs, J.E.; Walker, D.B.; Carroll, D.L.; Sun, Y.P. *J. Phys. Chem. B*, **2000**, *104*, 7071-7076.

(61) Dai L. *Carbon Nanotechnology*, 2006; pp: 113-120.

(62) Hamon, M.A.; Hui, H.; Bhowmik, P.; Itkis, H.E.; Haddon, R.C. *Appl. Phys. A: Mater. Sci. Process.* **2002**, *74*, 333-338.

(63) Chen, L.; Yuan, C.; Dou, H.; Gao, B.; Chen, S.; Zhang, X. *Electrochim. Acta*, **2009**, *54*, 2335-2341.

(64) Kong, B.; Zeng, J.; Luo, G.; Luo, S.; Wei, W.; Li, J. *Bioelectrochemistry*, **2009**, *74*, 289-294.

(65) Sugikawa, K.; Numata, M.; Kaneko, K.; Sada, K.; Shinkai, S. *Langmuir*, **2008**, *24*, 13270-13275.

(66) Lee, K-U; Cho, Y-H; Petty, M-C; Ahn, B-T *Carbon*, **2009**, *47*, 475-481.

(67) Kassim, A.; Earmul-Mahmud, H.N.M.; Yee, L.M.; Hanipah, N. *Pacif. J. Sci. Technol.* **2006**, *7*, 103-107.

(68) Petterson, A.L.; Carlsson, F.; Inganas, O.; Arwin, H. *Thin Solid Films*, **1998**, *313*, 855-879.

(69) Ouyang, J.Y.; Xu, Q.F.; Chu, C.W.; Yang, Y.; Li, G.; Shinar, J. *Polymer*, **2004**, *45*, 8443-8450.

(70) Kirchmeyer, S.; Reuter, K. *J. Mater. Chem.*, **2005**, *15*, 2077-2088.

(71) Jonas, F.; Morrison, J.T. *Synth. Met.*, **1997**, *3*, 1397-1398.

(72) Okuzaki, H.; Ashizawa, S.; Shinohara, Y.; Shinado, H.; Watanabe, Y. *Synth. Met.*, **2005**, *153*, 41-44.

(73) De Kok, M.M.; Buechel, M.; Vulto, S.I.E.; Weijtens, C.H.L; Van Elsbergen, V.; *Physica Status Solidi A*, **2004**, *201*, 1342-1359.

(74) Daoud, W.A.; Xin, J.H.; Szeto, Y.S. *Sensors and Actuators B*, **2005**, *109*, 329-333.

(75) Bratt-Leal, A.M.; Carpenedo, R.L.; McDevetti, T.C. *Biotechnol. Prog.*, **2009**, *25*, 43-51.

(76) Wei, G.; Ma, P. X. *Adv. Funct. Mater.*, **2008**, *18*, 3568-3582.

(77) Ross-Murphy, S.B. *Polymer*, **1992**, *33*, 2622-2627.

(78) Ren, S.Z.; Shi, W.F.; Zhang, W.B.; Sorensen, C.M. *Phys. Rev. A*, **1992**, *45*, 2416-2422.

(79) Yoshida, H.; Matsusaki, M.; Akashi, M. *Adv. Funct. Mater.*, **2009**, *19*, 1001-1007.

(80) Dubruel, P.; Unger, R.; Van Vlierberghe, S.; Cnudde, V.; Jacobs, P.J.S.; Schacht, E.; Kirkpatrick, C.J. *Biomacromolecules*, **2007**, *8*, 338-344.

(81) Mao, J.S.; Zhao, L.G.; Yin, Y.J.; Yao, K.D. *Biomaterials*, **2003**, *24*, 1067-1074.

(82) Brown, R.Q.; Mount, A.; Burg, K.J. *J. Biomed. Mater. Res. Part A*, **2005**, *74*, 488-494.

(83) Guo, T.; Zhao, J.; Chang, J.; Ding, Z.; Hong, H.; Chen, J.; Zhang, J. *Biomaterials*, **2006**, *27*, 1095-1103.

(84) Kim, H.W.; Kim, H.E.; Salih, V. *Biomaterials*, **2005**, *26*, 5221-5230.

(85) Holland, T.A.; Tabata, Y.; Mikos, A.G. *J. Control. Release*, **2005**, *101*, 111-125.

(86) Ko, I.K.; Iwata, H. *Ann. N. Y. Acad. Sci.*, **2001**, *944*, 443-455.

(87) Svensson, A.; Nicklasson, E.; Harrah, T.; Panilaitis, B.; Kaplan, D.L.; Brittberg, M.; Gatenholm, P. *Biomaterials*, **2005**, *26*, 419-431.

(88) Entcheva, E.; Bien, H.; Yin, L.; Chung, C.Y.; Farrell, M.; Kostov, Y. *Biomaterials*, **2004**, *25*, 5753-5762.

(89) Märtson, M.; Viljanto, J.; Hurme, T.; Saukko, P. *Eur. Surg. Res.*, **1998**, *30*, 426-432.

(90) Müller, F.A.; Müller, L.; Hofmann, I.; Greil, P.; Wenzel, M.M.; Staudenmaier, R.; *Biomaterials*, **2006,** *27*, 3955-3963.

(91) Tate, M.C.; Shear, D.A.; Hoffman, S.W.; Stein, D.G.; LaPlaca, M.C. *Biomaterials*, **2001**, *22*, 1113-1123.

(92) Cullen, B.; Watt, P.W.; Lundqvist, C.; Silcock, D.; Schmidt, R.J.; Bogan, D. *Int. J. Biochem. Cell Biol.*, **2002**, *34*, 1544-1556.

(93) Kino, Y.; Sawa, M.; Kasai, S.; Mito, M. *J. Surg. Res.*, **1998**, *79*, 71-76.

(94) Takata, T.; Wang, H.L.; Miyauchi, M. *Clin. Oral Implants Res.*, **2001**, *12*, 332-338.

(95) Yang, M.B.; Vacanti, J.P.; Ingber, D.E. *Cell Transplant*, **1994**, *3*, 373-385.

(96) LaIuppa, J.A.; McAdams, T.A.; Papoutsakis, E.T.; Miller, W.M. *J. Biomed. Mater. Res.*, **1997**, *36*, 347-359.

(97) Xing, Q.; Eadula, S.R.; Lvov, Y. *Biomacromolecules*, **2007**, *8*, 1987-1991.

(98) Schwinte, P.; Ball, V.; Szalontai, B.; Haikel, Y.; Voegel, J.; Schaaf, P. *Biomacromolecules*, **2002**, *3*, 1135-1143.

(99) Haynie, D.T.; Zhang, L.; Rudra, J.S.; Zhao, W.; Zhong, Y.; Palath, N. *Biomacromolecules*, **2005**, *6*, 2895-2913.

(100) Boraston, A.B.; Bolam, D.N.; Gilbert, H.J.; Davies, G.J. *Biochem. J.*, **2004**, *382*, 769-781.

(101) Brumer, H.; Zhou, Q.; Baumann, M.J.; Carlsson, K.; Teeri, T.T. *J. Am. Chem. Soc.*, 2004, *126*, 5715-5721.

(102) Wong, K.K.Y.; Richardson, J.D.; Mansfield, S. D. *Biotechnol. Prog.*, **2000**, *16*, 1025-1029.

(103) Lvov, Y.; Antipov, A.; Mamedov, A.; Möhwald, H.; Sukhorukov, G. *Nano Lett.*, **2001**, 1, 125-128.

(104) Piontek, K.; Antorini, M.; Choinowski, T. *J. Biol. Chem.*, **2002**, *277*, 37663-37669.

(105) Necochea, R.; Valderrama, B.; Dı'az-Sandoval, S.; Folch-Mallol, J.L.; Va'zquez-Duhalt, R.; Iturriaga, G. *FEMS Microbiol. Lett.*, **2005**, *244*, 235-241.

(106) Caruso, F.; Schuler, C. *Langumir*, **2000**, *16*, 9595-9603.

(107) Persson, P.V.; Hafrén, J.; Fogden, A.; Daniel, G.; Iversen, T. *Biomacromolecules*, **2004**, *5*, 1097-1101.

(108) Shutava, T.; Kommireddy, D.; Lvov, Y. *J. Am. Chem. Soc.*, **2006**, *128*, 9926-9934.

(109) Lvov, Y.; Caruso, F. *Anal. Chem.*, **2001**, *73*, 4212-4217.

(110) Derbal, L.; Lesot, H.; Voegel, J.; Ball, V. *Biomacromolecules*, **2003**, *4*, 1244-1263.

(111) Laska, J.; Wlodarczyk, J.; Zaborska, W. *J. Mol. Catal. B-Enzym.* **1999**, *6*, 549-553.

(112) Solna, R.; Skladal, P. *Electroanalysis*, **2005**, *17*, 2137-2146.

(113) Sigoillot, C.; Camarero, S.; Vidal, T.; Record, E.; Asther, M.; Perez-Boada, M.; Martinez, M.J.; Sigoillot, J.C.; Asther, M.; Colom, J.F.; Martinez, A.T. *J. Biotechnol.*, **2005**, *115*, 333-343.

(114) Chandra, R.P.; Lehtonen, L.K.; Ragauskas, A.J. *Biotechnol. Prog.*, **2004**, *20*, 255-261.

(115) Forzni, E.; Teijelo, M.; Nart, F.; Calvo, E.; Solís, V. *Biomacromolecules*, **2003**, *4*, 869-879.

(116)Aizenberg, J.; Black, A.J.; Whitesides, G.M. *Nature*, **1998**, *394*, 868-791.

(117)Naka, K.; Chujo, Y. *Chem. Mater.*, **2001**, *13*, 3245-3259.

(118)Shchukin, D.; Sukhorukov, G.; Price, R.; Lvov, Y. *Small*, **2005**, *5*, 510-513.

(119)Middleton, S.; Desmeules, J.; Scallan, A. *J. Pulp Paper Sci.*, **2003**, *29*, 241-247.

(120)Agarwal, M.; Xing, Q.; Shim, B.S.; Kotov, N.A.; Varahramyan K.; Lvov, Y. *Nanotechology*, **2009**, *20*, 21506.

(121)Kim, Y.H.; Moon, D.G.; Han, J.I. *IEEE Elect. Device Lett.*, **2004**, *25*, 702-704.

(122)Kim, J.; Seo, Y.B. *Smart Mater. Struct.*, **2002**, *11*, 355-360.

(123)Rigers, J.A.; Bao, Z. *PNAS,* **2001**, *98*, 4835-4840.

(124)Loh, K.J.; Lynch, J.P.; Shim, B.S.; Kotov, N.A. *J. Intell. Mater. Systm. Struct.* **2008**, *19*, 747-764.

(125)Shim, B.S.; Chen, W.; Doty, C.; Xu, C.; Kotov, N.A. *Nano Lett.*, **2008**, *8*, 4151-4157.

(126)O'Connell, M.J.; Boul, P.; Ericson, L.M.; Huffman, C.; Wang, Y.; Haroz, E.; Kuper, C.; Tour, J.; Ausman, K.D.; Smalley, R.E. *Chemic. Phys. Lett.* **2001**, *342*, 265-271.

(127)Shim, B.S.; Tang, Z.Y.; Morabito, M.P.; Agarwal, A.; Hong, H.P.; Kotov, N.A. *Chem. Mater.* **2007**, *19*, 5467-5474.

(128)Sano, M.; Lvov, Y.; Kunitake, T. *Ann. Rev. Mater. Sci.*, **1996**, *26*, 153-187.

(129)Vacca, P.; Nenna, G.; Miscioscia, R.; Palumbo, D.; Minarini, C.; Dala, D.D. *J. Phys. Chem. C*, **2009**, *113*, 5777-5783.

(130)Murugan, A.V.; Viswanath, A.K.; Campet, G.; Gopinath, C.S.; Vijayamohanan, K. *Appl. Phys. Lett.*, **2005**, *87*, 243511-243513.

(131)Renvall, S.; Sjöblom, M. *Eur. J. Surg.*, **1991**, *157*, 175-177.

(132)Noiset, O.; Schneider, Y.J.; Marchand-Brynaert, J. *J. Biomater. Sci. Polym. Ed.*, **1999**, *10*, 657-677.

(133)Poustis, J.; Baquey, C.; Chauveaux, D. *J. Biomater. Sci. Polym. Ed.* **1994**, *16*, 119-124.

(134)Zhao, F.; Grayson, W.L.; Ma, T.; Bunnell, B.; Lu, W.W. *Biomaterials*, **2006**, *27*, 1859-1867.

(135)Duan, X.; Sheardown, H. *Biomaterials*, **2006**, *27*, 4608-4617.

(136)Nabeta, M.; Sano, M. *Langmuir*, **2005**, *21*, 1706-1708.

(137)Zhao, F.; Ma, T. *Biotechnol. Bioeng.*, **2005**, *91*, 482-493.

(138)Averons, L.; Boquillon, N. *Carbohydrate Polymers*, **2004**, *56*, 111-122.

(139)Fricain, J.C.; Granja, P.L.; Barbosa, M.A.; De Jeso, D.; Barthe, N.; Baquey, C. *Biomaterials*, **2002**, *23*, 971-980.

(140)Kieswetter, K.; Schwartz, Z.; Hummert, T.W.; Cochran, D.L.; Simpson, J.; Dean, D.D.; Boyan, B.D. *J. Biomed. Mater. Res.*, **1996**, *32*, 55-63.

(141)Tuzlakoglu, K.; Bolgen, N.; Salgado, A.J.; Gomes, M.E.; Piskin, E.; Reis, R.L. *J. Mater. Sci. Mater. Med.*, **2005,** *16*, 1099-1104.

(142)Raj, R.G.; Kokta, B.V.; Dembele, F.; Sanschagrain, B. *J. Appl. Polym. Sci.*, **1989**, *38*, 1987-1996.

(143)Sehgal, A.; Ricks, S.; Warrick, J.; Boynton, A.L.; Murphy, G.P. *Anticancer Res.*, **1999**, *19*, 4947-4953.

(144)Rosso, F.; Giordano, A.; Barbarisi, M.; Barbarisi, A. *J. Cell. Physiol.*, **2004**, *199*, 174-180.

(145)Deguchi, S.; Tsudome, M.; Shen, Y.; Konishi, S.; Tsujii, K.; Ito, S. *Soft Mater.*, **2007**, *3*, 1170-1175.

(146)Green, C.F.; Scarpino, P.V.; Gibbs, S.G. *Aerobiologia*, **2003**, *19*, 159-169.

(147)Hendricks, C.W.; Doyle, J.D.; Hugley, B. *Appl. Environ. Microbiol.*, **1995**, *61*, 2016-2019.

(148)Litwin, J. *Developments in Biological Standardization*, **1985**, *60*, 237-242.

(149)Ko, I.K.; Kato, K.; Iwata, H. *J. Biomater. Sci. Polym. Ed.*, **2005**, *16*, 1277-12791.

(150)Ding, B.; Kim, J.; Kimura, E.; Shiratori, S. *Nanotechnology*, **2004**, *15*, 913-917.

(151)Sperling, L.H. *Introduction to Physical Polymer Science* 2001; pp. 499-500.